SANDIA NATIONAL LABORATORIES
WASTE ISOLATION PILOT PLANT

SUMMARY REPORT FOR THE 2026 COMPLIANCE RECERTIFICATION APPLICATION PERFORMANCE ASSESSMENT: INTERIM STATE REPOSITORY
REVISION 0

SARAH BRUNELL (Affiliate) Digitally signed by SARAH BRUNELL (Affiliate)
Date: 2025.12.10 12:15:54 -07'00'

Authentication

Author:	Sarah Brunell	Org.	8881
Author:	Brad Day	Org.	8881
Author:	Paul Docherty	Org.	8881
Author:	Dwayne Kicker	Org.	8881
Author:	Sungtae Kim	Org.	8881
Author:	Seth King	Org.	8881
Author:	Jennifer Long	Org.	8881
Author:	Justin Wilgus	Org.	8881
Author:	Todd R. Zeitler	Org.	8612
Technical Reviewer:	Clifford Hansen	Org.	8824
QA Reviewer:	Shelly R. Nielsen	Org.	8883
Management Reviewer:	Steve Wagner	Org.	8881

DECEMBER 2025

Information Only

EXECUTIVE SUMMARY

The Waste Isolation Pilot Plant (WIPP) was initially certified as a repository consisting of 10 panels, which were excavated for the long-term storage and placement of transuranic waste (U.S. EPA 1998). However, due to operational constraints, the entire volume of the 10 panels is no longer available for waste disposal. In March 2024, the U.S. Department of Energy (DOE) submitted the Replacement Panels Planned Change Request (RPPCR) to the U.S. Environmental Protection Agency (EPA) for approval of waste emplacement in two new panels. These panels, referred to as replacement panels, are located to the west of the existing operations area. The RPPCR received EPA approval in July of 2025 (U.S. EPA 2025).

The addition of the two replacement panels is not expected to provide adequate space for the disposal of the allowable waste volume designated for WIPP under the Land Withdrawal Act (LWA); thus, the 12-panel configuration is regarded as an interim state (IS) of the repository. The DOE may pursue approval for waste disposal in seven additional panels to accommodate the full allowable volume of waste. This hypothetical 19-panel configuration is considered the anticipated final state (FS) of the repository.

The DOE demonstrates compliance with containment requirements as outlined in the Certification Criteria of Title 40 CFR Part 191.13 through performance assessment (PA). PA calculations estimate the probability and consequences of potential radionuclide releases from the repository to the accessible environment over a regulatory period of 10,000 years following facility closure. WIPP PA models are utilized to support the periodic recertification of WIPP.

The 2026 Compliance Recertification Application (CRA-2026) represents the fifth recertification application submitted to the EPA. A PA has been carried out by Sandia National Laboratories to support the DOE's submission of the CRA-2026.

This report summarizes the CRA-2026 PA for the interim state repository and details the effects of the changes introduced and incorporated in the CRA-2026 PA. The results of the CRA-2026 PA are compared to those from the RPPCR PA, the most recent regulatory submission. In comparison to the RPPCR PA, the primary effects of these changes are slightly higher total releases, driven by increased contributions from spallings and direct brine releases, while releases through the Culebra, already small in the RPPCR, are further reduced to a negligible level. These findings confirm that the interim state repository configuration continues to meet containment requirements under 40 CFR Part 191.

Information Only

TABLE OF CONTENTS

EXECUTIVE SUMMARY II

1.0 INTRODUCTION 1

2.0 CHANGES SINCE THE RPPCR 2

2.1 Repository Design 2
2.2 Parameters Related to Repository Dimensions 4
2.3 Salado Flow and Transport Computational Grid 4
2.4 Waste Inventory 4
2.5 Baseline Actinide Solubilities 5
2.6 Solubility Uncertainty Distributions 5
2.7 Colloidal Enhancement Parameters 6
2.8 MgO Hydration Parameters 6
2.9 Lower Bound on Capillary Pressure in the Anhydrite Marker Beds 6
2.10 Porosity-Permeability Parameter Distribution 6
2.11 Minimum Brine Volume Needed for a DBR 7
2.12 Culebra Release Point Location 7
2.13 Drilling Rate and Borehole Plugging Pattern Probabilities 7
2.14 Parameters Not Updated as Anticipated in Analysis Plan AP-214 8

3.0 METHODOLOGY FOR THE CRA26_IS 9

3.1 Review of FEPs and Conceptual Models 9
3.2 Salado Flow 10
3.2.1 Repository Representation in BRAGFLO 10
3.2.2 Salado Flow Modeling Scenarios 11
3.3 Radionuclide Activities for Solid Releases 11
3.4 Cuttings, Cavings, and Spallings 12
3.5 Direct Brine Release Volumes 12
3.5.1 Initial Conditions 14
3.5.2 Modeling Scenarios 15
3.6 Mobilized Radionuclide Concentrations 15
3.7 Salado Transport 16
3.8 Culebra Flow and Transport 16

Information Only

3.9 Release Construction Methodology 18
3.10 Sensitivity Analysis 19
3.11 Run Control 19

4.0 RESULTS 20
4.1 Inventory 20
4.1.1 Total Waste Volume 20
4.1.2 Inventory by EPA Units 21
4.1.3 Waste Stream Activity Concentration 24
4.1.4 Total Radionuclide Activity 25
4.2 Salado Flow 28
4.3 Cuttings, Cavings, and Spallings 32
4.3.1 Cuttings and Cavings 32
4.3.2 Spallings 33
4.4 Direct Brine Release Volumes 38
4.5 Mobilized Radionuclide Concentrations 42
4.6 Salado Transport 47
4.7 Culebra Flow and Transport 50
4.8 Releases by Release Mechanism 54
4.8.1 Undisturbed Repository Releases 54
4.8.2 Cuttings and Cavings Releases 54
4.8.3 Spallings Releases 57
4.8.4 Direct Brine Releases 59
4.8.5 Long-Term Radionuclide Transport 62
4.9 Total Releases 66
4.9.1 Sensitivity Analysis for Total Releases 68
4.9.2 Comparison to CRA-2019 71

5.0 CONCLUSIONS 73

REFERENCES 74

Information Only

LIST OF FIGURES

Figure 1. Interim State Repository Layout 3
Figure 2. BRAGFLO Grid for the CRA26_IS with Modeled Area Descriptions 10
Figure 3. CRA26_IS and RPPCR DBR Grid with Simulated Intrusion Locations 13
Figure 4. Regions Used to Transfer Initial Pressure and Saturation from the BRAGFLO Salado Grid to the DBR Grid 14
Figure 5. Culebra Modeling Domain 18
Figure 6. Total Activity in WIPP CH- and RH-TRU Waste from Closure to 10,000 Years After Closure, in Units of (a) Curies (Ci) and (b) EPA Units. 26
Figure 7. Mean Net Brine Flow into the Waste Panel 29
Figure 8. Mean Brine Consumption in the Waste Panel 30
Figure 9. Mean Brine Saturation in the Waste Panel 30
Figure 10. Mean Total Repository Gas Generation 31
Figure 11. Mean Normalized Total Repository Gas Generation 31
Figure 12. Mean Brine Pressure in the Waste Panel 32
Figure 13. Non-Zero Spallings Release Volume by Intrusion Scenario 36
Figure 14. Non-Zero Spallings Release Volume by Intrusion Location 36
Figure 15. Spallings Release Concentration from Closure to 10,000 Years 37
Figure 16. DBR Volume Frequency, All Non-Zero Releases, Replicate 1 41
Figure 17. DBR Volumes, All Non-Zero Releases, Replicate 1 41
Figure 18. DBR Volumes by Scenario, All Non-Zero Releases, Replicate 1 42
Figure 19. Largest Contributors in Curies to Inventory at Closure in the Waste Area 43
Figure 20. Comparison of Mean Concentrations 46
Figure 21. DBR Concentration Versus Time Used for Determining DBRs, All Vectors 46
Figure 22. Cumulative Lumped Radionuclide Releases 48
Figure 23. Total Cumulative Radionuclide Releases vs Time 49
Figure 24. Particle Travel Paths and Travel Time to the LWB Exceedance Probabilities, Full Mining Scenario 51
Figure 25. Particle Travel Paths and Travel Time to the LWB Exceedance Probabilities, Partial Mining Scenario 52
Figure 26. Exceedance Probability of Cumulative Mass to the LWB in 10,000 Years for Full Mining Scenario 53

Information Only

Figure 27. Exceedance Probability of Cumulative Mass to the LWB in 10,000 Years for Partial Mining Scenario 53
Figure 28. Mean Cuttings and Cavings Volume Scaled by the FVW Factor for Replicate 1 55
Figure 29. Cuttings and Cavings Releases for Replicate 1 of the CRA26_IS 56
Figure 30. Overall Mean Cuttings and Cavings Releases 56
Figure 31. Mean Spallings Volume Scaled by the FVW Factor for Replicate 1 58
Figure 32. Spallings Releases for Replicate 1 of the CRA26_IS 58
Figure 33. Overall Mean Spallings Releases 59
Figure 34. Mean Direct Brine Volumes for Replicate 1 60
Figure 35. Direct Brine Releases for Replicate 1 of the CRA26_IS 61
Figure 36. Overall Mean Direct Brine Releases 61
Figure 37. Mean Activity Entering the Culebra by Radionuclide for Replicate 1 of the CRA26_IS 63
Figure 38. Overall Mean Activity Entering the Culebra 63
Figure 39. Releases Through the Culebra by Radionuclide and Release Point for Replicate 1 of the CRA26_IS 65
Figure 40. Overall Mean Releases Through the Culebra 65
Figure 41. Overall Mean Releases Components for the CRA26_IS 67
Figure 42. Overall Mean Total Releases 67
Figure 43. Overall Mean Total Releases 72

Information Only

LIST OF TABLES

Table 1. Changed Repository Parameters 4
Table 2. Inventory Iron, CPR, and Decay Heat Concentrations 5
Table 3. Updated Minimum Brine Volume Parameter 7
Table 4. Location of Culebra Release Point 2 7
Table 5. Drilling Rate and Plugging Pattern Probabilities 8
Table 6. BRAGFLO Modeling Scenarios for the CRA26_IS 11
Table 7. DBR Scenarios 15
Table 8. WIPP CH- and RH-TRU Waste Streams by Total Scaled Volume from the RPPCR and CRA26_IS Inventories 21
Table 9. WIPP CH- and RH-TRU Waste Streams by Total EPA Units; Time 0 (Calendar Year 2083) and 10,000 Years (Calendar Year 12,083) From the CRA26_IS Inventory 23
Table 10. WIPP CH- and RH-TRU Waste Streams Ordered by Activity Concentration at Closure (Calendar Year 2,083) and at 10,000 Years Post-Closure (Calendar Year 12,083) from CRA26_IS Inventory 24
Table 11. Total Activity (EPA Units) for Dominant Isotopes in WIPP CH- and RH-TRU Waste at Closure and at 10,000 Years Post-Closure 27
Table 12. Cavings Area Statistics for CRA26_IS and RPPCR 33
Table 13. Spallings Volume Summary, Replicate 1 35
Table 14. DBR Volume Summary, Replicate 1 40
Table 15. Mean Mobile Concentration Limits in mol/L 44
Table 16. Mean Lumped Radionuclide Mobile Concentration Limits in mol/L 45
Table 17. Mean Cumulative Lumped Radionuclides Releases Through a Borehole to the Culebra at 10,000 Years in EPA Units 48
Table 18. Statistics on the Overall Mean Cuttings and Cavings Release 57
Table 19. Statistics on the Overall Mean Spallings Release 59
Table 20. Statistics on the Overall Mean Direct Brine Release 62
Table 21. Statistics on the Overall Mean Activity Entering the Culebra 64
Table 22. Statistics on the Overall Mean Releases Through the Culebra 66
Table 23. Statistics on the Overall Mean for Total Release 68
Table 24. Stepwise Ranked Regression Analysis for Mean Total Releases for Replicate 1 of the RPPCR and CRA26_IS 69
Table 25. Stepwise Ranked Regression Analysis for Mean Total Releases for Replicate 2 of the RPPCR and CRA26_IS 70

Information Only

Table 26. Stepwise Ranked Regression Analysis for Mean Total Releases for Replicate 3 of the RPPCR and CRA26_IS.....70

Table 27. Statistics on the Overall Mean for Total Release 72

Information Only

1.0 INTRODUCTION

The Waste Isolation Pilot Plant (WIPP), located in southeastern New Mexico, has been developed by the U.S. Department of Energy (DOE) for the geologic disposal of transuranic (TRU) waste. The containment of TRU waste at the WIPP is regulated by the U.S. Environmental Protection Agency (EPA) under Title 40 of the Code of Federal Regulations (CFR), Part 191.

The DOE demonstrates compliance with the containment requirements of 40 CFR 191.13 by means of performance assessment (PA) as described in the Certification Criteria of Title 40 CFR Part 194. Sandia National Laboratories (SNL) conducts PAs at the request of the DOE. The PA calculations estimate the probability and consequences of potential radionuclide releases from the repository to the accessible environment over a regulatory period of 10,000 years following facility closure. The PA models are continuously maintained and updated with new information, which typically leads to refinements and modifications in both the models and their parameters. Additionally, planned changes to the repository and its components necessitate updates to the WIPP PA models.

All previous WIPP certifications have been based on a repository consisting of 10 panels. In March 2024, the DOE submitted the Replacement Panels Planned Change Request (RPPCR) to seek EPA approval for waste emplacement in two new panels, referred to as replacement panels, located to the west of the existing operations area (Bollinger 2024). The RPPCR received EPA approval in July of 2025 (U.S. EPA 2025).

The addition of the two replacement panels is not expected to provide sufficient space for the disposal of the allowable waste volume designated for the WIPP under the Land Withdrawal Act (LWA). The 12-panel configuration is thus regarded as an interim state (IS) of the repository. The DOE may seek approval for waste disposal in up to seven additional panels to accommodate the full allowable volume of waste. This 19-panel configuration is considered the anticipated final state (FS) of the repository.

The CRA-2026 is the fifth recertification application for the WIPP submitted by the DOE for EPA approval. The PA executed by SNL in support of the CRA-2026 PA is described in AP-214 (Hansen et al. 2025). This report summarizes the results of the CRA-2026 PA for the interim state repository.

Information Only

2.0 CHANGES SINCE THE RPPCR

Several changes are incorporated in the CRA-2026 PA relative to the RPPCR that impact the results. These changes include:

- The repository design.
- Parameters related to repository dimensions.
- The waste inventory.
- Baseline actinide solubilities.
- Solubility uncertainty distributions.
- Colloid concentration parameters for humic and microbial colloids.
- MgO hydration parameters.
- The Salado flow and transport computational grid.
- A new lower bound on capillary pressure in the anhydrite marker beds.
- Revisions to the porosity-permeability parameter distribution.
- The minimum brine volume needed for a direct brine release (DBR).
- The location of the Culebra release point (CRP) for the replacement waste panels.
- The drilling rate and probabilities of borehole plugging patterns.

Changes listed above are discussed in more detail in the sections that follow.

2.1 Repository Design

This analysis represents the 12-panel interim state repository consisting of ten original and two replacement panels. Figure 1 depicts the interim state repository. The RPPCR considered the anticipated final repository state, which included a total of 19 waste panels and the entire allowable inventory volume.

Information Only

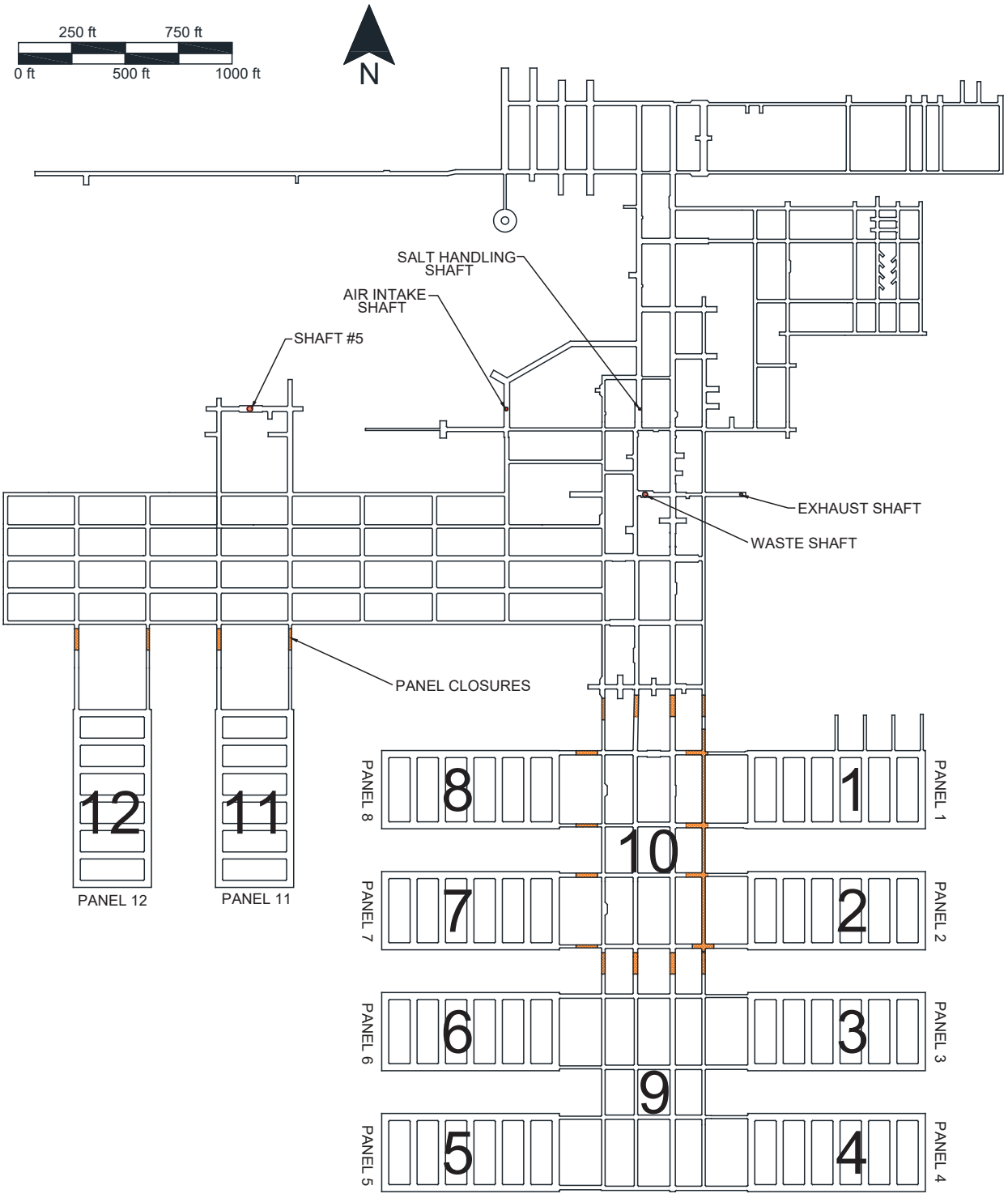


Figure 1. Interim State Repository Layout

Information Only

2.2 Parameters Related to Repository Dimensions

The repository design (Section 2.1) requires changes to several parameters describing repository dimensions. Brunell (2025) revises four parameters to align with the as-built dimensions of the original 10 waste panels and the planned dimensions of the replacement and additional waste panels.. The parameters include:

- the waste storage volume (REFCON:VREPOS).
- the area of the berm placed over the waste panels (REFCON:ABERM).
- the area allocated for contact-handled (CH) waste disposal (REFCON:AREA_CH).
- the fraction of the repository volume occupied by CH waste (REFCON:FVW).

Although not listed in AP-214 as an anticipated change (Hansen et al. 2025), the area for emplaced remote-handled (RH) waste (REFCON:AREA_RH) is revised by King (2025c) due to the reduced inventory volume used in the CRA26_IS PA calculation (see Section 2.2). The updated values are provided in Table 1.

Table 1. Changed Repository Parameters

Material	Property	RPPCR Value	CRA26_IS Value	Units
REFCON	VREPOS	853,284.89	560,722.29	m^3
REFCON	ABERM	1,268,303	750,000	m^2
REFCON	AREA_CH	216,952	141,511	m^2
REFCON	FVW	0.197	0.279	-
REFCON	AREA_RH	15,760	3,528	m^2

Table 1 from Day and King (2025).

2.3 Salado Flow and Transport Computational Grid

Dimensions in the computational grid for the Salado flow (BRAGFLO) and transport (NUTS) calculation are changed to be consistent with the interim state repository dimensions (Section 2.1). Day (2025a) modifies the computational grid based on as-built excavation footprint dimensions within the existing repository, plans for future excavations, and the planned change for alternative panel closure locations for Panels 1 and 2 (Knerr 2020).

2.4 Waste Inventory

The LWA establishes a statutory limit on the volume of waste that can be disposed of in the WIPP repository, set at 175,564 m^3 (6,200,000 ft^3). Current assessments indicate that the interim state repository will accommodate less waste than the LWA volume. Ward (2025) provided an assessment of the projected waste storage capacity at 157,837.92 m^3, which includes 156,247.12 m^3 of Contact-Handled (CH) waste and 1,584.80 m^3 of Remote-Handled (RH) waste. Based on

Information Only

information collected up to December 31, 2023, the Interim State Performance Assessment Inventory Report – 2024 (ISPAIR-2024; Van Soest 2025) offers an inventory estimate scaled to the waste volume specified by Ward. Kicker (2025) conducted a screening analysis of the inventory estimates for the ISPAIR-2024 to define the inventory-related input parameters for the PA calculations.

Table 2 compares aspects of the CRA26_IS and RPPCR inventories, normalized by the waste storage volume of each repository (REFCON:VREPOS).

Table 2. Inventory Iron, CPR, and Decay Heat Concentrations

Input	Unit	RPPCR Value	CRA26_IS Value	CRA26_IS to RPPCR Ratio
Iron	kg/m^3	87.51	126.83	1.45
CPR	kg/m^3	25.02	40.48	1.62
Decay Heat	$watt/m^3$	0.22	0.43	1.95

Table 2 from Day and King (2025).

2.5 Baseline Actinide Solubilities

Thermodynamic calculations are used to compute the baseline solubilities for actinides in the +III, +IV, and +V oxidation states in GWB and ERDA-6 brines for five multiples of the minimum brine volume for a DBR event. These baseline solubility calculations account for inventory components and thus are updated to be consistent with inventory estimates. Domski (2025b) reports the baseline solubility values based on the CRA26_IS inventory.

Currently there is no thermodynamic model for WIPP actinides in the +VI oxidation state. The Los Alamos National Laboratory Actinide Chemistry and Repository Science Program (LANL-ACRSP) has performed experimental investigations on U(+VI) solubility under WIPP-relevant conditions. Based on this experimental work, Kaplan et al. (2025) recommends a solubility of 3×10^{-6} M for actinides in the +VI oxidation state in both Salado and Castile brines.

2.6 Solubility Uncertainty Distributions

Actinide solubility uncertainty distributions, which are independent of the repository inventory, are updated for CRA-2026, as documented in Domski (2025a). A literature review was conducted to identify relevant studies published prior to the CRA-2026 cutoff date. Based on this review, the uncertainty distribution for +III actinide solubilities (SOLMOD3:SOLVAR) is updated. No new literature was found for +IV actinide solubilities; therefore, no update to the +IV solubility uncertainty distribution is made.

Information Only

2.7 Colloidal Enhancement Parameters

Based on updates to the thermodynamic model and baseline solubility values, Mariner (2025) reevaluated the proportionality constant for humic colloids. Mariner recommends updated values for radionuclides in the +III oxidation state for both Castile and Salado brines (PHUMOX3:PHUMCIM and PHUMOX3:PHUMSIM). Mariner recommends no change to values for radionuclides in the +IV oxidation state.

In previous WIPP PA calculations, microbial colloid enhancement parameters (PROPMIC and CAPMIC) have been specified for each element (parameter materials AM, NP, PU, TH, and U). For the CRA-2026 PA, the microbial enhancement parameters have been specified for each element-oxidation state (materials AM+3, NP+4, NP+5, PU+3, PU+4, U+4, and U+6), in order to more closely align to the experimental data used to derive the parameter values. Kaplan et al. (2025) recommends the microbial colloid parameter values for the CRA-2026 PA.

2.8 MgO Hydration Parameters

The rate of hydration of MgO to form brucite, $Mg(OH)_2$, in the Salado flow model is specified for humid (WAS_AREA:BRUCITEH), Castile brine inundated (WAS_AREA:BRUCITEC), and Salado brine inundated (WAS_AREA:BRUCITES) conditions. Although changes to the MgO hydration rate parameters were not anticipated in AP-214 (Hansen et al. 2025), Nemer (2025) recommends new parameter distributions for the Castile and Salado brine inundated conditions. King (2025a) redefines the recommended distributions to be compatible with the WIPP PA code LHS.

2.9 Lower Bound on Capillary Pressure in the Anhydrite Marker Beds

To improve numerical stability of the Salado flow model when using the modified van Genuchten-Parker capillary pressure function in the anhydrite marker beds, the PA code BRAGFLO was updated to Version 8.00 (WIPP PA 2025) to implement a new capillary pressure model which incorporates a lower bound on the capillary pressure. This lower bound is applied when brine saturations exceed one minus the residual gas saturation. Day (2025b) sets the lower bound on capillary pressure to 1 atm (101325 Pa), with the PO_MIN property of the S_MB139, S_ANH_AB, and S_MB138 materials, and applied the new capillary pressure model by setting the CAP_MOD property to 6 for the same materials.

2.10 Porosity-Permeability Parameter Distribution

King (2025a) redefines the distribution for the parameter representing the relationship between porosity and permeability in a run-of-mine salt panel closure system during the secondary time duration (PCS_T2:POR2PERM). Initially defined as a truncated normal distribution, this parameter is revised, along with the MgO hydration parameters (Section 2.8), to a cumulative distribution characterized by discrete data points. This change constitutes a deviation from AP-214 (Hansen et al. 2025).

Information Only

2.11 Minimum Brine Volume Needed for a DBR

The parameter representing minimum brine volume required for a direct brine release (DBR), GLOBAL:DBRMINBV, is revised by Brunell (2025) to be consistent with geomechanical modeling that predicts repository porosity and with the repository geometry described in Section 2.1. The value used in the CRA-2026 IS PA is presented in Table 3.

Table 3. Updated Minimum Brine Volume Parameter

Material	Property	RPPCR Value	CRA-2026 IS Value	Units
GLOBAL	DBRMINBV	33,804	6,314	m^3

2.12 Culebra Release Point Location

For the RPPCR, the Culebra release point CRP 2 was located at the centroid of Panels 11, 12, and 13 in a 19-panel representation of the WIPP repository. For the interim state repository with only replacement Panels 11 and 12 beyond the original 10, CRP 2 is relocated to the centroid of Panels 11 and 12 (Wilgus and Brunell 2025). The updated coordinates are shown in Table 4. The location of CRP 1 remains unchanged. CRP 3 and CRP 4 are outside the 12-Panel repository footprint, and are not evaluated for CRA26_IS (Wilgus and Bethune 2025)

Table 4. Location of Culebra Release Point 2

Analysis	UTM (x)	UTM (y)	SECO (i)	SECO (j)
RPPCR	612828.31	3581621.38	52	81
CRA-2026	612929.61	3581621.38	54	81

Table 1 from Wilgus and Brunell (2025).

2.13 Drilling Rate and Borehole Plugging Pattern Probabilities

The DOE surveys drilling activity in the Delaware Basin to meet the requirements established in 40 CFR Part 194.33. Local well operators are surveyed annually to provide the WIPP project with information on drilling practices, encounters with Castile brine, and related data. Survey results through August 2024 are documented in the 2024 *Waste Isolation Pilot Plant Delaware Basin Monitoring Annual Report* (DBMAR) (U.S. DOE 2025).

Information Only

Survey results are used in WIPP PA to define the frequency of hypothetical drilling intrusions into the WIPP repository (parameter GLOBAL:LAMBDAD) and to determine the probabilities associated with different plugging configurations used to seal the wellbore. The possible configurations are grouped into three plugging patterns for PA purposes; probabilities associated with each pattern are represented by the parameters GLOBAL:ONEPLG, GLOBAL:TWOPLG, and GLOBAL:THREEPLG. The methodology for updating these parameter values is provided in King (2025b). A summary of the updated drilling rate and plugging pattern probabilities is presented in Table 5.

Table 5. Drilling Rate and Plugging Pattern Probabilities

Material	Property	RPPCR Value	CRA-2026 Value	Units
GLOBAL	LAMBDAD	0.01389	0.01534	$km^{-2}\ yr^{-1}$
GLOBAL	ONEPLG	0.366	0.359	-
GLOBAL	TWOPLG	0.430	0.464	-
GLOBAL	THREEPLG	0.204	0.177	-

Table 1 from King (2025b).

2.14 Parameters Not Updated as Anticipated in Analysis Plan AP-214

AP-214 (Hansen et al. 2025) indicates that several parameters were expected to be updated for CRA-2026. Specifically, the parameter specifying the likelihood of low or high oxidation state for an actinide (property OXCUTOFF for materials NP, PU, and U) and the parameters related to mineral and intrinsic colloids (properties CONCMIN and CONCINT for materials AM, NP, PU, TH, and U) were anticipated to undergo revisions. Kaplan et al. (2025) re-examines the basis for these parameter values and recommends the continued use of the RPPCR values. As a result, no changes were made to these parameters for CRA-2026.

Information Only

3.0 METHODOLOGY FOR THE CRA26_IS

The WIPP PA calculations estimate the probability and consequence of potential radionuclide releases from the repository to the accessible environment for a regulatory period of 10,000 years after facility closure. It is conceivable that the WIPP repository might be disturbed by exploratory drilling for natural resources during the 10,000-year regulatory period. Drilling could create additional pathways for radionuclide transport, especially in the Culebra, and could potentially release material directly to the surface. In addition, hypothetical mining for potash within the Land Withdrawal Boundary (LWB) might alter flow in the overlying geologic units and may locally accelerate transport through the Culebra. The disturbed scenarios used in PA modeling are designed to capture the range of possible releases that could result from these hypothetical drilling and mining activities.

The PA accommodates both aleatory (i.e., stochastic) and epistemic (i.e., subjective) uncertainty in its constituent models. Aleatory uncertainty pertains to unknowable future events such as intrusion times and locations that may affect repository performance. It is accounted for by the generation of random sequences of future events. Epistemic uncertainty concerns parameter values that are assumed to be constants; the constants' true values are uncertain due to a lack of knowledge about the system. An example of a parameter with epistemic uncertainty is the permeability of a material. Epistemic uncertainty is accounted for by sampling parameter values from assigned distributions using Latin Hypercube Sampling, discussed in King and Zeitler (2025e). One set of all sampled values required to run a WIPP PA calculation is termed a vector. Each set of 100 vectors is termed a replicate, and three sets of 100 vectors (e.g., three replicates) are used in a full WIPP PA analysis. For each vector, 10,000 possible sequences of future events (e.g., futures) are simulated to address aleatory uncertainty. The releases for each of the 10,000 simulated futures are tabulated for each of the 100 vectors in each of the 3 replicates.

For a random variable, the complementary cumulative distribution function (CCDF) provides the probability of the variable being greater than a particular value. By regulation, PA results are presented as a distribution of CCDFs of releases (U.S. EPA 1996). Each individual CCDF summarizes the likelihood of releases across the 10,000 futures simulated for one vector of parameter values. The uncertainty in parameter values results in a distribution of CCDFs.

3.1 Review of FEPs and Conceptual Models

A FEPs assessment was performed for the CRA-2026 analysis according to SP 9-4 to determine if any of the changes implemented in this analysis affect current baseline FEP screening arguments or decisions. The FEPs assessment found that no changes to the FEP baseline were warranted (Kirkes and McCormick 2025).

The CRA-2026 conceptual models are unchanged from those of the RPPCR. The differences between the CRA-2026 and the RPPCR described in Section 2.0 do not reflect changes to the conceptual models on which the CRA-2026 and RPPCR are based. The 12-panel interim state repository in the CRA-2026 PA comprises a subset of the 19 waste panels in the final state repository. Features and processes that influence flow and transport are the same in both the interim and final state repositories.

Information Only

3.2 Salado Flow

The BRAGFLO code calculates the flow of brine and gas in the vicinity of the WIPP repository over a 10,000-year regulatory compliance period. The results of these calculations are used by other WIPP PA codes to calculate potential radionuclide releases to the accessible environment.

The following subsections summarize the approach and methodology for Salado flow modeling as described by Day and King (2025).

3.2.1 Repository Representation in BRAGFLO

The computational grid and associated material map used by BRAGFLO for CRA26_IS includes changes from the RPPCR BRAGFLO grid to accommodate as-built excavation footprint dimensions within the existing repository, plans for future excavations, and the planned change for alternative panel closure locations for Panels 1 and 2. The flaring of the far-field Salado was re-calculated based on the altered dimensions of the WIPP repository. The distance to the North LWB was calculated as the minimum distance from the westernmost edge of the excavated repository to the nearest land withdrawal boundary (to the west) and the distance to the South LWB was calculated as the minimum distance from the southernmost edge of the excavated repository to the nearest land withdrawal boundary (to the south) (Day 2025a). The generic BRAGFLO computational grid with modeled area descriptions and cell dimensions for the CRA26_IS is shown in Figure 2. Detailed material maps associated with the six modeling scenarios are further defined in Section 4.2 of Day and King (2025).

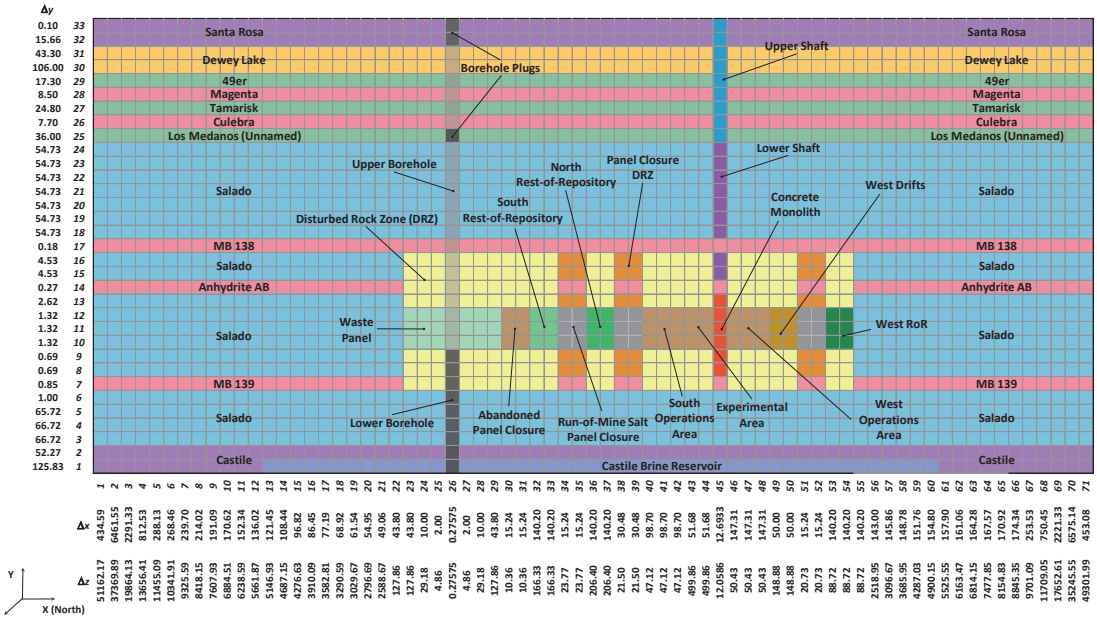


Figure 4 from Day and King (2025). Δx, Δy, and Δz dimensions in meters.

Figure 2. BRAGFLO Grid for the CRA26_IS with Modeled Area Descriptions

Information Only

3.2.2 Salado Flow Modeling Scenarios

The six BRAGFLO modeling scenarios used in the CRA-2026 PA are unchanged from those used for the RPPCR PA. A single representative borehole intrusion can be used in the South repository for both South and West repository intrusions (King 2021). Results obtained in the six scenarios are used to initialize flow and material properties in subsequent codes in the PA computational suite (e.g., in the calculation of direct brine release volumes). The scenarios include one undisturbed scenario (S1-BF), four scenarios that include a single inadvertent drilling intrusion into the repository (S2-BF to S5-BF), and one scenario investigating the effect of two intrusions into a single waste panel (S6-BF). Two types of intrusions, denoted as E1 and E2, are considered. An E1 intrusion assumes the borehole passes through a waste-filled panel and into a region of pressurized brine that may exist under the repository in the Castile formation, while an E2 intrusion assumes that the borehole passes through the repository but does not encounter pressurized brine. BRAGFLO results obtained in Scenario S6-BF are only used to calculate radionuclide transport to the Culebra (Section 3.8). Table 6 summarizes the six scenarios used in the Salado flow calculation. A total of 1,800 separate Salado flow simulations are run (3 replicates × 6 scenarios × 100 vectors). Day and King (2025) describe results from scenarios S1-BF, S2-BF, S4-BF, and S6-BF. Results from scenarios S2-BF and S3-BF are generally similar to each other, as are results from S4-BF and S5-BF.

Table 6. BRAGFLO Modeling Scenarios for the CRA26_IS

Scenario	Description
S1-BF	Undisturbed Repository
S2-BF	E1 intrusion at 350 years
S3-BF	E1 intrusion at 1,000 years
S4-BF	E2 intrusion at 350 years
S5-BF	E2 intrusion at 1,000 years
S6-BF	E2 intrusion at 1,000 years; E1 intrusion at 2,000 years.

Table 3 from Day and King (2025).

3.3 Radionuclide Activities for Solid Releases

Activity in waste encountered during a hypothetical drilling event is quantified using the metric of EPA units. The activity in EPA units for a radionuclide is the initial source term activity (in Ci) of that radionuclide divided by the product of the waste unit factor (WUF) and the release limit (in Ci/unit of waste) for the same radionuclide (Sanchez et al. 1997). Release limits and the number of Ci in an EPA unit vary by radionuclide.

The activity in EPA units at each time interval of interest for each of the major radionuclides in each waste stream is calculated by the WIPP PA code EPAUNI. EPAUNI also calculates the activity of the entire waste stream in EPA units (at each of the specified time intervals) and the probability of encountering each waste stream during a drilling intrusion.

Information Only

EPAUNI models ten radionuclides (^{241}Am, ^{244}Cm, ^{137}Cs, ^{238}Pu, ^{239}Pu, ^{240}Pu, ^{241}Pu, ^{90}Sr, ^{233}U, and ^{234}U), which account for 99.85% of the EPA units at the time of repository closure in the CRA26_IS (Kicker 2025, Table 10).

3.4 Cuttings, Cavings, and Spallings

The volume of solid material (in m^3) brought to the surface due to inadvertent human intrusion through drilling is assessed using the WIPP PA code CUTTINGS_S. This code calculates the volume of material removed through three distinct release mechanisms: cuttings, cavings, and spallings.

Cuttings refer to the repository waste that is directly impacted by the drill bit. These materials are immediately transported to the surface via the cooling fluid circulated through the borehole during drilling. The volume of cuttings corresponds to the repository material intersected by the borehole.

Cavings occur when waste materials that originally bordered the borehole on its exterior erode into the cooling fluid due to frictional effects. If the shear stresses exerted by the cooling fluid at the borehole wall exceed the shear strength of the surrounding matrix materials, erosion will take place, resulting in the removal of wall material. This process can lead to a local increase in the borehole diameter, which may cause the volume of waste removed to exceed the volume of the borehole initially cut through the waste. As the borehole diameter increases, the fluid shear stresses at the outer boundary decrease. If these stresses diminish to a point where the failure stress of the wall material equals or exceeds the fluid shear stress, the caving process will cease.

Spallings occur when the repository is pressurized at the time of intrusion. If the internal pressure within the repository exceeds the hydrostatic pressure of the cooling fluid column, materials originally surrounding the borehole but located interior to the repository-fluid interface may deform inward to replace the materials removed by the cutting bit and erosive brine. The solid fraction of these materials is referred to as spallings. In cases where repository materials are more permeable, pressurized gas may seep through the matrix, carrying loose particles with it. Conversely, if the repository pressures are too low, spalling events will not occur.

Additionally, the CUTTINGS_S code calculates information about the pressure, saturation, porosity, and crushed panel height, which is used as initial conditions for direct brine release calculations.

3.5 Direct Brine Release Volumes

If the WIPP repository were to be penetrated by a borehole while under conditions of sufficient repository brine pressure and saturation, brine could migrate up through the intruding borehole to reach the land surface. Such an event is defined as a direct brine release (DBR). As with previous WIPP PAs, the BRAGFLO DBR analysis uses the BRAGFLO code to numerically evaluate the volumetric flux of brine that enters the borehole over the duration of the release. The following subsections summarize the approach and methodology for DBR volume modeling as described by Zeitler (2025).

Information Only

The BRAGFLO_DBR model explicitly represents the vicinity of the waste panels, including specific repository features like individual panels and panel closures, in a 2-dimensional rectilinear grid. Like the BRAGFLO Salado Model (Section 3.2.1), the grid dips 1° to the south.

The DBR numerical grid and material map used in the CRA26_IS PA is the same as that used in the RPPCR calculations and is shown in Figure 3. The reduced repository area included in the CRA26_IS representation of the WIPP in Salado flow calculations did not result in a change to the DBR grid representation, as it already adequately considers the connections between the Salado flow results and DBR initial conditions for each of the waste regions. With the short duration of DBR simulations, there is very little communication across panel closures; therefore, there is not a need to have an explicit representation of repository volume outside of the panel closures containing the intrusion locations. Four drilling locations are considered in the CRA26_IS PA: "U" (for upper, since it is up-dip), "M" (for middle), and "L" (for lower, since it is down-dip), and "O" (for other). These intrusion locations are shown in Figure 3. Additional details on the DBR model are described in Zeitler (2025).

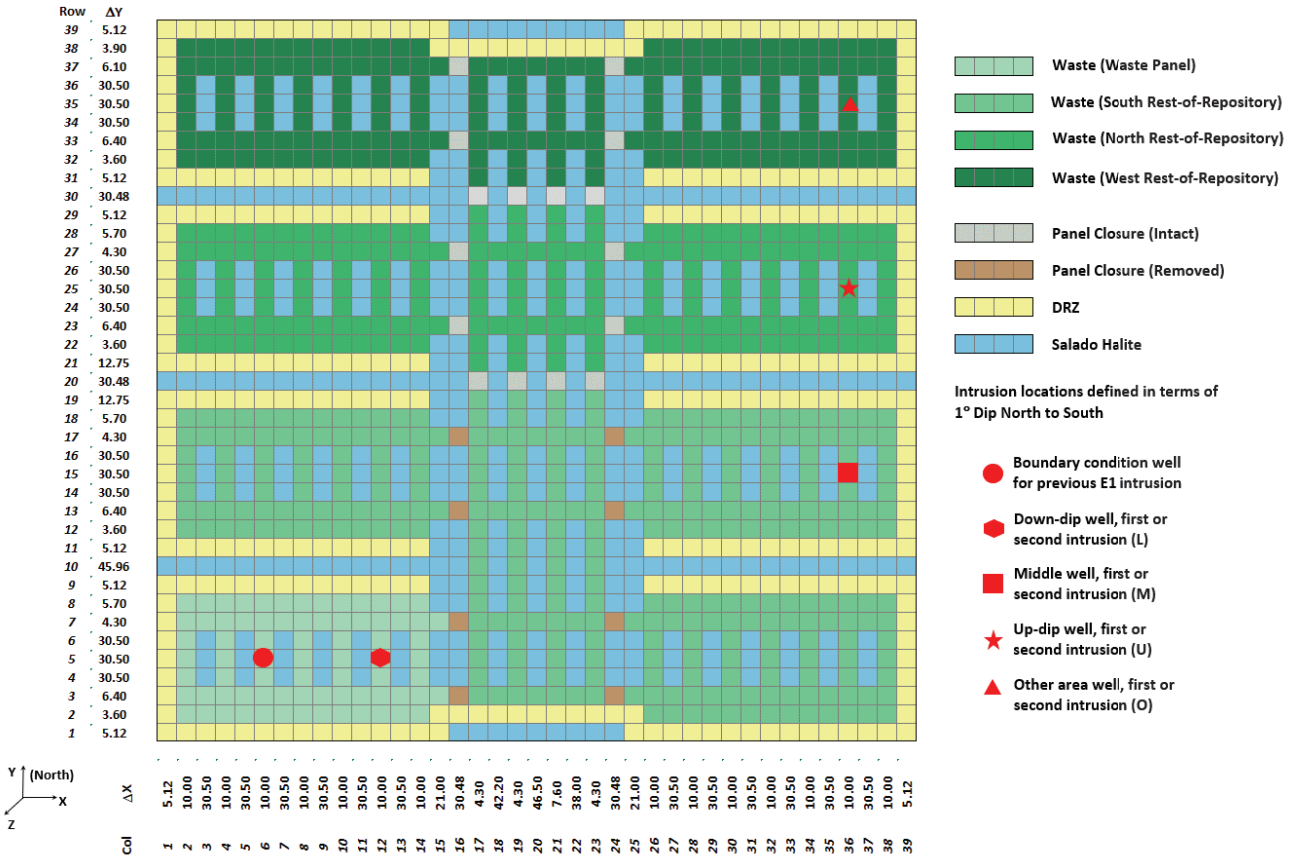


Figure 3. CRA26_IS and RPPCR DBR Grid with Simulated Intrusion Locations

Information Only

3.5.1 Initial Conditions

Brine pressures and brine saturations calculated during the BRAGFLO Salado flow simulations (Section 4.2) are volume-averaged and used as initial conditions in the DBR simulations. Figure 4 illustrates the method used to transfer initial conditions in the waste for the CRA26_IS. The BRAGFLO grid aggregates waste panels into four waste-bearing regions: Waste Panel, South Rest-of-Repository, North Rest-of-Repository, and West Rest-of-Repository (Day and King 2025). In Figure 4, these regions are denoted Waste Panel, SRoR, NRoR and WRoR, respectively. At the time of the intrusion, the volume-averaged pressure and saturation from the four waste-filled regions in the BRAGFLO grid are used as the initial pressure and saturation for corresponding waste regions in the DBR grid. Consistent with the designations L, M, U and O for the intrusion locations, the DBR grid waste regions will be referred to as Lower, Middle, Upper, and Other. As indicated in Figure 4, conditions in the BRAGFLO Waste Panel map to the Lower waste region in the DBR grid; likewise, BRAGFLO SRoR conditions map to the Middle DBR region, NRoR to the Upper DBR region, and WRoR to the Other DBR region. Note that pressure and saturation are allowed to change during the DBR volume calculations.

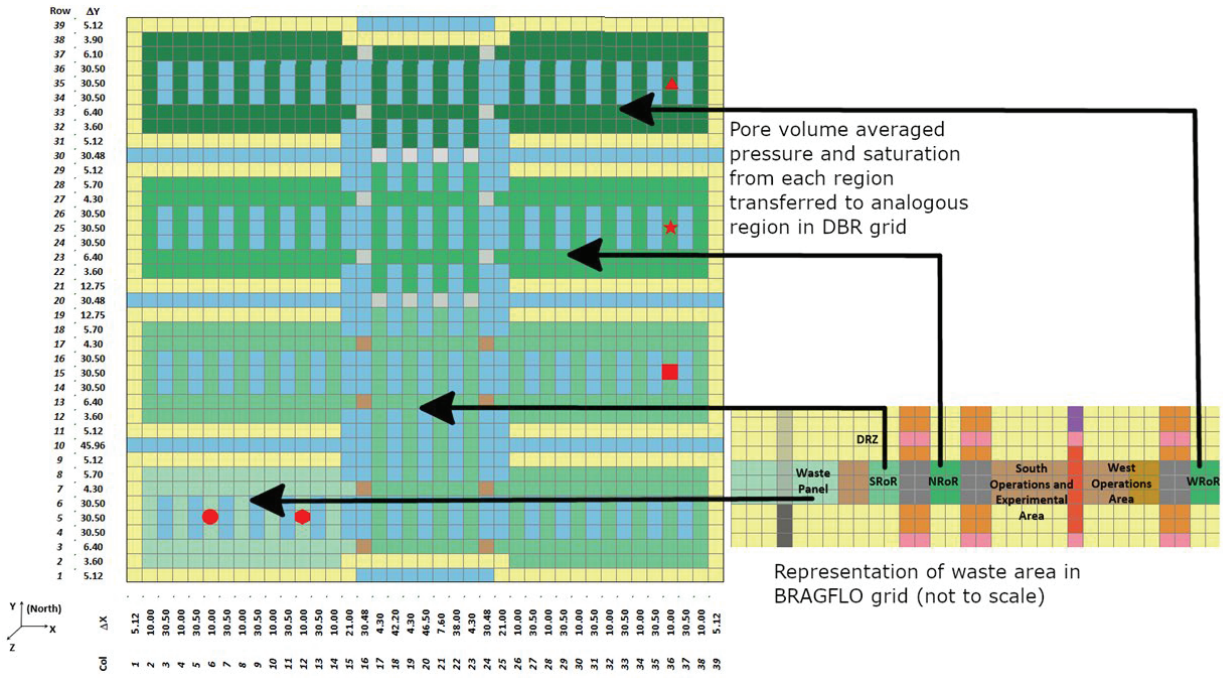


Figure 4. Regions Used to Transfer Initial Pressure and Saturation from the BRAGFLO Salado Grid to the DBR Grid

Information Only

3.5.2 Modeling Scenarios

In performing DBR volume calculations, five of the BRAGFLO Salado flow model scenarios, S1-BF to S5-BF, are used to set the initial conditions for the DBR volume calculations at the time of intrusion. The five BRAGFLO Salado flow scenarios (Section 3.2.2) capture the long-term behavior of the repository under three different conditions: undisturbed (E0); intersected by a borehole that continues down to a hypothetical pressurized brine reservoir below the repository (E1); and intersected by a borehole that does not intersect pressurized regions below the repository (E2). DBR volume calculations map the resulting BRAGFLO pressure and saturation conditions at a suite of intrusion times onto the DBR model grid and simulate flow to the intrusion. The scenarios and intrusion times used for the CRA26_IS, presented in Table 7, are the same as those used for the RPPCR. There are a total of 104 combinations, or DBR simulations, for each parameter vector.

Table 7. DBR Scenarios

Scenario	Description
S1-DBR	Initially undisturbed repository (E0 conditions). Intrusion at the L, M, U, or O location at 100; 350; 1,000; 3,000; 5,000; or 10,000 years: 24 combinations.
S2-DBR	Initial E1 intrusion at 350 years followed by a second intrusion at the L, M, U, or O location at 550; 750; 2,000; 4,000; or 10,000 years: 20 combinations.
S3-DBR	Initial E1 intrusion at 1,000 years followed by a second intrusion at the L, M, U, or O location at 1,200; 1,400; 3,000; 5,000; or 10,000 years: 20 combinations.
S4-DBR	Initial E2 intrusion at 350 years followed by a second intrusion at the L, M, U, or O location at 550; 750; 2,000; 4,000; or 10,000 years: 20 combinations.
S5-DBR	Initial E2 intrusion at 1,000 years followed by a second intrusion at the L, M, U, or O location at 1,200; 1,400; 3,000; 5,000; or 10,000 years: 20 combinations.

3.6 Mobilized Radionuclide Concentrations

The code PANEL simulates radionuclide decay and mobilization in brine in the repository throughout the 10,000-year regulatory period. PANEL performs three essential functions in PA. First, it determines radionuclide concentrations in brine as a function of time. Second, it calculates radionuclide transport releases to the Culebra for the E2E1 scenario, which involves a borehole intrusion into the repository followed by a borehole intrusion into a hypothetical pressurized brine reservoir beneath the repository. Third, PANEL determines the mobile concentration limits of five "lumped" radionuclides. The lumped radionuclides, namely, AM241L, PU238L, PU239L, U234L, and TH230L are described by Leigh and Trone (2005).

Kicker (2025) reports a total of 168 radionuclides in the repository for the CRA-2026_IS. PANEL models decay and ingrowth for 30 of the radionuclides; and, for 26 of the 30, PANEL determines both concentrations and E2E1 transport releases. Kim et al. (2024) estimate, for the RPPCR, that

Information Only

the radionuclides included in PA account for more than 99% of the DBRs and more than 90% of the transport releases predicted to occur using the total inventory of the repository.

PANEL reports the sum of radionuclide concentrations for use by the code CCDFGF in calculating DBRs. PANEL combines E2E1 releases determined for individual radionuclides to form releases for the five lumped radionuclides. Lumped E2E1 releases are PANEL's contribution to *to Culebra* releases. Lumped radionuclide mobile concentration limits determined by PANEL are used by code NUTS.

3.7 Salado Transport

Code NUTS simulates transport in the Salado formation for BRAGFLO intrusion scenarios S1-BF through S5-BF, while transport for scenario S6-BF is handled by PANEL. The NUTS transport model accounts for contaminant advection in the aqueous phase, dissolution and precipitation, and radioactive decay (Shinta 1997). The transport equations are solved on the same two-dimensional computational grid used by BRAGFLO. Additionally, NUTS relies on BRAGFLO for values of brine flow rate, brine saturation, and porosity, all of which are functions of space and time. PANEL's simpler transport model treats the waste area as a whole and accounts only for radionuclide decay, radionuclide ingrowth, and brine flow out of the repository up through an intruding borehole.

NUTS considers three pathways for potentially significant transport releases: (i) along anhydrite marker beds to the LWB; (ii) up the repository shaft to the Culebra; and (iii) up through an intruding borehole to the Culebra. Releases through the marker beds and shaft are effectively zero, as discussed in Section 4.8.1. Releases up the borehole to the Culebra are the NUTS contribution to *to Culebra* releases.

For efficiency, NUTS works with the lumped radionuclides. In addition, NUTS uses screening simulations to identify vectors likely to contribute appreciably to transport releases. Only screened-in vectors take part in full transport simulations. PANEL's transport calculations are carried out for all vectors. The NUTS and PANEL *to Culebra* releases are used by CCDFGF to calculate *from Culebra* releases at the LWB.

3.8 Culebra Flow and Transport

The Culebra Dolomite Member (Culebra) of the Rustler Formation is the most likely subsurface release pathway of radionuclides to the LWB (Beauheim and Holt 1990; Holt 1997). It is hypothesized that subsidence of the Culebra due to potash mining leads to fracturing, resulting in higher Culebra transmissivities and altered groundwater flow patterns (Wallace 1996). WIPP PA accounts for these potential changes in transmissivity by simulating flow and transport within the Culebra under full and partial mining conditions.

Conceptual handling of Culebra flow and transport is unchanged since 2008 (Hart et al. 2008; Burgess et al. 2008). The model domain and discretization are the same for CRA26_IS as in the RPPCR calculations (Kuhlman 2010; Bethune 2023; Figure 5). Groundwater flow in the Culebra is calculated with MODFLOW6 simulating steady state flow using mining modified transmissivity fields at two resolutions:

Information Only

1) A 100-m grid used in the T-field calibrations (Bowman et al. 2023) and particle tracking simulations.
2) A 50-m grid used in the mass transport simulations.

Other key model domain features shown in Figure 5 include no flow (inactive cells) and constant head boundaries, recharge cells (Kuhlman 2010), and the extent of mineable potash (Cranston 2009).

Radionuclide transport is simulated by placing a 1 kg source term (^{241}Am, ^{239}Pu, ^{230}Th, and ^{234}U) into the Culebra at discrete release points above the waste panels then tabulating the cumulative fraction of mass that crosses the LWB at 50-year intervals. Transport of the ^{230}Th daughter product of ^{234}U decay is calculated and tracked as a separate species. In the results section (see Section 4.7), ^{230}Th refers to the ^{234}U daughter product and ^{23A}Th refers to the ^{230}Th released at the release point.

The 19-panel repository representation modeled in the RPPCR implemented four Culebra release points spanning the repository footprint. Mass transport of radionuclides in the 12-panel interim state repository is represented only with CRP 1 and CRP 2 (Figure 5). For the CRA26_IS, CRP 2 was relocated to the centroid of Panels 11 and 12 (Wilgus and Brunell 2025; see Section 2.12).

Flow field patterns from each CRP are characterized by tracking a single, non-sorbing particle through the modified flow fields to the LWB for each combination of release point, transmissivity field, parameter vector, and mining scenario with code DTRKMF. Radionuclide transport is simulated with code SECOTP2D and accounts for physical processes not modeled in particle track simulations.

There are five steps in estimating radionuclide transport through the Culebra, including:

Step 1. Construction of 1,000 base geostatistical realizations of Culebra hydraulic transmissivity (T), anisotropy, storativity, and recharge fields (collectively referred to as "T-fields").

Step 2. Calibration of the T-fields to observed head and pumping drawdowns including selection of a final set of the 100 best fit realizations.

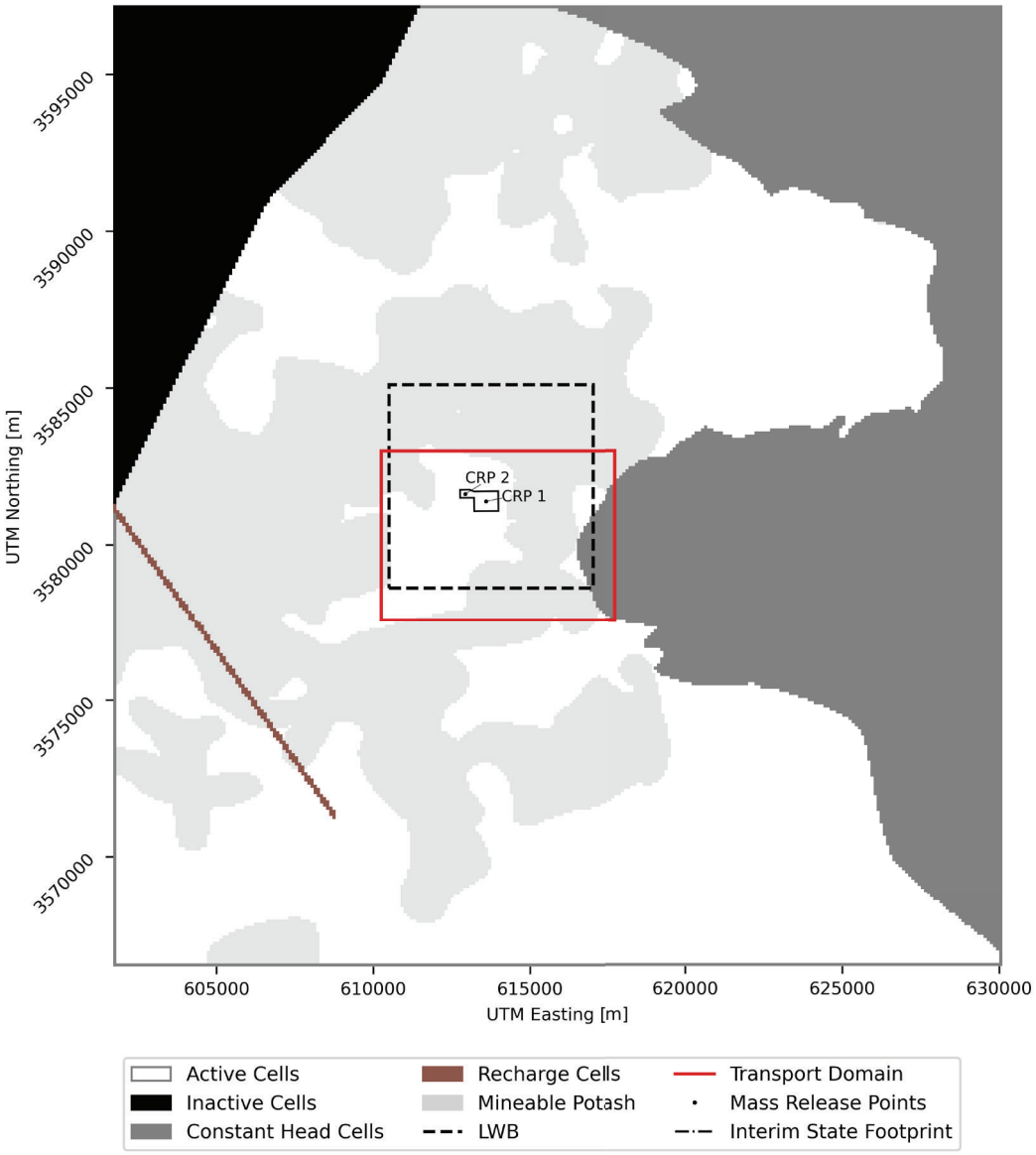
Step 3. Modification of the T-fields to account for potential subsidence due to potash mining beneath the Culebra.

Step 4. Calculation of steady-state groundwater flow-fields for each mining-modified T-field using MODFLOW6.

Step 5. Calculation of radionuclide transport through the Culebra to the LWB for each simulated flow-field and release location using SECOTP2D.

Steps 1 and 2 produce 100 equally likely T-fields that provide input to Step 3. The work presented in this summary report is limited to Step 3 through Step 5. The output of Step 5 is used by the WIPP PA code CCDFGF to calculate potential radionuclide releases through the Culebra to the accessible environment (King et al. 2025d; see Section 4.8.5.2). A more complete overview of methodology is described in Wilgus and Bethune (2025).

Information Only



Derived from Wilgus and Bethune (2025).

Figure 5. Culebra Modeling Domain

3.9 Release Construction Methodology

The conceptual structure of the CCDFGF calculation in the CRA26_IS remains consistent with the methodology used in the RPPCR. For each member of a sample of uncertain parameters, many 10,000-year futures are randomly generated. Each future comprises a sequence of simulated drilling intrusions and mining events. Drilling location, whether a brine pocket is penetrated, and the type of plugging pattern are randomly determined. The simulation of many possible realizations, or futures, characterizes the aleatory uncertainty of the results.

Information Only

For each drilling intrusion, direct releases are tabulated using output from the other models described in Section 3.0. Over the course of the entire future, releases through the Salado and Culebra to the LWB are recorded using output from the Salado and Culebra transport models. The switch from partial mining to full mining conditions occurs randomly with a probability of 1% per 100 years. The total of these various releases at the end of the 10,000-year period yields a datum for total releases. The collection of total release data points, over all futures, comprises one complementary cumulative distribution function (CCDF) of releases. The code CCDFGF generates the random futures and constructs the CCDFs. A more complete description of the CCDF calculation methodology can be found in King et al. (2025d).

Based on the number of panel closures separating the waste panels the RPPCR classified each pair of waste panels into one of four groups: same, connected, adjacent, and non-adjacent. For the CRA26_IS, the panel neighbor assignments follow the same methodology as the RPPCR but are adjusted to reflect the smaller repository footprint, which includes only 12 panels in the interim state analysis compared to 19 panels in the RPPCR (Hansen et al. 2023). For CRA26_IS, panel intrusion probabilities were updated using area ratios from Day (2025a).

3.10 Sensitivity Analysis

Stepwise linear multiple rank regression analyses were performed to determine the relative importance of the sampled parameters in the uncertainty in releases using the code STEPWISE. Sensitivity analysis results for the CRA26_IS analysis are compared to the results of the RPPCR analysis. The sensitivity analysis identifies parameters which contribute most to the uncertainty in a model result (King et al. 2025d).

3.11 Run Control

A full description of the run control for CRA26_IS, including names and locations of input and output files, can be found in Long (2025). The WIPP PA Parameter Database (PAPDB), ParamDB, is used as the source for parameter values. Parameter specifications and sampled values can be found in Feng and Kicker (2025).

Information Only

4.0 RESULTS

This section summarizes the CRA26_IS process model results and release calculations detailed in each of the analysis reports (Brunell and Kicker 2025; Day and King 2025; Docherty and Kim 2025, Kim and Kicker 2025; King et al. 2025d; Wilgus and Bethune 2025; Zeitler 2025). PA process model results are shown for the inventory, repository conditions, direct release mechanisms, and subsurface transport mechanisms. Results of PA process models are compared to the RPPCR, and are shown for Replicate 1 only, unless otherwise stated; results of Replicates 2 and 3 are generally similar to those from Replicate 1. Finally, CCDFs of cumulative releases for each release mechanism, total releases, and the sensitivity analysis for total releases are discussed. Some results in this report are presented as box and whisker plots. The box bottom and top edges indicate the 25th and 75th percentiles, the box interior line indicates the 50th percentile (median), and the open square indicates the mean. The extended vertical lines with horizontal bars (the whiskers) indicate the 2nd and 98th percentiles, while the diamond markers exterior to the bars are discrete outliers.

4.1 Inventory

Inventory analysis results for the CRA26_IS analysis (based on CRA26_IS inventory data from Van Soest, 2025a) are presented in this section and compared to inventory analysis results for the RPPCR (Kicker 2023).

4.1.1 Total Waste Volume

Table 8 presents the ten predominant waste streams by volume in the RPPCR (out of a total of 591 waste streams) and CRA26_IS (out of a total of 590 waste streams) inventories. These ten waste streams account for approximately 51.71% of the total waste volume in the CRA26_IS and 53.90% in the RPPCR. In both inventories, SR-CH-PP is the waste stream with the largest volume, contributing 16.15% of the total volume in the CRA26_IS and 20.33% in the RPPCR.

In the PAIR-2022 report (Van Soest 2022), the waste inventory was scaled up to 175,564 m^3, which is the statutory capacity for WIPP as set by the WIPP Land Withdrawal Act. However, in the ISPAIR-2024 report (Van Soest, 2025a), the waste inventory was scaled to 157,832 m^3, reflecting the waste capacity of a 12-panel repository (Ward, 2025). The discrepancies between the WIPP waste capacity and the total volume in Table 8 are 41 m^3 in the CRA26_IS (from 157,832 m^3 to 157,873 m^3) and 10 m^3 in the RPPCR (from 175,564 m^3 to 175,574 m^3). These discrepancies are attributed to the scale factors, which were rounded to three significant figures.

Information Only

Table 8. WIPP CH- and RH-TRU Waste Streams by Total Scaled Volume from the RPPCR and CRA26_IS Inventories

Rank Order	RPPCR Waste Stream ID	RPPCR Stream Type	RPPCR Volume (m^3)	CRA26_IS Waste Stream ID	CRA26_IS Stream Type	CRA26_IS Volume (m^3)
1	SR-CH-PP	CH	3.57×10^4	SR-CH-PP	CH	2.55×10^4
2	RL200-02	CH	1.19×10^4	LA-MHD01.001	CH	9.75×10^3
3	WP-BN510	CH	9.63×10^3	WP-BN510	CH	9.63×10^3
4	LA-MHD01-Pits	CH	7.74×10^3	RL200-02	CH	8.48×10^3
5	LA-MHD01.001	CH	6.94×10^3	RLPFP-01	CH	6.16×10^3
6	RLPFP-01	CH	6.34×10^3	LA-MHD01-Pits	CH	5.46×10^3
7	WP-ID-SDA-SLUD	CH	5.19×10^3	WP-ID-SDA-SLUDGE	CH	5.20×10^3
8	WP-RF029.01	CH	4.31×10^3	WP-RF029.01	CH	4.31×10^3
9	WP-BNINW216	CH	3.47×10^3	WP-LA-MHD01.001	CH	3.65×10^3
10	WP-BN510.1	CH	3.42×10^3	WP-BNINW216	CH	3.50×10^3
•	•	•	•	•		•
•	•	•	•	•		•
•	•	•	•	•		•
Last	WP-LA-OS-00-04	CH	2.69×10^{-3}	WP-LA-OS-00-04	CH	2.69×10^{-3}
Total			**175,574**	**Total**		**157,873**

4.1.2 Inventory by EPA Units

Table 9 presents the ten waste streams that predominantly contribute to the total EPA units in the CRA26_IS, accounting for approximately 86.59% of the total inventory at closure and 91.93% at 10,000 years post-closure. In the CRA26_IS inventory, the top two waste streams are SR-KAC-PuOx-2 and SR-KAC-PuOx. These waste streams contribute 34.91% and 21.87%, respectively, of the total EPA units at closure, while they account for 48.68% and 23.51% at 10,000 years post-closure. At the closure year of 2083, the RPPCR inventory contains 10,025 EPA units (Kicker 2023) and the CRA26_IS waste inventory contains 10,000 EPA units (Table 9).

Information Only

For the SR-KAC-PuOx-2 waste stream, which has the highest activity, the CRA26_IS reports a total of 2.72×10^6 Ci at closure: 1.74×10^6 Ci of ^{239}Pu, 4.01×10^5 Ci of ^{241}Am, 3.82×10^5 Ci of ^{240}Pu, 1.41×10^5 Ci of ^{241}Pu, and 4.98×10^4 Ci of ^{238}Pu (Van Soest 2025b, Table 5-1). This waste stream was not included in the RPPCR inventory. The waste stream with the highest activity at closure in the RPPCR is SR-KAC-PuOx, which has a total of 2.48×10^6 Ci: 1.15×10^6 Ci of ^{239}Pu, 6.84×10^5 Ci of ^{241}Am, 3.87×10^5 Ci of ^{240}Pu, 1.59×10^5 Ci of ^{241}Pu, and 9.67×10^4 Ci of ^{238}Pu (Van Soest 2022, Table 5-1).

By 10,000 years post-closure, the total number of EPA units decreases to 3,344 in the RPPCR (Kicker 2023, Table 3) and 4,005 in the CRA26_IS (Table 9). The top two waste streams at this time in the CRA26_IS remain SR-KAC-PuOx-2 and SR-KAC-PuOx, which together contain 72.19% of the total EPA units. Overall, ten waste streams account for approximately 91.93% of the repository activity at the end of the regulatory period.

Information Only

Table 9. WIPP CH- and RH-TRU Waste Streams by Total EPA Units; Time 0 (Calendar Year 2083) and 10,000 Years (Calendar Year 12,083) From the CRA26_IS Inventory

Rank Order	Waste Stream ID at closure	Stream Type at closure	EPA Units at closure	Waste Stream ID after 10,000 years	Stream Type after 10,000 years	EPA Units after 10,000 years
1	SR-KAC-PuOx-2	CH	3.49×10^{3}	SR-KAC-PuOx-2	CH	1.95×10^{3}
2	SR-KAC-PuOx	CH	2.19×10^{3}	SR-KAC-PuOx	CH	9.41×10^{2}
3	SR-CH-PP	CH	1.17×10^{3}	SR-CH-PP	CH	3.59×10^{2}
4	L-MHD01.001	CH	6.66×10^{2}	LA-MHD01-Pits	CH	9.96×10^{1}
5	LA-MHD01-Pits	CH	3.63×10^{2}	LA-MHD01.001	CH	9.67×10^{1}
6	WP-LA-MHD01.001	CH	2.40×10^{2}	WP-RF118.01	CH	7.60×10^{1}
7	WP-RF009.01	CH	1.79×10^{2}	WP-LA-MHD01.001	CH	6.71×10^{1}
8	WP-RF118.01	CH	1.41×10^{2}	WP-RF009.01	CH	6.22×10^{1}
9	WP-SR-W027-221H-HET	CH	1.32×10^{2}	WP-BN510	CH	1.52×10^{1}
10	WP-SR-MD-PAD1	CH	9.21×10^{1}	WP-RF003.01	CH	1.43×10^{1}
• • •	• • •	• • •	• • •	• • •		• • •
590	LB-T002	CH	1.83×10^{-7}	WP-OR-LWT-CH-HET	CH	2.27×10^{-12}
Total			**10,000**	**Total**		**4,005**

Information Only

4.1.3 Waste Stream Activity Concentration

The activity concentration (EPA units/m^3) for each waste stream is calculated at closure and at 10,000 years post-closure. The ten waste streams that exhibit the highest activity concentrations in the CRA26_IS at each time point are listed in Table 10. Due to radioactive decay, the EPA units of each waste stream, and, thus, the concentration of activity in the waste, decreases by 10,000 years post-closure. The varying distributions of radionuclides within each waste stream, along with their different decay rates, lead to a non-constant decrease in activity concentration. Consequently, the group of the top ten waste streams by activity concentration at closure is not the same as that at 10,000 years post-closure.

Table 10. WIPP CH- and RH-TRU Waste Streams Ordered by Activity Concentration at Closure (Calendar Year 2,083) and at 10,000 Years Post-Closure (Calendar Year 12,083) from CRA26_IS Inventory

Rank Order	Waste Stream ID at closure	Stream Type at closure	EPA units per m^3 at closure	Waste Stream ID after 10,000 years	Stream Type after 10,000 years	EPA units per m^3 after 10,000 years
1	OR-OXIDE-CH-HET	CH	6.75×10^{0}	WA-SR-KAC-PUOX	CH	1.65×10^{-1}
2	WA-SR-KAC-PUOX	CH	3.42×10^{0}	SR-KAC-PuOx-2	CH	1.49×10^{-1}
3	SR-KAC-PuOx	CH	3.39×10^{0}	SR-KAC-PuOx	CH	1.46×10^{-1}
4	SR-KAC-PuOx-2	CH	2.66×10^{0}	WP-SR-KAC-PUOX	CH	1.35×10^{-1}
5	WP-SR-KAC-PUOX	CH	2.42×10^{0}	OR-OXIDE-CH-HET	CH	7.27×10^{-1}
6	WP-LA-OS-00-01.001	CH	1.56×10^{0}	WP-LA-OS-00-04	CH	7.09×10^{-1}
7	LA-OS-00-01.001	CH	1.27×10^{0}	LA-OS-00-01.001	CH	3.34×10^{-1}
8	WP-LA-OS-00-04	CH	1.21×10^{0}	WP-RLRFETS.001	CH	2.77×10^{-1}
9	WP-RF005.02	CH	7.06×10^{-1}	WP-RF118.01	CH	2.26×10^{-1}
10	WP-RLHMOX.001	CH	6.65×10^{-1}	WP-RLHMOX.001	CH	2.13×10^{-1}
• •	• •	• •	• •	• •	• •	• •
590	LB-T002	CH	4.14×10^{-7}	WP-OR-LWT-CH-HET	CH	3.60×10^{-12}
Overall waste streams			**6.33×10^{-2}**	**Overall waste streams**		**2.54×10^{-2}**

Information Only

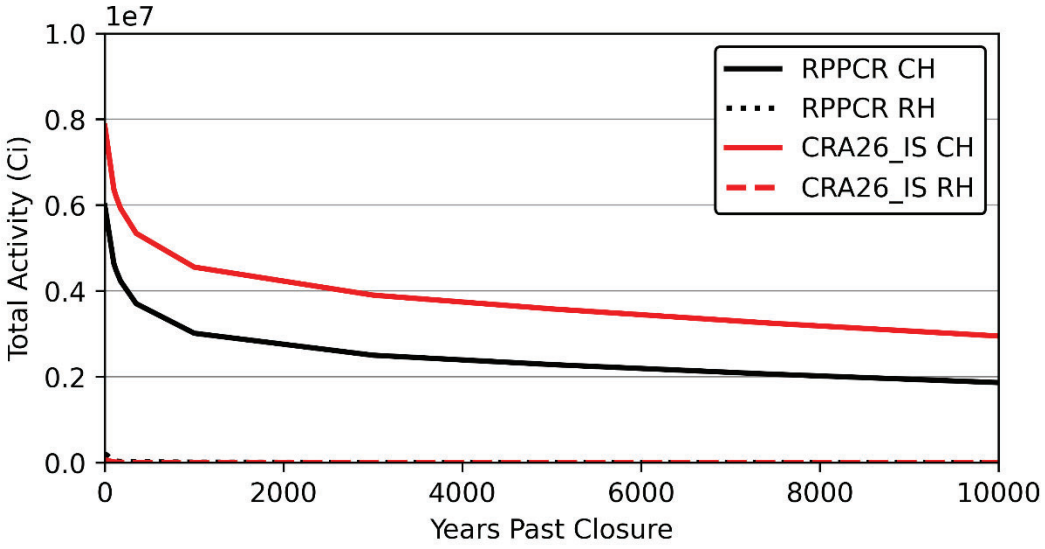
4.1.4 Total Radionuclide Activity

Figure 6 compares the total activity (in Ci and EPA units) as a function of time for the CH and RH waste inventories. The RH waste contributes minimally in terms of both Ci and EPA units. In Figure 6(a), the total activity in Ci for the CRA26_IS is higher than that for the RPPCR over the regulatory period, primarily due to an increased inventory of ^{239}Pu.

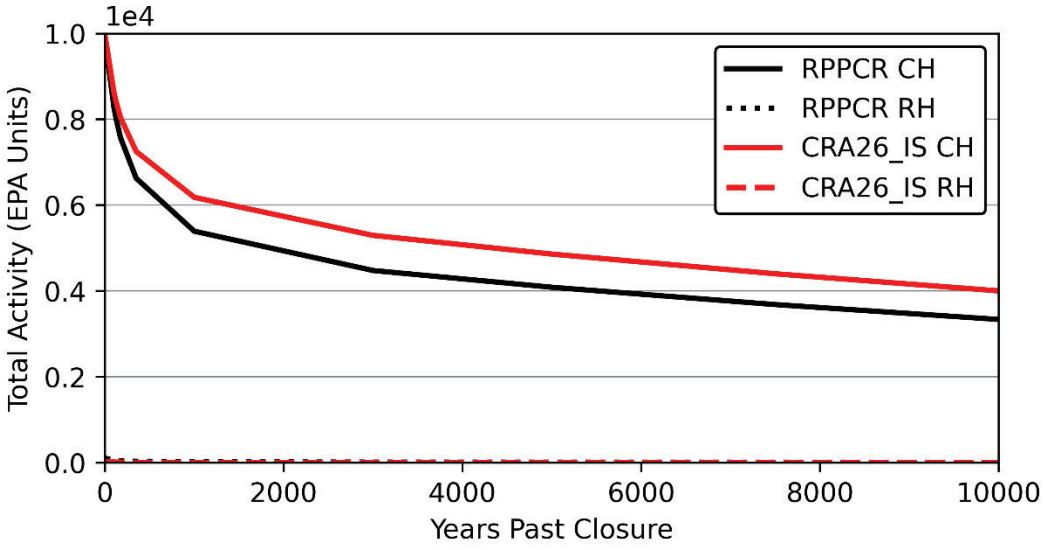
In Figure 6(b), however, the total activity in EPA units for the CRA26_IS is nearly identical to that for the RPPCR at closure. This is attributed to the fact that the EPA unit value represents radioactivity in curies normalized by the WUF factor, which is defined as the total curies of the transuranic radionuclides at closure divided by one million curies. The WUF factors used are 5.59 for the RPPCR and 7.37 for the CRA26_IS. As time progresses after closure, the total activity in EPA units for the CRA26_IS becomes greater than that for the RPPCR due to the increased inventory of ^{239}Pu, which has a relatively long half-life.

The total activity for the dominant WIPP radionuclides in EPA units at closure and at 10,000-years post-closure is displayed in Table 11. The initial activity of the inventory is dominated by ^{241}Am, ^{238}Pu, ^{239}Pu and ^{240}Pu. Since the inventories of ^{241}Am and ^{238}Pu decay rapidly, the total activity of the inventory is primarily dominated by ^{239}Pu at later times (beyond 2,000 years), with a smaller contribution from ^{240}Pu. The radionuclides ^{244}Cm, ^{137}Cs, ^{241}Pu, ^{90}Sr, ^{233}U, and ^{234}U do not appreciably contribute to the total activity at any time throughout the 10,000-year regulatory period.

Information Only



(a) Total activity (in Ci)



(b) Total activity (in EPA units)

Figure 6. Total Activity in WIPP CH- and RH-TRU Waste from Closure to 10,000 Years After Closure, in Units of (a) Curies (Ci) and (b) EPA Units.

Information Only

Table 11. Total Activity (EPA Units) for Dominant Isotopes in WIPP CH- and RH-TRU Waste at Closure and at 10,000 Years Post-Closure

Radionuclide	Half-life (y)	RPPCR Activity at Closure (EPA Units)	RPPCR Activity after 10,000 Years (EPA Units)	CRA26_IS Activity at Closure (EPA units)	CRA26_IS Activity after 10,000 Years (EPA units)
^{241}Am	432.7	2.55×10^{3}	2.79×10^{-4}	2.11×10^{3}	2.31×10^{-4}
^{244}Cm	18.1	-	-	-	-
^{137}Cs	30.07	1.65×10^{1}	0.00	4.32×10^{0}	0.00
^{238}Pu	87.7	2.32×10^{3}	0.00	1.87×10^{3}	0.00
^{239}Pu	24100	3.88×10^{3}	2.91×10^{3}	4.76×10^{3}	3.57×10^{3}
^{240}Pu	6560	1.24×10^{3}	4.29×10^{2}	1.26×10^{3}	4.37×10^{2}
^{241}Pu	14.29	-	-	-	-
^{90}Sr	28.8	1.11×10^{1}	0.00	2.64×10^{0}	0.00
^{233}U	159200	9.49×10^{-1}	9.08×10^{-1}	4.46×10^{-1}	4.27×10^{-1}
^{234}U	246000	1.21×10^{0}	1.99×10^{0}	8.89×10^{-1}	1.52×10^{0}
Total		**1.00×10^{4}**	**3.34×10^{3}**	**1.00×10^{4}**	**4.00×10^{3}**

Information Only

4.2 Salado Flow

Repository conditions influencing releases including brine pressures and saturations within the waste areas of the repository are summarized and compared with corresponding results from the RPPCR. Some of the changes introduced in the CRA26_IS have significant impacts on the Salado flow results. Differences in the mean results are shown and discussed here. Day and King (2025) explore more differences in the overall distribution of results and results for additional areas of the repository. Individual vectors might not display the same trends as the mean results. Changes included in the CRA-2026 IS that most substantially affect Salado flow results as compared to the RPPCR are (Day and King 2025):

- Increased inventory iron mass, CPR mass, and decay heat leading to increased gas generation and brine consumption on a per waste area volume basis.
- Changes in panel areas and volumes leading to increases in net brine flow into the repository for the representative waste panel, south rest-of-repository, and north rest-of-repository and decreases for the west rest-of-repository that impact net brine flow into these areas from the adjacent DRZ.

In summary, the mean net brine inflows into the representative waste panel, South Rest-of-Repository, and North Rest-of-Repository are larger for CRA26_IS due to the grid modifications to better align the modeling grid with as-built dimensions, that increase the area/volume of these regions in comparison to RPPCR. The increased area correlates to an increase in the brine available within the adjacent DRZ which flows into these waste areas. Net brine inflow for the representative waste panel is shown in Figure 7. On a per-panel basis, the same is true for the West Rest-of-Repository, but the West Rest-of-Repository in CRA26_IS consists of only two panels whereas for RPPCR it consists of nine panels. Thus, the net brine inflow for the West Rest-of-Repository is significantly larger for RPPCR and contributes such that the total net brine flow into the repository is greater for RPPCR in comparison to CRA26_IS.

In all reported scenarios and on a volume-normalized basis, the mean brine consumption resulting from chemical reactions within each of the waste areas is greater for CRA26_IS in comparison to RPPCR due to the effects of the increased MgO hydration rate and increased gas generation rates coupled to higher concentrations of iron, CPR, and decay heat in the waste areas. Brine consumption in the representative waste panel is shown in Figure 8. As a result of the consumption of brine outpacing the net inflow of brine into waste areas for CRA26_IS, brine saturations are observed to be significantly decreased over all reported waste areas and scenarios in comparison to RPPCR. Brine saturation in the representative waste panel is shown in Figure 9.

Primarily due to the decreased size of the West Rest-of-Repository, total gas generation from all sources is less for CRA26_IS in comparison to RPPCR. However, when gas generation is normalized to the repository waste volume (REFCON:VREPOS), all sources of gas generation are observed to be proportionally greater for CRA26_IS, particularly in scenarios with a Castile intrusion and associated higher post-intrusion brine saturations. Total and normalized total repository gas generation from all sources are shown in Figure 10 and Figure 11, respectively. Inventory concentrations contributing to gas generation are higher in CRA26_IS such that with available brine, volume-normalized gas generation outpaces that seen in RPPCR.

Information Only

Mean brine pressures over all waste areas and scenarios without a Castile intrusion are generally lower for CRA26_IS in comparison to RPPCR due primarily to the reduced brine saturation facilitated by increased brine consumption in relation to net brine inflow. However, for scenarios with a Castile intrusion, the increased brine saturation and associated gas generation for CRA26_IS that is supported by a higher concentration of gas generating inventory constituents leads to marginally higher mean and max pressures than in the RPPCR. Mean brine pressure in the representative waste panel is shown in Figure 12.

Brine flows away from the repository (up the borehole, shaft, and out through anhydrite layers) are similar between the CRA26_IS and RPPCR and relatively low in volume.

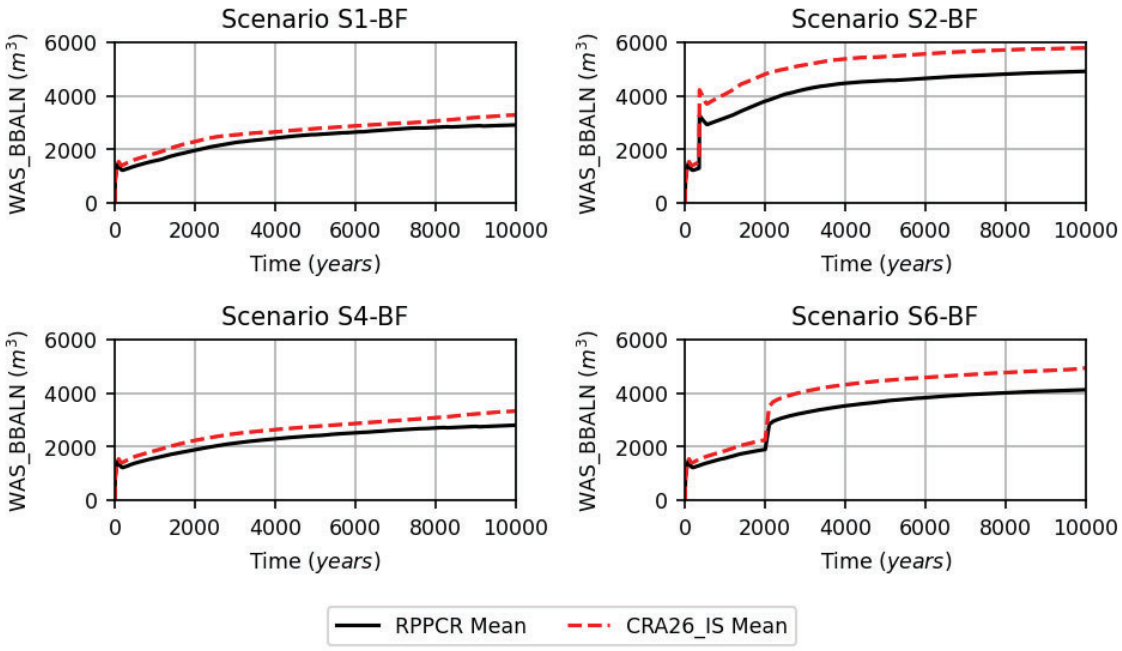


Figure 109 from Day and King (2025).

Figure 7. Mean Net Brine Flow into the Waste Panel

Information Only

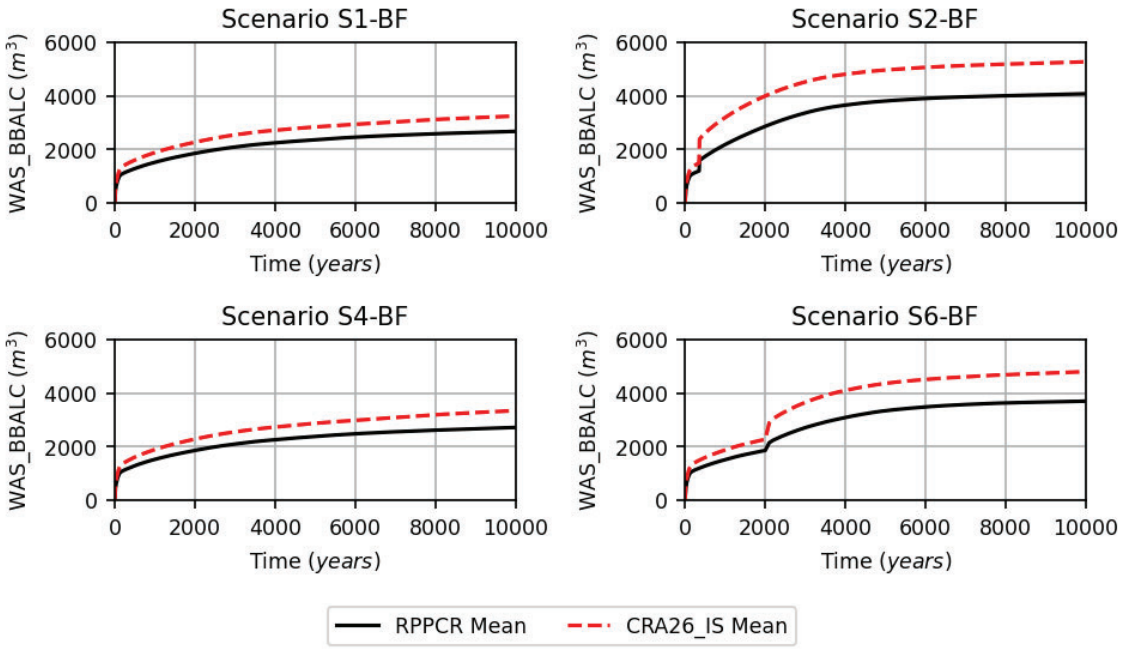
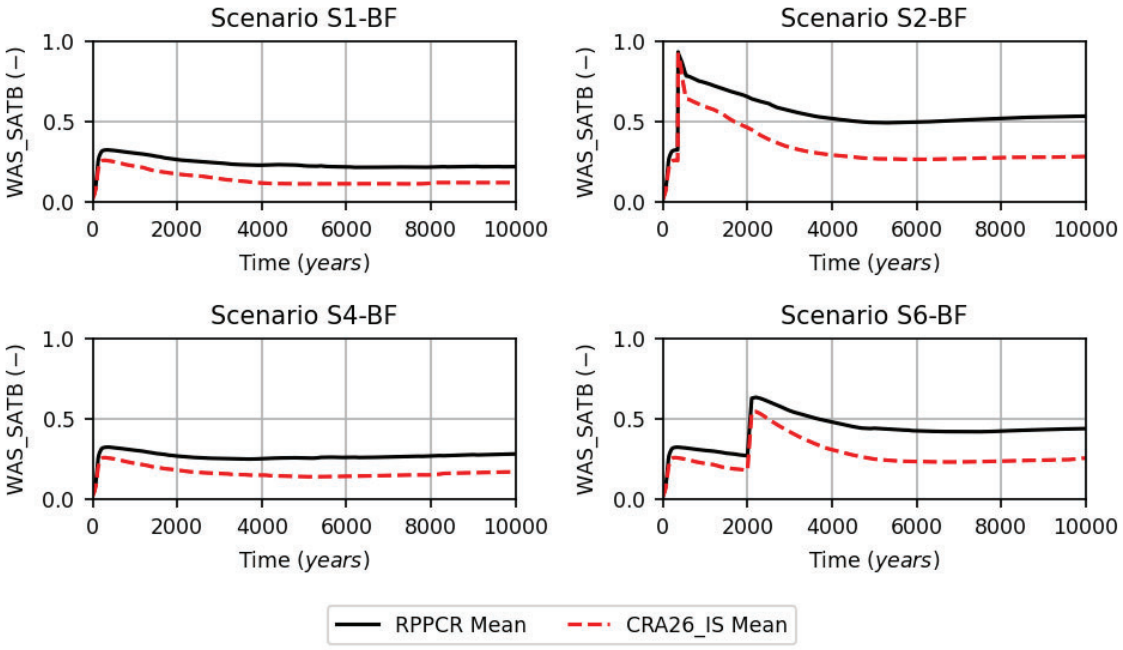


Figure 110 from Day and King (2025).

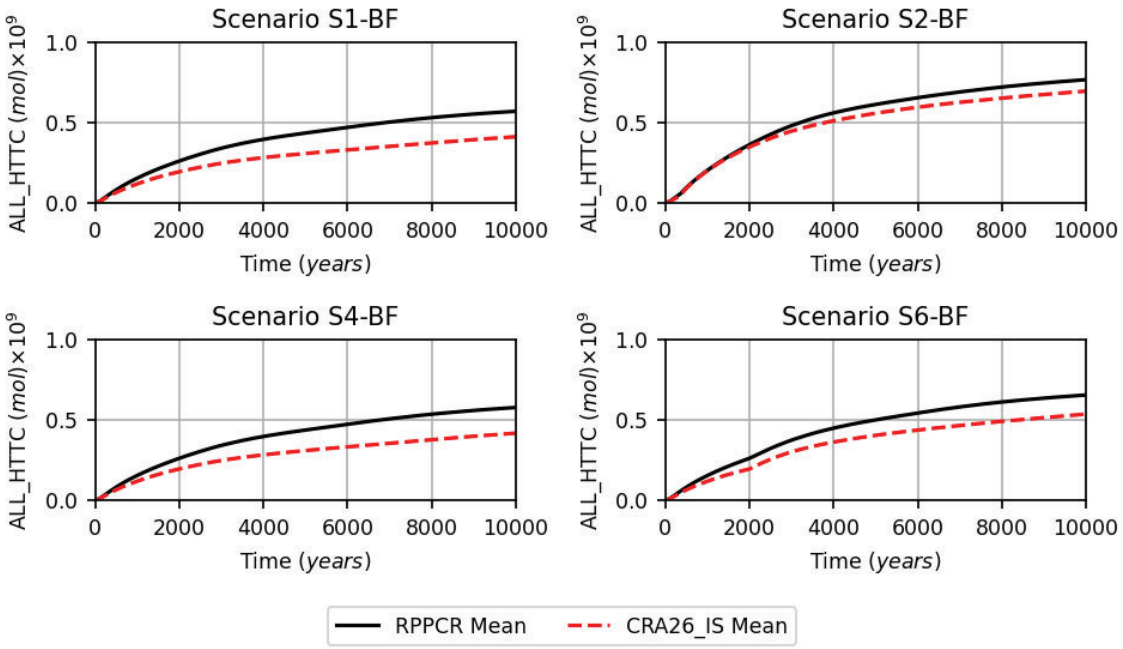
Figure 8. Mean Brine Consumption in the Waste Panel



Compiled from Figures 43, 52, 58, and 62 from Day and King (2025).

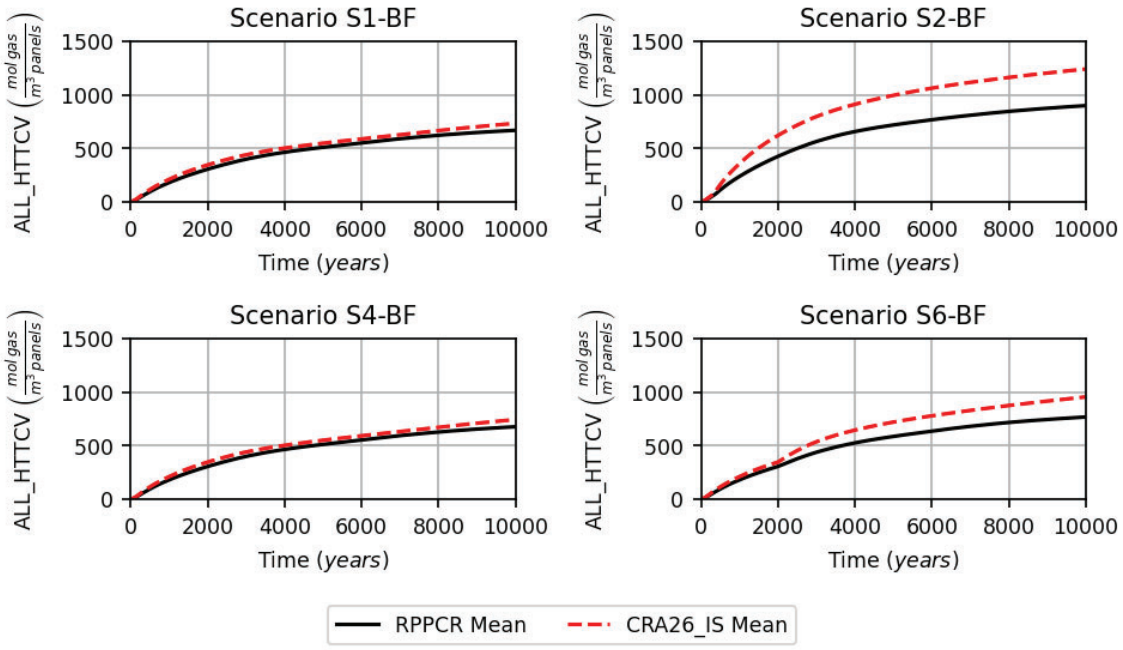
Figure 9. Mean Brine Saturation in the Waste Panel

Information Only



Compiled from Figures 82, 84, and 86 from Day and King (2025).

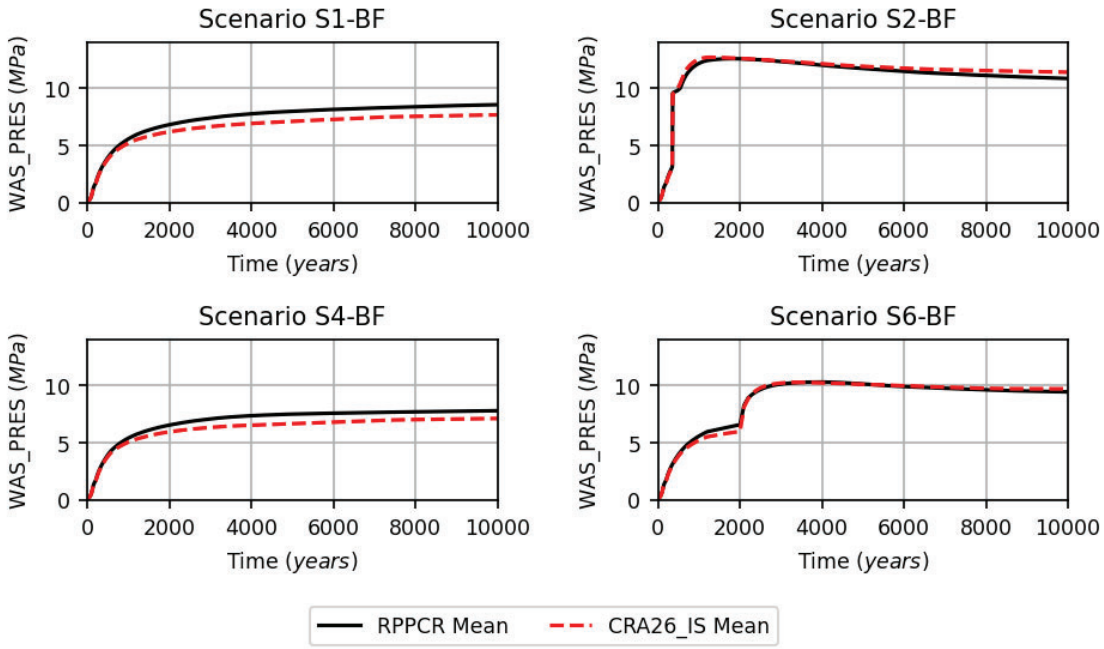
Figure 10. Mean Total Repository Gas Generation



Compiled from Figures 83, 85, and 87 from Day and King (2025).

Figure 11. Mean Normalized Total Repository Gas Generation

Information Only



Compiled from Figures 16, 25, 31, and 35 from Day and King (2025).

Figure 12. Mean Brine Pressure in the Waste Panel

4.3 Cuttings, Cavings, and Spallings

This section describes the calculations of the volume of solids released from the WIPP repository from an intrusion borehole. The PA codes CUTTINGS_S and DRSPALL are used to calculate these volumes which include cuttings, cavings, and spallings. Changes included in the CRA-2026 IS that most substantially affect cuttings, cavings, and spallings results as compared to the RPPCR are:

- Changes in panel areas and volumes leading to changes in brine pressures and resulting in similar but variable pressure trend comparisons across scenarios and intrusion locations.
- Increase in inventory concentrations over time leading to increased spallings concentrations.

Cuttings, cavings, and spallings releases are analyzed across four distinct areas of the repository: the lower ('L') area, which includes only Panel 5; the middle ('M') area, comprising the connected Panels 3, 4, 6, and 9; the upper ('U') repository area, consisting of Panels 1, 2, 7, 8, and 10; and the other ('O') repository area, which encompasses Panels 11 and 12. For more information on the solids release calculation, see Brunell and Kicker (2025).

4.3.1 Cuttings and Cavings

The results obtained for the CRA26_IS are consistent with those from the RPPCR. There were no changes to parameters associated with the cuttings and cavings processes in the CRA26_IS. Furthermore, cuttings and cavings volumes are independent of repository conditions so there are

Information Only

no changes between the RPPCR and the CRA26_IS. A summary of statistics for cavings is presented in Table 12, which highlights the mean and maximum cavings areas, as well as the number of vectors without cavings.

Table 12. Cavings Area Statistics for CRA26_IS and RPPCR

Analysis	Mean Cavings Area (m^2)	Mean Non-Zero Cavings Area (m^2)	Maximum Cavings Area (m^2)	Number of Realizations Without Cavings
CRA26_IS	0.011	0.021	0.110	49
RPPCR	0.011	0.021	0.110	49

4.3.2 Spallings

Spallings releases are calculated by multiplying the estimated spallings volumes by the concentrations of radionuclides present in Contact Handled (CH) waste at the time of intrusion. This methodology ensures that the assessment reflects the radionuclide concentrations relevant to the specific conditions in the repository during each intrusion event. The spallings volumes, as detailed in Section 4.3.2.1, are derived from the pressure conditions within the repository waste areas (Figure 2). Section 4.3.2.2 discusses the spallings concentrations, which are based on the average activity per volume of CH-TRU waste. While the spallings volumes remain generally consistent across analyses, the spallings concentrations increase from the RPPCR to the CRA26_IS.

4.3.2.1 Spallings Volume

The spallings volume calculations for the RPPCR and the CRA26_IS utilize DRSPALL solids release volumes as outlined by Kirchner et al. (2014; 2015). Individual borehole spallings releases are influenced by repository conditions, particularly the pressures present in the waste areas. It is important to note that conservative assumptions embedded in the spallings volume calculations may lead to an overestimation of these volumes (U.S. DOE, 2019, Appendix MASS).

The intrusion scenarios and times employed in the calculation of spallings release volumes are presented in Table 7; these same scenarios are also used for calculating DBR volumes. Time-dependent spallings volumes are determined by interpolating the spallings volumes calculated by DRSPALL to align with the time-dependent repository pressures derived from BRAGFLO. Summary statistics of spallings volumes are provided in Table 13 and shown in Figure 13 and Figure 14 for the CRA26_IS and RPPCR.

The mean nonzero spallings volume remain relatively consistent across analyses, with the highest occurring in the undisturbed scenario S1-DBR, with volumes of 1.76 m^3 for the RPPCR and 2.06 m^3 for the CRA26_IS. Among the subsequent intrusion scenarios S2-DBR through S5-DBR, S5-

Information Only

DBR has the highest mean nonzero volume of 1.73 m^3 in CRA26_IS and 1.48 m^3 in the RPPCR, while S3-DBR shows the lowest mean at 1.10 m^3 in the CRA26_IS and 1.08 m^3 in the RPPCR.

The percentage of realizations with nonzero spallings volume remains relatively consistent across analyses. Scenario S2-DBR, involving an early-time intrusion into a brine pocket, shows the highest percentage of realizations with nonzero spallings for both RPPCR (33.75%) and CRA26_IS (34.80%). For each analysis, scenario S1-DBR has the lowest percentage across all scenarios (13.83% for RPPCR and 11.54% for CRA26_IS). The percentage of non-zero realizations decreased slightly from RPPCR to CRA26_IS in the O locations. The decreased brine saturation (discussed in Section 4.2) contributes to lower brine pressure, ultimately leading to smaller spallings volumes in this area.

Information Only

Table 13. Spallings Volume Summary, Replicate 1

Scenario	Location	Mean Spallings Volume (m^3) RPPCR	Mean Spallings Volume (m^3) CRA26_IS	Fraction of Sim. with Nonzero Releases RPPCR	Fraction of Sim. with Nonzero Releases CRA26_IS	Mean of Non-Zero Spallings Releases (m^3) RPPCR	Mean of Non-Zero Spallings Releases (m^3) CRA26_IS
S1-DBR	**All**	**0.24**	**0.24**	**13.83%**	**11.54%**	**1.76**	**2.06**
S1-DBR	L	0.28	0.28	15.67%	13.33%	1.80	2.13
S1-DBR	M	0.28	0.28	15.67%	13.33%	1.80	2.12
S1-DBR	U	0.27	0.27	14.00%	12.83%	1.90	2.09
S1-DBR	O	0.14	0.12	10.00%	6.67%	1.43	1.75
S2-DBR	**All**	**0.39**	**0.41**	**33.75%**	**34.80%**	**1.16**	**1.18**
S2-DBR	L	0.54	0.60	48.60%	50.60%	1.12	1.18
S2-DBR	M	0.54	0.59	48.20%	50.60%	1.12	1.17
S2-DBR	U	0.33	0.33	25.20%	26.60%	1.30	1.26
S2-DBR	O	0.15	0.12	13.00%	11.40%	1.18	1.08
S3-DBR	**All**	**0.36**	**0.38**	**33.25%**	**34.75%**	**1.08**	**1.10**
S3-DBR	L	0.44	0.51	45.20%	49.20%	0.98	1.04
S3-DBR	M	0.44	0.51	44.80%	49.20%	0.98	1.04
S3-DBR	U	0.37	0.36	27.60%	27.60%	1.32	1.29
S3-DBR	O	0.19	0.15	15.40%	13.00%	1.25	1.13
S4-DBR	**All**	**0.20**	**0.20**	**15.20%**	**13.15%**	**1.33**	**1.52**
S4-DBR	L	0.21	0.23	17.20%	15.00%	1.23	1.54
S4-DBR	M	0.21	0.23	17.20%	15.00%	1.22	1.53
S4-DBR	U	0.24	0.23	16.20%	14.80%	1.50	1.57
S4-DBR	O	0.15	0.11	10.20%	7.80%	1.43	1.36
S5-DBR	**All**	**0.28**	**0.28**	**18.85%**	**15.90%**	**1.48**	**1.73**
S5-DBR	L	0.30	0.32	20.80%	18.20%	1.43	1.76
S5-DBR	M	0.30	0.32	20.80%	18.20%	1.42	1.76
S5-DBR	U	0.33	0.32	20.00%	18.00%	1.66	1.76
S5-DBR	O	0.19	0.14	13.80%	9.20%	1.39	1.57
All Scenarios	**All Locations**	**0.29**	**0.30**	**22.63%**	**21.63%**	**1.30**	**1.38**
All	**L**	0.35	0.38	28.96%	28.65%	1.22	1.34
All	**M**	0.35	0.38	28.81%	28.65%	1.22	1.34
All	**U**	0.31	0.30	20.35%	19.69%	1.50	1.53
All	**O**	0.16	0.13	12.38%	9.50%	1.33	1.34

Information Only

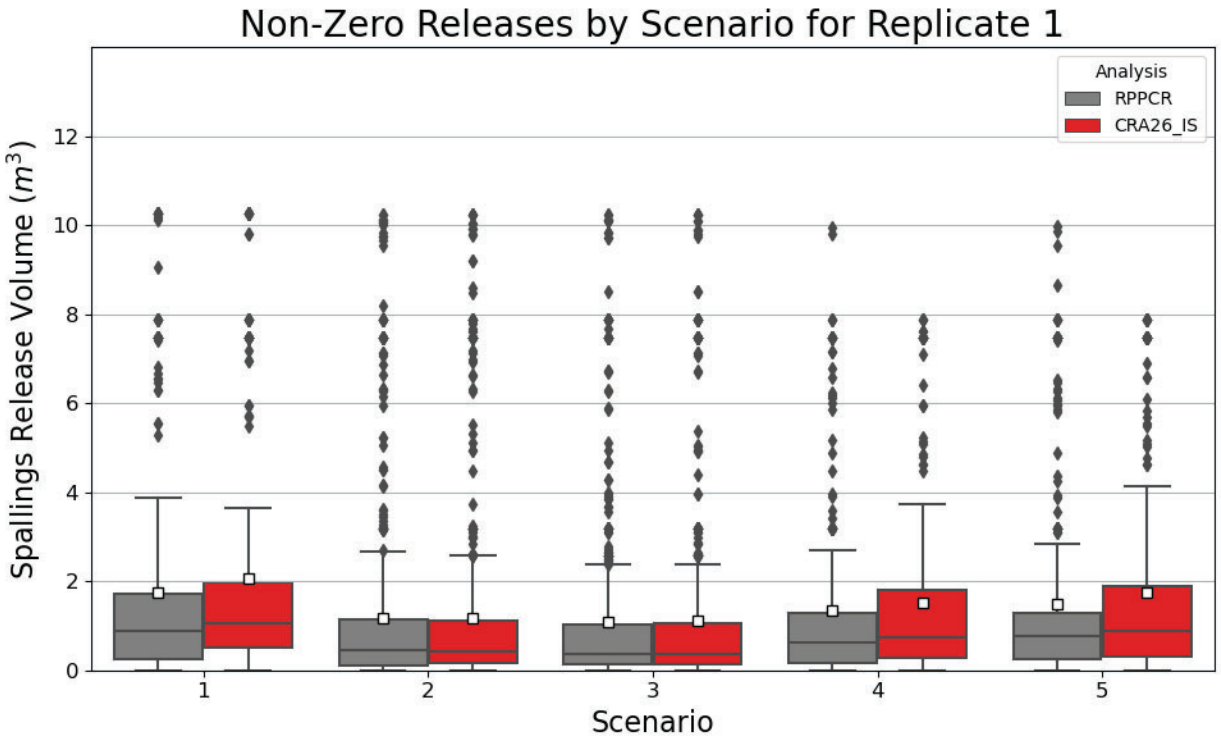


Figure 13. Non-Zero Spallings Release Volume by Intrusion Scenario

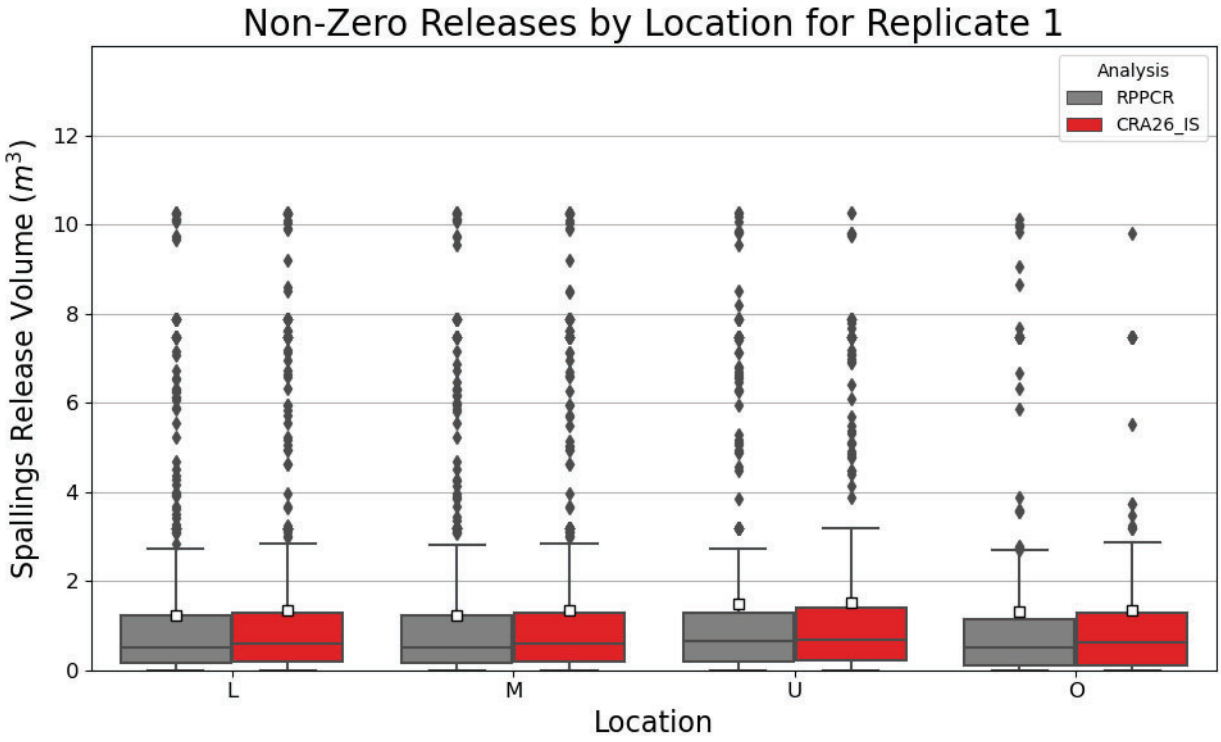


Figure 14. Non-Zero Spallings Release Volume by Intrusion Location

Information Only

4.3.2.2 Spallings Concentration

The spallings concentration over the 10,000-year regulatory period, expressed in EPA units per cubic meter of waste, is illustrated in Figure 15. The figure illustrates that the CRA26_IS inventory consistently exhibits higher radionuclide concentrations over time than the RPPCR inventory. Although the total inventory volume in the CRA26_IS is lower than that used in the RPPCR, as discussed in Section 4.1, the elevated concentrations can be attributed to the increased levels of ^{239}Pu in the CRA26_IS inventory compared to the RPPCR inventory.

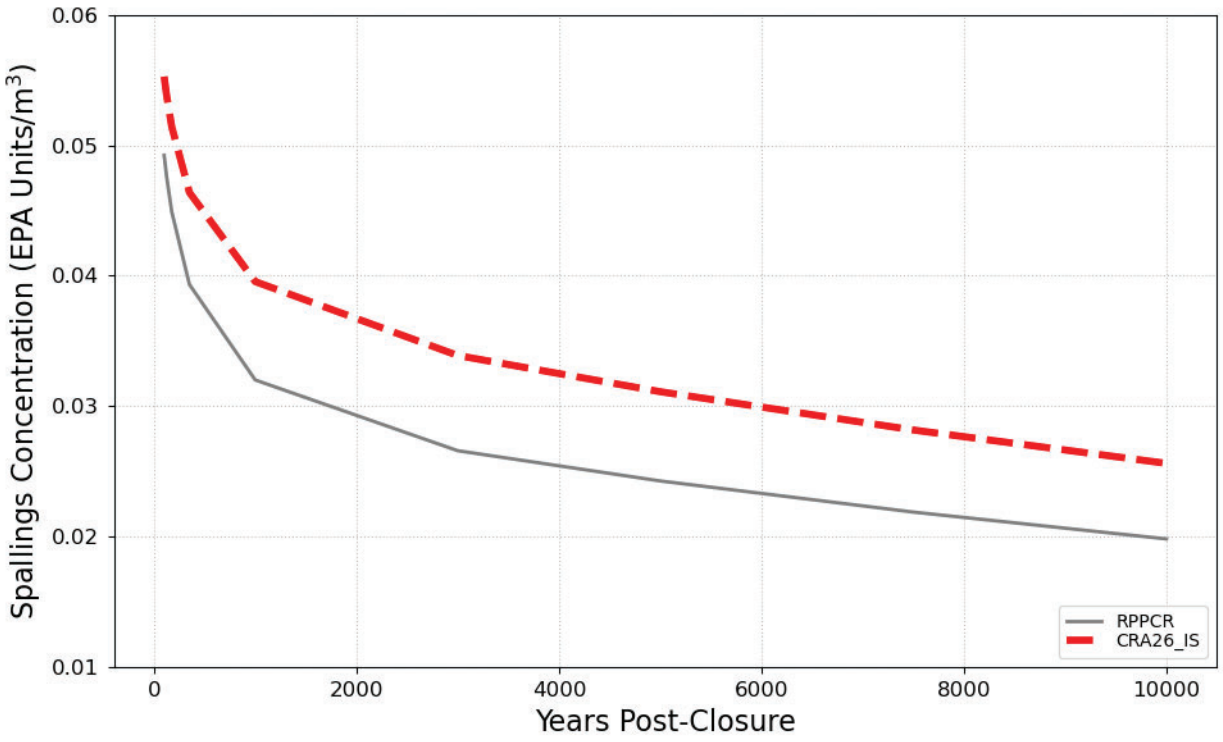


Figure 15. Spallings Release Concentration from Closure to 10,000 Years

Information Only

4.4 Direct Brine Release Volumes

Mean brine releases, the fraction of simulations with non-zero releases, and the mean of non-zero brine releases for Replicate 1 are summarized in Table 14. The number of non-zero brine releases is plotted in Figure 16 by brine release volume, and the distribution of non-zero brine release volumes is plotted in Figure 17. Figure 18 shows the distribution of non-zero release volumes broken down by scenario. Changes included in the CRA26_IS that are observed to most substantially affect DBR results as compared to the RPPCR are (Zeitler 2025):

- Increased gas generation and brine consumption on a per waste area volume basis, leading to increased brine pressure and decreased brine saturation in waste areas (see Section 3.2).

Pressure and saturation from the Salado flow simulations are initial conditions in the DBR calculation. Changes in the CRA26_IS that affect these initial conditions strongly affect both the number of DBRs and the volume of brine released in a DBR.

Making an overall comparison of DBR volumes for the RPPCR and the CRA26_IS:

(i) The number of non-zero DBR volumes decreased for the CRA26_IS across all scenarios.

(ii) The CRA26_IS saw small magnitude releases decrease in frequency (Figure 16), while large magnitude releases (greater than 50 m^3) increased slightly in frequency (though they represent a very small fraction of release events) (Figure 17).

(iii) Mean and median non-zero release volumes all decreased for the CRA26_IS, while maximum non-zero release volumes increased (Figure 17). Overall, the mean non-zero release volume decreased by about 10% (Table 14).

(iv) For the CRA26_IS, mean non-zero release volumes are decreased for scenarios S1-DBR, S2-DBR, and S3-DBR, but increased for the other two scenarios (Figure 18). Median release volumes are decreased for all scenarios except S4-DBR. Maximum release volumes are increased for all scenarios except S1-DBR.

(v) For both the RPPCR and the CRA26_IS, the largest fraction of non-zero DBR volumes occurs at the L intrusion location and decreases as the intrusion location moves to the north, that is, up dip to the M, U, and O locations (Table 14). The largest mean non-zero release volume also occurs at the L intrusion location and decreases as the intrusion location moves to the north to the M intrusion location, but then increases for the U intrusion location, and finally decreases to the lowest volume for the O intrusion location.

(vi) Releases from the O intrusion location contribute to RPPCR and CRA26_IS DBR volumes; however, O intrusion releases are less frequent and mean volumes are smaller compared to the L, M and U intrusion locations (Table 14).

As described in Section 4.2, the CRA26_IS Salado flow results show a decrease in mean brine pressures for scenarios without an E1 intrusion and an increase in mean brine pressures for scenarios with an E1 intrusion (except for the westernmost waste areas). Additionally, there is an observed decrease in brine saturation. The combination of these effects could lead to mixed impacts on the number of non-zero DBR volumes across scenarios. Day and King (2025) also point out that maximum brine pressure for any individual vector in Replicate 1 is generally greater in the CRA26_IS and there is a substantial decrease in brine saturation; these are effects that could also lead to mixed impacts on the magnitudes of the largest DBR volumes.

Information Only

Comparing CRA26_IS and RPPCR DBR volumes at individual intrusion locations (in Table 14, rows directly beneath the "All Scenarios" label), DBR volumes for all intrusion locations follow the overall trend of a decreased frequency of non-zero DBR volumes and with decreased mean non-zero release volumes in the CRA26_IS. In both analyses, DBR volumes from the L location have the greatest frequency and mean non-zero release volume. DBR volumes at the M location have decreased frequency and mean non-zero release volumes compared to the L location, but the mean non-zero release volumes are also lower compared to the U intrusion location for Replicate 1 in both analyses.

Scenarios with an E1 intrusion (S2-DBR and S3-DBR) have a decreased frequency of non-zero DBR volumes in the CRA26_IS; additionally, mean non-zero release volumes in the CRA26_IS are decreased by about 20-25% compared with those in the RPPCR (Table 14). The decrease in mean non-zero release volumes can be attributed to reduced brine saturation for scenarios with E1 intrusion, despite increased brine pressures (Section 4.2) and despite the observed increase in the number of large magnitude releases (Figure 17).

Scenarios without an E1 intrusion (S1-DBR, S4-DBR and S5-DBR) saw the frequency of non-zero DBR volumes also decrease in the CRA26_IS, while mean non-zero releases were reduced by about 20% for S1-DBR and increased by about 10-20% for the other two scenarios (Table 14). The decreased frequency in non-zero DBR volumes can be attributed to decreased brine saturation, as well as decreased mean pressure for scenarios without an E1 intrusion (Day and King 2025). The increased mean DBR volumes for scenarios S4-DBR and S5-DBR can be attributed to increased maximum pressures in CRA26_IS.

Information Only

Table 14. DBR Volume Summary, Replicate 1

Intrusion Location	Mean Brine Released (m^3)		Fraction of Simulations with Non-Zero Releases		Mean of Non-Zero Brine Releases (m^3)	
	RPPCR	CRA26_IS	RPPCR	CRA26_IS	RPPCR	CRA26_IS
S1-DBR	**0.67**	**0.30**	**8.96%**	**5.04%**	**7.48**	**6.05**
L	1.77	0.78	15.17%	9.67%	11.67	8.11
M	0.34	0.20	6.67%	3.67%	5.13	5.53
U	0.42	0.19	8.33%	4.83%	5.02	3.87
O	0.15	0.05	5.67%	2.00%	2.67	2.28
S2-DBR	**2.24**	**1.32**	**37.70%**	**27.75%**	**5.94**	**4.77**
L	5.73	3.66	74.60%	62.40%	7.67	5.87
M	2.45	1.20	55.60%	39.20%	4.41	3.06
U	0.59	0.33	13.80%	6.60%	4.25	5.06
O	0.19	0.10	6.80%	2.80%	2.73	3.57
S3-DBR	**1.40**	**0.69**	**33.30%**	**22.10%**	**4.21**	**3.13**
L	3.73	1.94	68.00%	51.00%	5.48	3.81
M	0.95	0.52	40.00%	27.20%	2.37	1.91
U	0.67	0.25	15.80%	6.80%	4.22	3.68
O	0.26	0.06	9.40%	3.40%	2.80	1.70
S4-DBR	**0.89**	**0.68**	**12.45%**	**7.75%**	**7.18**	**8.79**
L	2.02	1.76	18.40%	15.20%	10.97	11.55
M	0.79	0.52	12.60%	6.80%	6.29	7.65
U	0.58	0.35	12.00%	6.40%	4.86	5.44
O	0.18	0.10	6.80%	2.60%	2.69	3.84
S5-DBR	**1.18**	**0.70**	**14.90%**	**7.90%**	**7.91**	**8.88**
L	2.68	2.07	21.40%	15.20%	12.52	13.61
M	1.00	0.40	14.20%	6.60%	7.04	6.08
U	0.76	0.28	14.60%	6.40%	5.18	4.32
O	0.28	0.06	9.40%	3.40%	2.96	1.79
All Scenarios						
L	**3.13**	**1.99**	**38.58%**	**29.88%**	**8.11**	**6.67**
M	**1.08**	**0.55**	**25.08%**	**16.19%**	**4.30**	**3.43**
U	**0.60**	**0.28**	**12.73%**	**6.15%**	**4.67**	**4.48**
O	**0.21**	**0.07**	**7.54%**	**2.81%**	**2.78**	**2.56**
ALL	**1.25**	**0.72**	**20.98%**	**13.76%**	**5.97**	**5.26**

Table 4 from Zeitler (2025).

Information Only

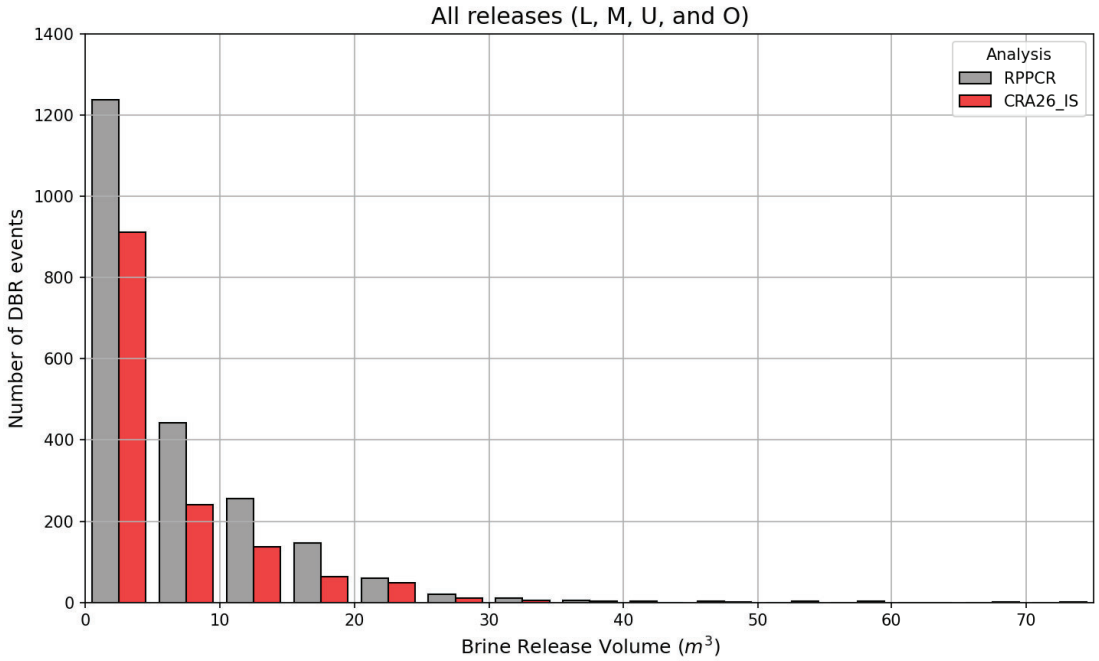


Figure 6 from Zeitler (2025).

Figure 16. DBR Volume Frequency, All Non-Zero Releases, Replicate 1

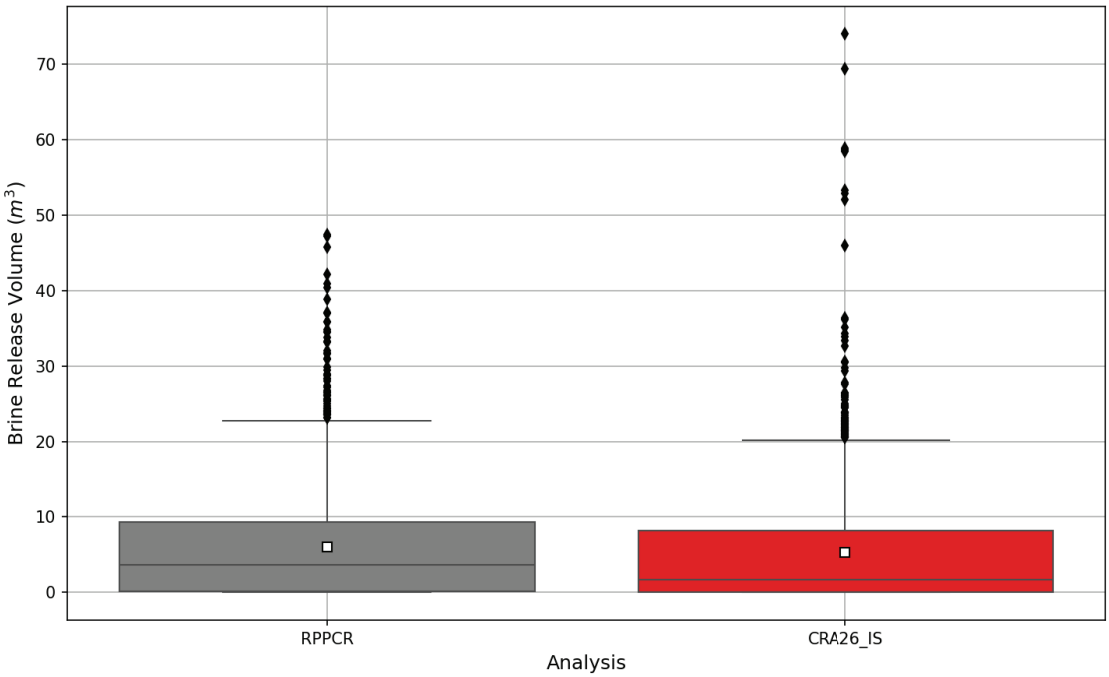


Figure 7 from Zeitler (2025).

Figure 17. DBR Volumes, All Non-Zero Releases, Replicate 1

Information Only

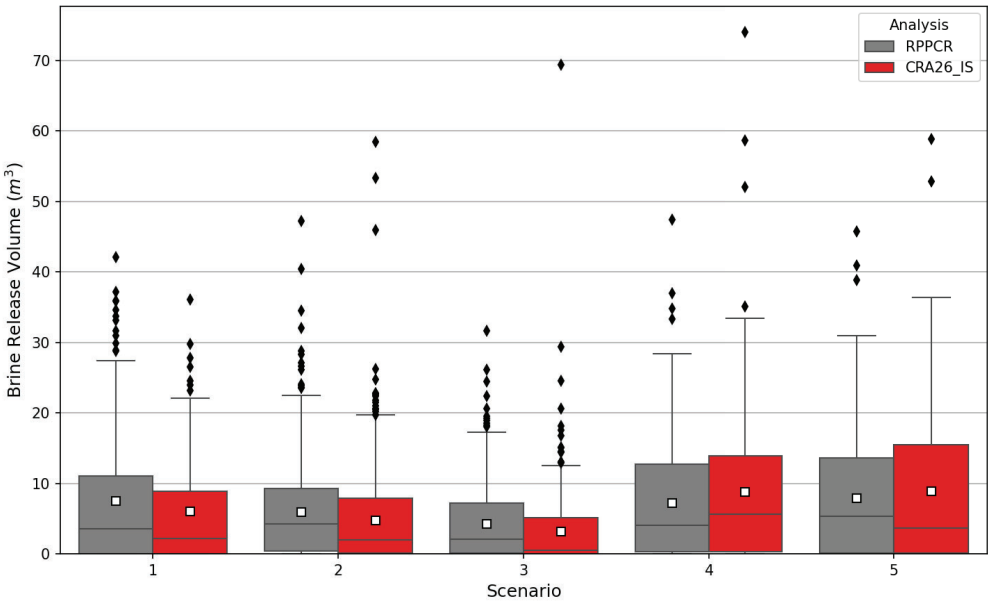


Figure 8 from Zeitler (2025).

Figure 18. DBR Volumes by Scenario, All Non-Zero Releases, Replicate 1

4.5 Mobilized Radionuclide Concentrations

Changes included in the CRA-2026_IS that are observed to most substantially affect radionuclide mobilization results as compared to the RPPCR are:

- The total activity at repository closure increased from 6.51×10^6 Ci in the RPPCR to 8.05×10^6 Ci for the CRA26_IS (Kicker 2025).
- The transuranic inventory of alpha-emitting radionuclides with half-lives greater than 20 years at repository closure increased from 5.59×10^6 Ci in the RPPCR to 7.37×10^6 Ci for the CRA26_IS (Kicker 2025).
- DBRMINBV (the minimum brine volume for a DBR to occur) is reduced from 33,804 m^3 in the RPPCR to 6,314 m^3 in the CRA26_IS, consistent with new geomechanical modeling (Brunell 2025).
- Proportionality constants (for concentration relative to solubility) and cap values for microbial colloids are specified by actinide in the RPPCR and, as recommended by Kaplan et al. (2025), by actinide and oxidation state in the CRA26_IS.
- Proportionality constants for humic colloids, which are specified by oxidation state and brine type, are updated for the CRA26_IS by Mariner (2025).

Information Only

The PANEL code models radionuclide mobilization for a group of five interconnected waste panels, designated as the waste area (Docherty and Kim 2025, Section 5.1). Inventory in the waste area is obtained from total inventory by multiplying by the factor 5×REFCON:VPANLEX/REFCON:VREPOS, that is, by five times the volume of one panel, divided by the volume of the repository. Parameter REFCON:VPANLEX is 46,097.65 m^3 in both analyses; however, REFCON:VREPOS decreased from 853,284.89 m^3 in the RPPCR to 560,722.29 m^3 in the CRA26_IS. Figure 19 illustrates the twelve largest contributors to waste area inventory, based on curies at closure, of the 30 radionuclides considered by PANEL. The five largest contributors in order, in both analyses, are ^{239}Pu, ^{241}Am, ^{238}Pu, ^{240}Pu, and ^{241}Pu. The inventory of each of these radionuclides has increased in the CRA26_IS. The significant increase in ^{239}Pu in the CRA26_IS is due to the addition of waste stream SR-KAC-PuOx-2 (Van Soest 2025).

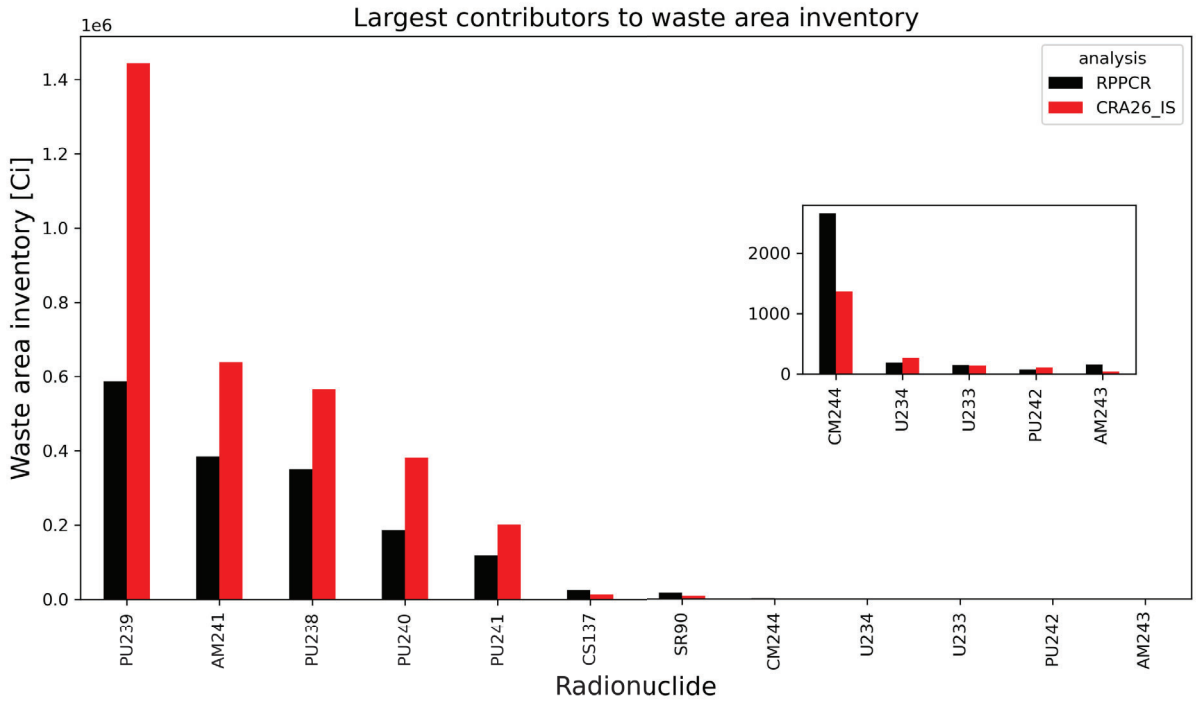


Figure 8 from Docherty and Kim (2025).

Figure 19. Largest Contributors in Curies to Inventory at Closure in the Waste Area

Mobile concentration limits in the CRA26_IS are affected by changes to baseline solubilities and to microbial and humic colloid enhancement parameters (Docherty and Kim 2025, Section 5.2). Less significant is an update to the cumulative probability distribution describing An(III) solubility uncertainty factors for the CRA26_IS (Docherty and Kim 2025, Figure 15).

In both ERDA-6 and GWB brines, An(III) baseline solubilities are about 4 times larger in the CRA26_IS than in the RPPCR, An(IV) baseline solubilities are similar in the two analyses, and An(V) baseline solubilities show a modest increase in the CRA26_IS. Domski (2025c) notes that

Information Only

the total moles of organic ligands are nearly the same in the two analyses, so that decreasing the minimum brine volume (DBRMINBV) in the CRA26_IS increases organic ligand concentrations, affecting An(III) and An(V) solubilities.

A thermodynamic model has not been developed for U(VI). The RPPCR uses 1×10^{-3} mol/L for the U(VI) baseline solubility, a value specified by the EPA (U.S. EPA 2006) and in use since the CRA-2004 PABC. The CRA26_IS updates the U(VI) baseline solubility to 3×10^{-6} mol/L, based on recent experimental work by Kaplan et al. (2025). U(VI) baseline solubility does not depend on brine type.

The proportionality constant for microbial colloids (PROPMIC) increases by a factor of about 10 for Pu(III), decreases somewhat for Am(III), and otherwise is unchanged for the CRA26_IS. The cap value for microbial colloids (CAPMIC) increases by a factor of about 400 for Pu(III) in the CRA26_IS. CAPMIC also increases for Pu(IV), U(IV), and U(VI), decreases for Np(IV), Np(V), and Am(III), and remains the same for Th(IV). Humic proportionality constants either increase in the CRA26_IS or are the same as the RPPCR values. See Docherty and Kim (2025, Section 5.2.4) for tables of the colloid parameters.

PANEL determines mobile concentration limits for the primary actinides, which are used to constrain radionuclide concentrations (Docherty and Kim 2025, Section 3.1.5). Table 15 lists mean values of the mobile concentration limits, determined for the minimum volume of brine for a DBR to occur. The mean values in both brine types increase in the CRA26_IS for Pu and Am, decrease for U and Np, and are largely unchanged for Th.

Table 15. Mean Mobile Concentration Limits in mol/L

Brine	Analysis	PU	U	NP	AM	TH
ERDA-6	RPPCR	7.43×10^{-7}	5.08×10^{-4}	2.35×10^{-6}	4.69×10^{-6}	6.27×10^{-7}
ERDA-6	CRA26_IS	3.20×10^{-6}	3.71×10^{-6}	2.23×10^{-6}	1.66×10^{-5}	6.25×10^{-7}
GWB	RPPCR	7.21×10^{-7}	5.08×10^{-4}	1.68×10^{-6}	4.59×10^{-6}	6.19×10^{-7}
GWB	CRA26_IS	3.22×10^{-6}	3.12×10^{-6}	6.97×10^{-7}	1.67×10^{-5}	6.19×10^{-7}

Table 12 from Docherty and Kim (2025).

PANEL determines lumped radionuclide mobile concentration limits for use by code NUTS. Table 16 lists mean values of the lumped radionuclide mobile concentration limits (for the minimum brine volume). Mean values in both brine types increase in the CRA26_IS for PU238L, PU239L and AM241L, and decrease for U234L. The mean values for TH230L are approximately the same for both brines and both analyses.

Information Only

Table 16. Mean Lumped Radionuclide Mobile Concentration Limits in mol/L

Brine	Analysis	PU238L	PU239L	U234L	AM241L	TH230L
ERDA-6	RPPCR	1.48×10^{-9}	7.43×10^{-7}	3.46×10^{-7}	4.69×10^{-6}	3.85×10^{-9}
ERDA-6	CRA26_IS	4.25×10^{-9}	3.20×10^{-6}	2.79×10^{-9}	1.66×10^{-5}	3.62×10^{-9}
GWB	RPPCR	1.44×10^{-9}	7.21×10^{-7}	3.46×10^{-7}	4.59×10^{-6}	3.80×10^{-9}
GWB	CRA26_IS	4.27×10^{-9}	3.22×10^{-6}	2.35×10^{-9}	1.67×10^{-5}	3.59×10^{-9}

Table 13 from Docherty and Kim (2025).

PANEL determines the concentrations of 26 radionuclides for a period of 10,000 years starting at repository closure. The concentrations are summed for use in determining of DBRs (Docherty and Kim 2025, Section 3.1.8). Figure 20 shows mean concentration in EPA units/m^3 as a function of time for ^{241}Am, ^{239}Pu, and ^{240}Pu in ERDA-6 brine and minimum brine volume (the mean is taken over the 100 vectors of Replicate 1). The three radionuclides, along with the fast-decaying ^{238}Pu, are the largest contributors to inventory at closure (Figure 19). Also shown in Figure 20 is the mean of the sum of the 26 radionuclides, designated CDBR. At closure, CDBR in the CRA26_IS is 2.6 times the RPPCR value; at 10,000 years, CDBR in the CRA26_IS is 2.1 times the RPPCR value. The CRA26_IS increases are attributed to larger inventory (Figure 19) and increased mobile concentration limits for Pu and Am (Table 15).

Figure 21 plots the sum of concentrations in ERDA-6 brine for all 100 vectors of Replicate 1. At early times, ^{241}Am is the primary component of the sum of radionuclides. As ^{241}Am decays it becomes inventory limited (Docherty and Kim, Figure 29) and ^{239}Pu contributes most to the sum.

Information Only

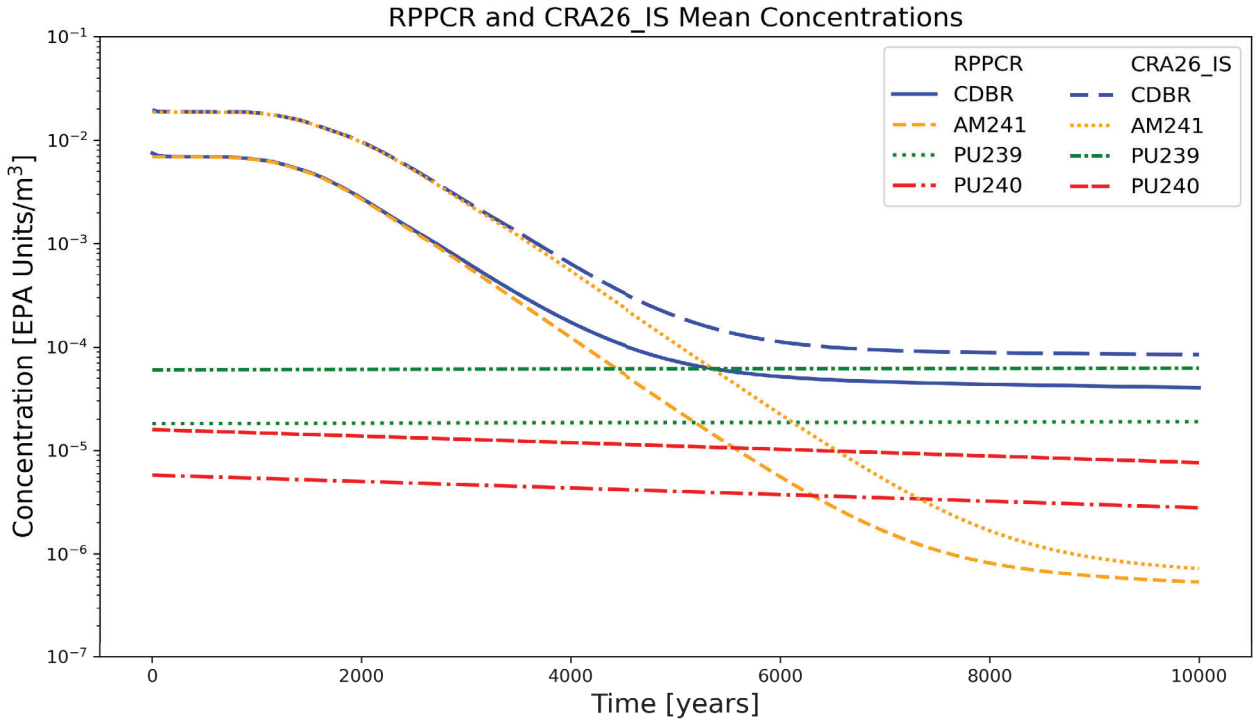


Figure 27 from Docherty and Kim (2025).

Figure 20. Comparison of Mean Concentrations

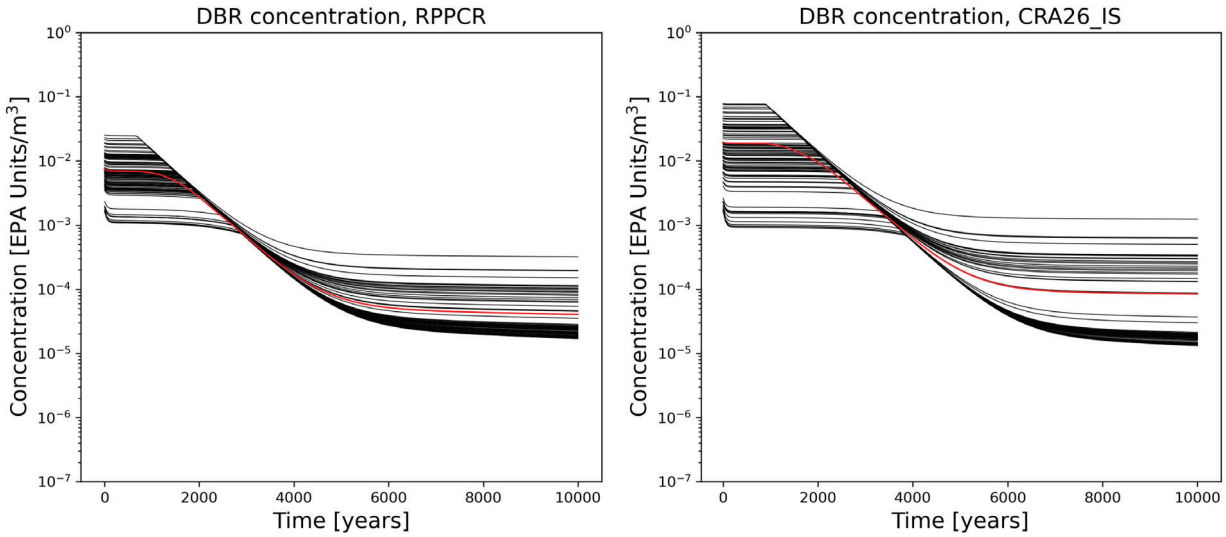


Figure 31 from Docherty and Kim (2025).

Figure 21. DBR Concentration Versus Time Used for Determining DBRs, All Vectors

Information Only

4.6 Salado Transport

Radionuclide transport up through an intruding borehole is the primary pathway for radionuclide mass transport in the Salado. Releases up a borehole to the Culebra are called *to Culebra* releases (though they are not releases in terms of WIPP regulatory compliance). NUTS determines lumped radionuclide *to Culebra* releases for screened-in vectors in BRAGFLO scenarios 2-5. Releases for screened-out vectors are set to zero. PANEL determines lumped radionuclide *to Culebra* releases for all vectors in BRAGFLO scenario 6. Figure 22 shows cumulative *to Culebra* releases at 10,000 years for scenarios 2-6, as well as total releases for each scenario – obtained by summing the accumulated releases of all five lumped radionuclides. Screened-out vectors have been included when making the box plots and affect the mean values shown (boxes marking 25th through 75th percentiles are absent from the plots where less than 25% of vectors are screened in.) For scenarios 4 and 5, no vectors were screened in for the CRA26_IS and only a few for the RPPCR. Mean cumulative *to Culebra* releases are listed in Table 17.

AM241L and PU239L are the dominant *to Culebra* releases in both analyses. For scenarios 2-5, the mean cumulative releases of all lumped radionuclides are decreased in the CRA26_IS compared to the RPPCR, attributed to reduced brine flow up the borehole (Docherty and Kim 2025, Table 14). Releases for scenario 6, which utilizes a simpler transport model, are similar in the two analyses. Scenario 6 has the highest total cumulative releases in both analyses.

The complete history of total cumulative *to Culebra* releases is plotted for scenarios 2-6 in Figure 23. The red lines in the figures are mean total cumulative releases. For most simulations, the majority of the releases occur in the first few hundred years after the borehole plug degrades (plug degradation occurs 200 years after the intrusion). For scenario 6, where an E2 intrusion at 1,000 years is followed by an E1 at 2,000 years, most of the releases occur after the E1 intrusion.

Information Only

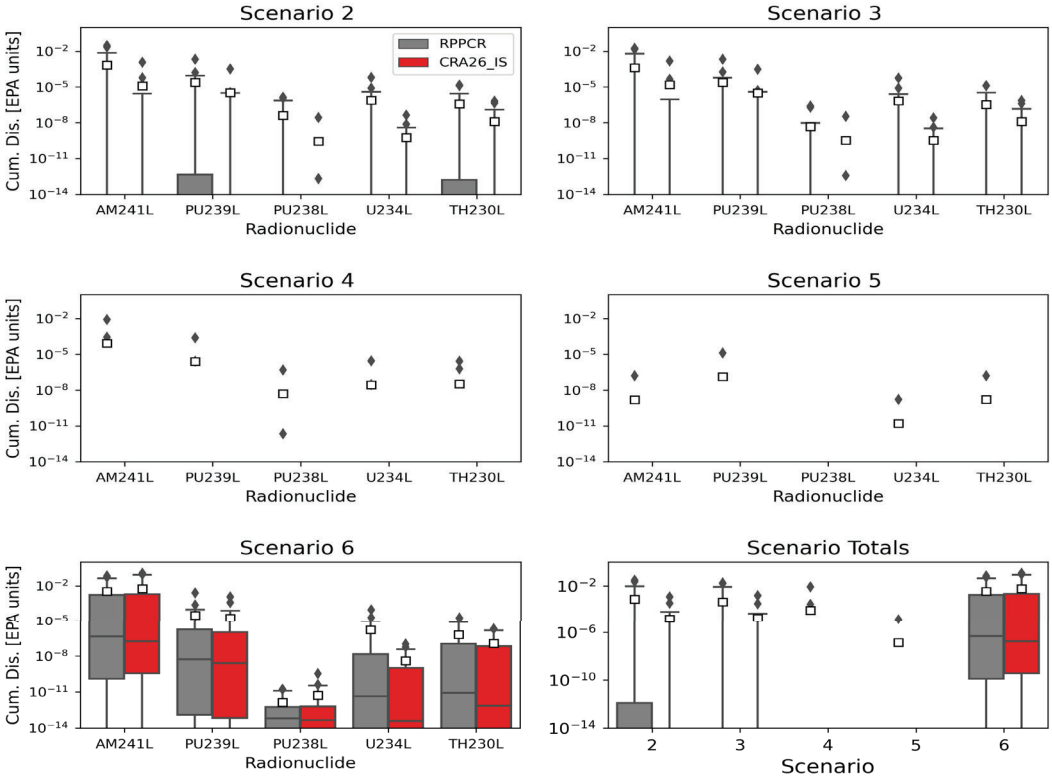


Figure 39 from Docherty and Kim (2025).

Figure 22. Cumulative Lumped Radionuclide Releases

Table 17. Mean Cumulative Lumped Radionuclides Releases Through a Borehole to the Culebra at 10,000 Years in EPA Units

Analysis	Scenario	AM241L	PU239L	PU238L	U234L	TH230L	TOTAL
RPPCR	2	6.99E-04	2.54E-05	4.12E-08	7.69E-07	3.85E-07	7.26E-04
RPPCR	3	4.08E-04	2.44E-05	4.77E-09	6.94E-07	3.50E-07	4.34E-04
RPPCR	4	8.43E-05	2.46E-06	4.90E-09	2.82E-08	3.22E-08	8.69E-05
RPPCR	5	1.58E-09	1.31E-07	2.05E-22	1.65E-11	1.64E-09	1.34E-07
RPPCR	6	3.40E-03	3.19E-05	1.39E-12	1.60E-06	6.23E-07	3.43E-03
CRA26_IS	2	1.23E-05	3.40E-06	2.83E-10	5.71E-10	1.26E-08	1.57E-05
CRA26_IS	3	1.51E-05	3.13E-06	3.46E-10	3.42E-10	1.30E-08	1.83E-05
CRA26_IS	4	0.00E+00	0.00E+00	0.00E+00	0.00E+00	0.00E+00	0.00E+00
CRA26_IS	5	0.00E+00	0.00E+00	0.00E+00	0.00E+00	0.00E+00	0.00E+00
CRA26_IS	6	5.89E-03	1.88E-05	5.34E-12	3.89E-09	1.14E-07	5.91E-03

Table 17 from Docherty and Kim (2025).

Information Only

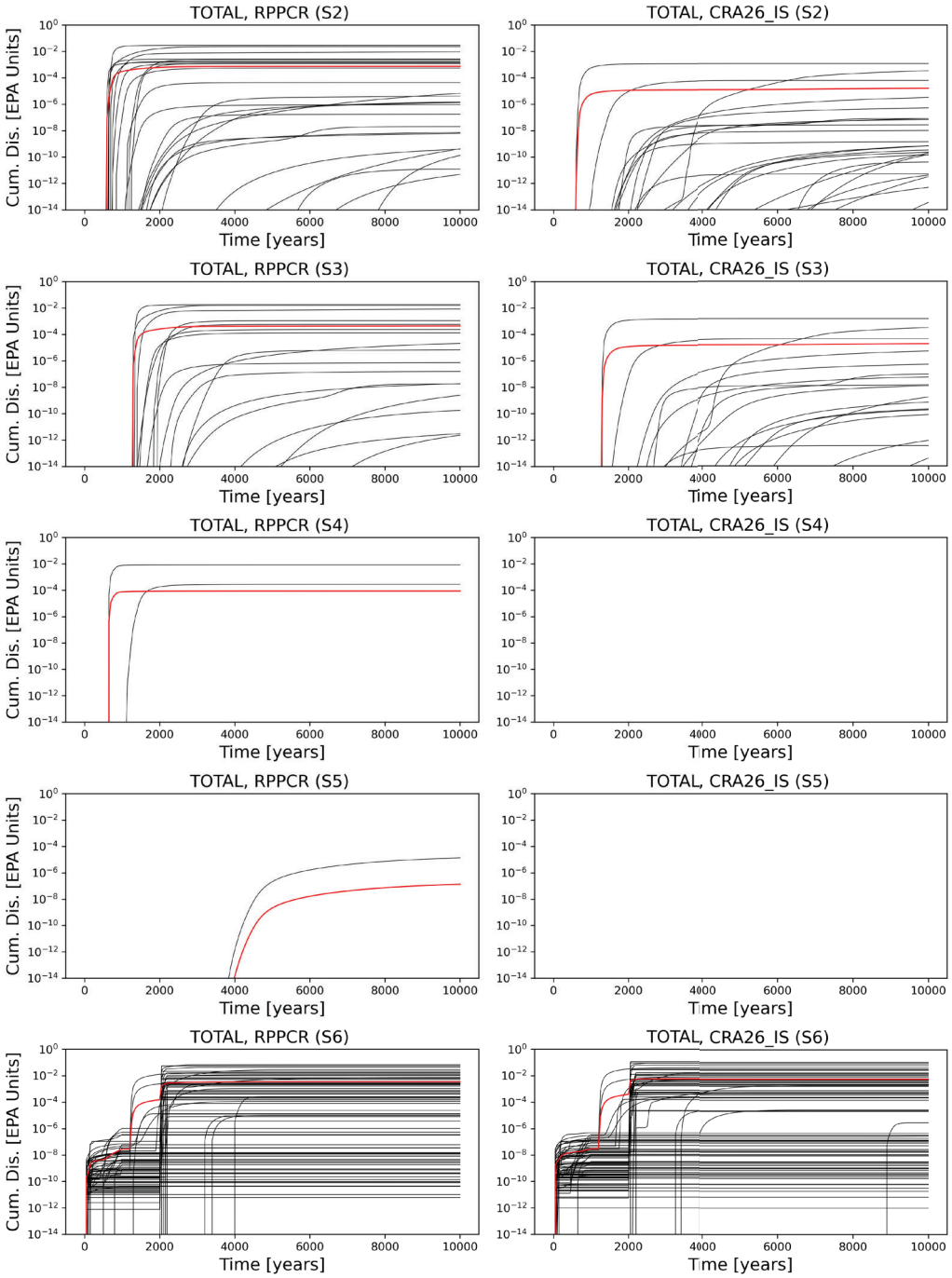


Figure 47 from Docherty and Kim (2025).

Figure 23. Total Cumulative Radionuclide Releases vs Time

Information Only

4.7 Culebra Flow and Transport

This section presents results from the CRA26_IS particle tracking and radionuclide mass transport calculations for full and partial mining scenarios and compares the results to the RPPCR. Flow field results are omitted because they are identical to the RPPCR (Wilgus and Bethune 2025). The only modification made in the CRA26_IS since the RPPCR that impacts results was a small change in the location of CRP 2 (see Section 2.12), the effects of which are insignificant. CRP 1 results are unchanged in the CRA26_IS relative to the RPPCR. A full set of replicate statistics are provided in Wilgus and Bethune (2025).

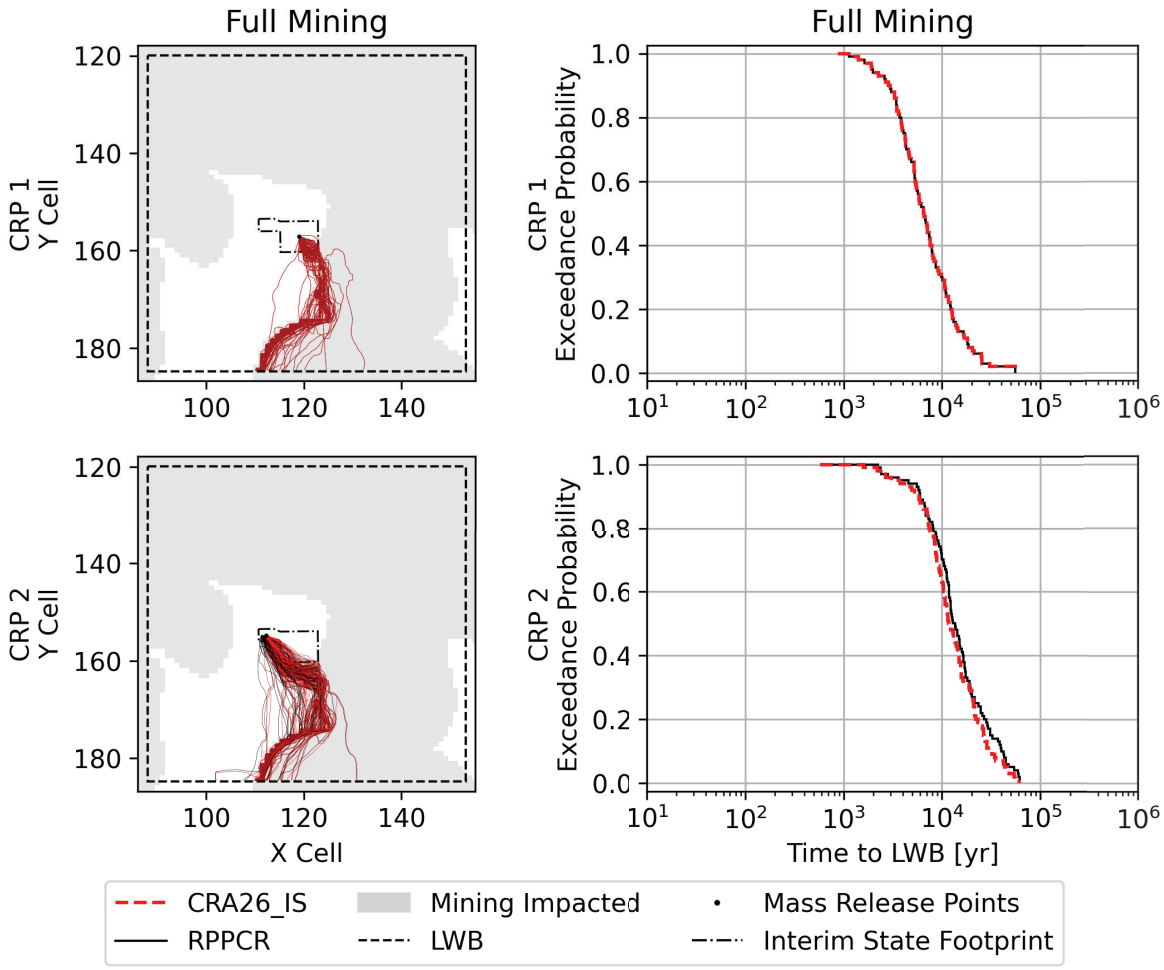
Figure 24 and Figure 25 show the spatial distribution of all 100 particle tracks alongside the cumulative distribution of the time taken for a particle to reach the LWB from each release point for full and partial mining scenarios, respectively. Time to LWB is shown on a logarithmic scale on the x-axis of the cumulative distribution plots from 10 to 10,000 years. Conceptually, the cumulative particle travel time distribution subplots (plotted as exceedance probability) describe the likelihood of a particle crossing the LWB within the range of observed particle travel times.

As in the RPPCR, particle tracks from CRP 1 and CRP 2 show downstream flow generally oriented toward the south. In the full mining scenario, particle tracks show the flow field is typically oriented toward the full mining impacted area to the southeast, then deflects along the mining affected region interface to the southern LWB. The partial mining particle tracks are more broadly distributed across the east-west direction. CRP 2 particle tracks from the CRA26_IS and RPPCR show slight initial differences near the release point, but differences diminish near the LWB. Travel times to the LWB are shorter in the full mining scenario, with travel times from CRP 1 shorter than from CRP 2. Relative to the RPPCR, CRP 2 travel times to the LWB in CRA26_IS are slightly shorter at most probabilities.

Figure 26 and Figure 27 show exceedance probability curves of cumulative mass of each tracked radionuclide reaching the LWB by 10,000 years for full and partial mining scenarios, respectively. Mass discharge is shown on a logarithmic scale on the x-axis from 10^{-9} to 1 kg. Some partial mining scenario subplots display no results due to the low predictions of mass to the LWB.

Cumulative releases at 10,000 years are higher in the full mining scenario than in the partial mining scenario for all radionuclides across all displayed probability ranges. CRP 2 releases are generally lower than CRP 1 for all radionuclides. Amongst the radionuclides, ^{241}Am shows the lowest releases, while ^{234}U, shows the highest releases in both the full and partial mining scenarios. Relative to the RPPCR, CRP 2 cumulative discharge in the CRA26_IS is similar or slightly increased.

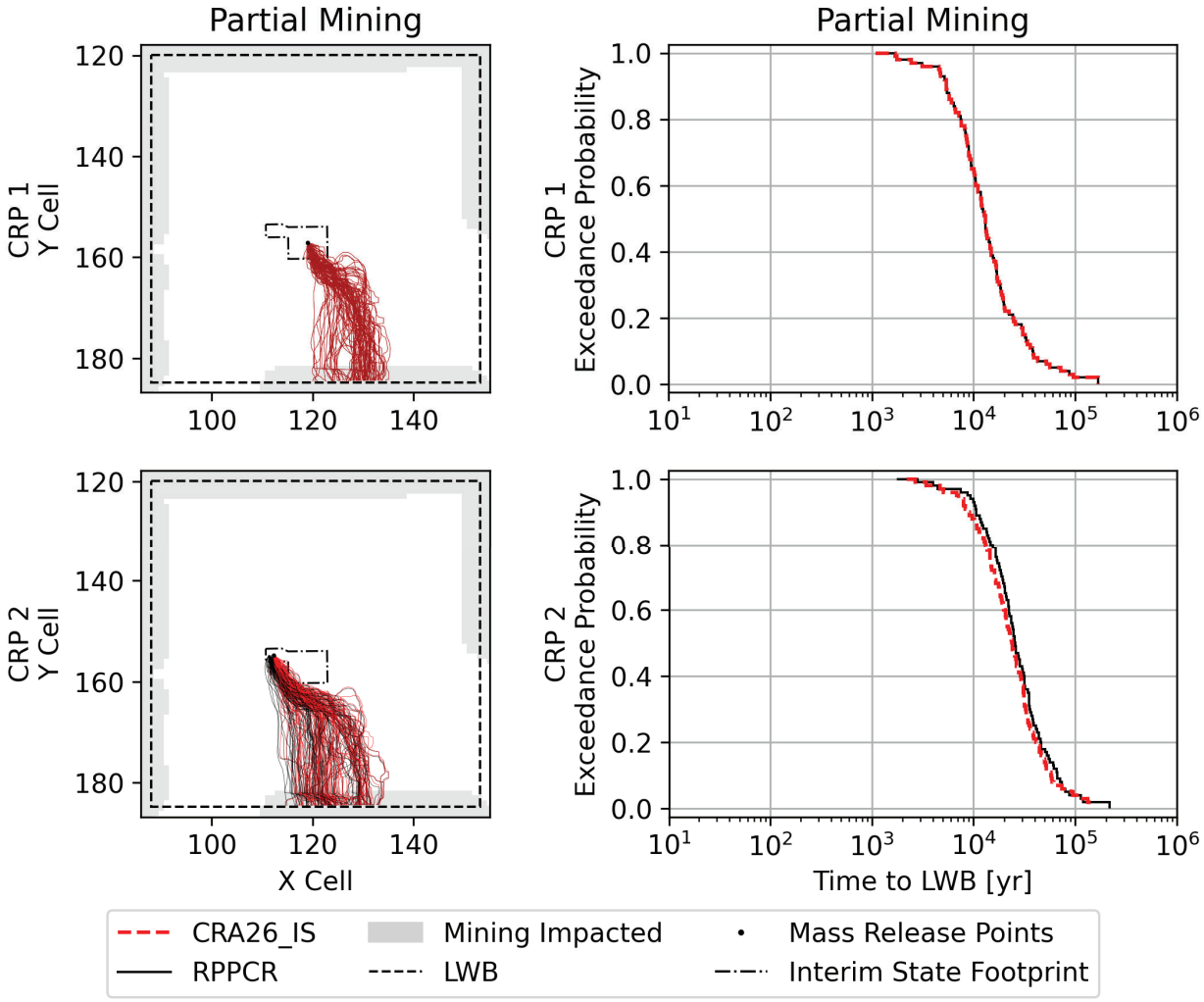
Information Only



Derived from Figure 9 and 10 of Wilgus and Bethune (2025).

Figure 24. Particle Travel Paths and Travel Time to the LWB Exceedance Probabilities, Full Mining Scenario

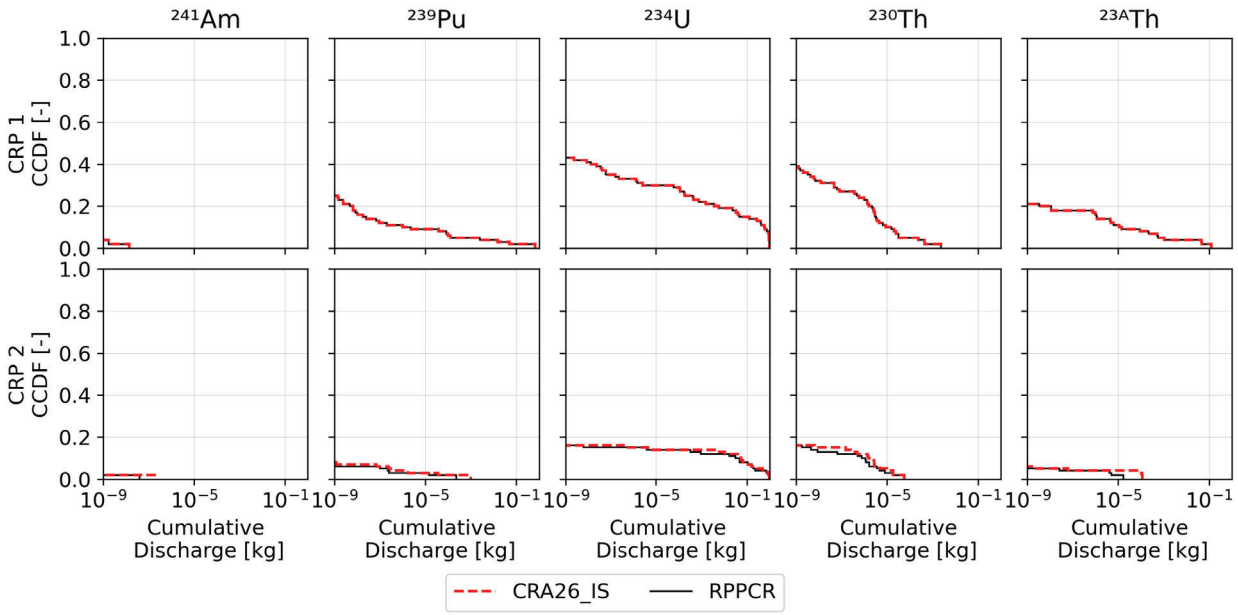
Information Only



Derived from Figure 9 and 10 of Wilgus and Bethune (2025).

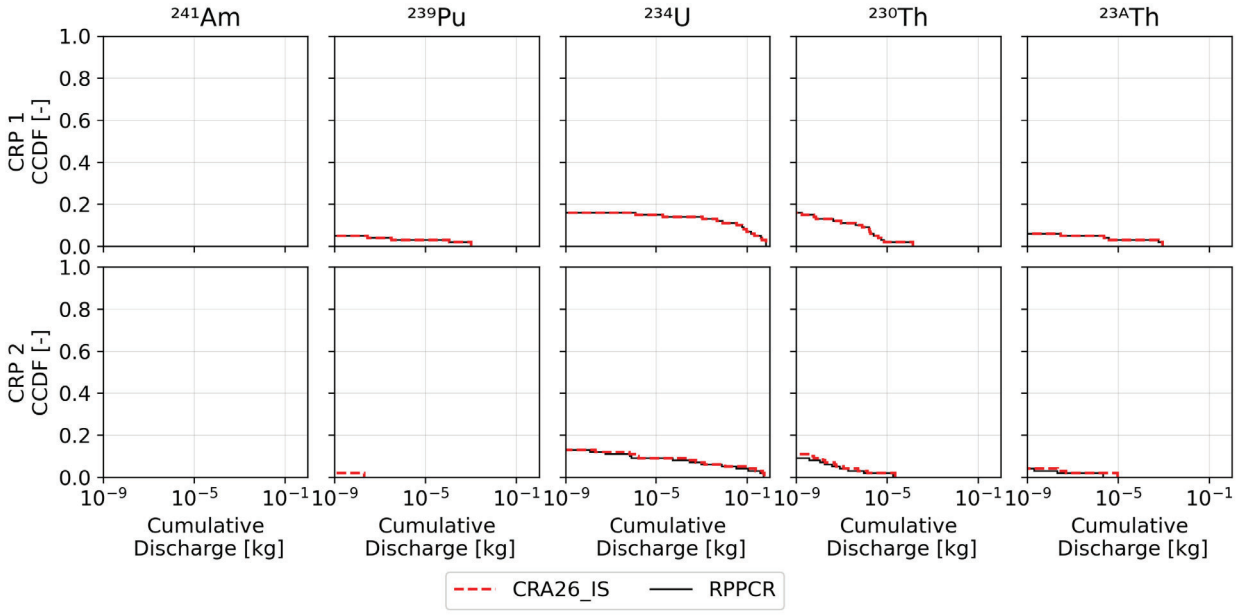
Figure 25. Particle Travel Paths and Travel Time to the LWB Exceedance Probabilities, Partial Mining Scenario

Information Only



Derived from Figures 15 through 19 of Wilgus and Bethune (2025).

Figure 26. Exceedance Probability of Cumulative Mass to the LWB in 10,000 Years for Full Mining Scenario



Derived from Figures 15 through 19 of Wilgus and Bethune (2025).

Figure 27. Exceedance Probability of Cumulative Mass to the LWB in 10,000 Years for Partial Mining Scenario

Information Only

4.8 Releases by Release Mechanism

This section summarizes the results of the CRA26_IS analysis for releases from the undisturbed repository and each of the four disturbed repository release mechanisms (cuttings and cavings, spallings, direct brine releases, and long-term transport releases through the Culebra) that contribute to total releases. The results presented here are based on the normalized release analysis documented in King et al. (2025d). Complementary cumulative distribution functions (CCDFs) of releases for each release pathway are compared to results from the RPPCR analysis. Changes included in the CRA-2026 IS that were observed to most substantially affect release results as compared to the RPPCR are (King et al. 2025d):

- An increase in the drilling rate, which leads to an increase in the number of intrusion events.
- A reduction in the repository footprint, which reduces the number of intrusion events but increases the fractional volume of repository occupied by waste.
- An increase in waste activity concentration, which leads to an increase in activity of solids releases.

4.8.1 Undisturbed Repository Releases

The undisturbed repository performance scenario includes two potential release pathways: transport through the marker beds and transport up the shaft. Screening runs using a non-sorbing, highly soluble tracer determine which vectors had the potential to transport radionuclides to the accessible environment. Full Salado transport simulations are then performed for all screened-in vectors.

As in the RPPCR, no vectors in the CRA26_IS exceed the screening criterion for the undisturbed repository. Consequently, no vectors show radionuclide transport through the Salado to the LWB or through the shafts to the Culebra. These results confirm that radionuclide transport under undisturbed conditions is effectively zero, and no releases from the undisturbed repository are calculated for the CRA26_IS.

4.8.2 Cuttings and Cavings Releases

For each intrusion, cuttings and cavings releases are calculated based on the cuttings volume, cavings volume, and radionuclide concentration of the intersected waste. The cuttings and cavings volumes for individual boreholes in the CRA26_IS are unchanged from the RPPCR. However, the smaller repository footprint and reduced drilling rate in the CRA26_IS results in fewer boreholes per future, leading to smaller cuttings and cavings volumes overall.

Despite the smaller repository footprint, cuttings and cavings waste release volumes are comparable between the CRA26_IS and the RPPCR due to the higher fraction of the repository volume occupied by contact-handled waste (FVW) in the CRA26_IS. Figure 28 shows the mean cuttings and cavings volume scaled by the FVW factor for Replicate 1, illustrating the impact of repository configuration on waste release volumes.

CCDFs for cuttings and cavings releases are presented in Figure 29 for Replicate 1 of the CRA26_IS. The CCDFs show slightly higher releases at lower probabilities in the CRA26_IS

Information Only

compared to the RPPCR, driven by increased radionuclide activity concentrations in the waste inventory. The overall mean cuttings and cavings releases, along with the 95% confidence interval, are presented in Figure 30. Table 18 provides statistics on the overall mean cuttings and cavings release at the compliance limit probabilities.

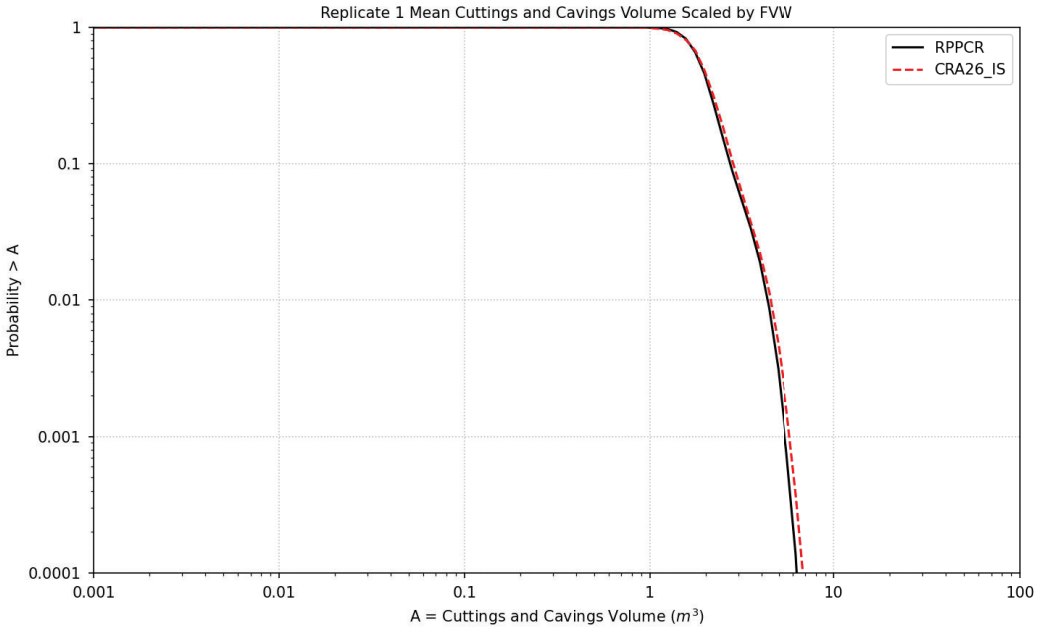


Figure 4 of King et al. (2025d).

Figure 28. Mean Cuttings and Cavings Volume Scaled by the FVW Factor for Replicate 1

Information Only

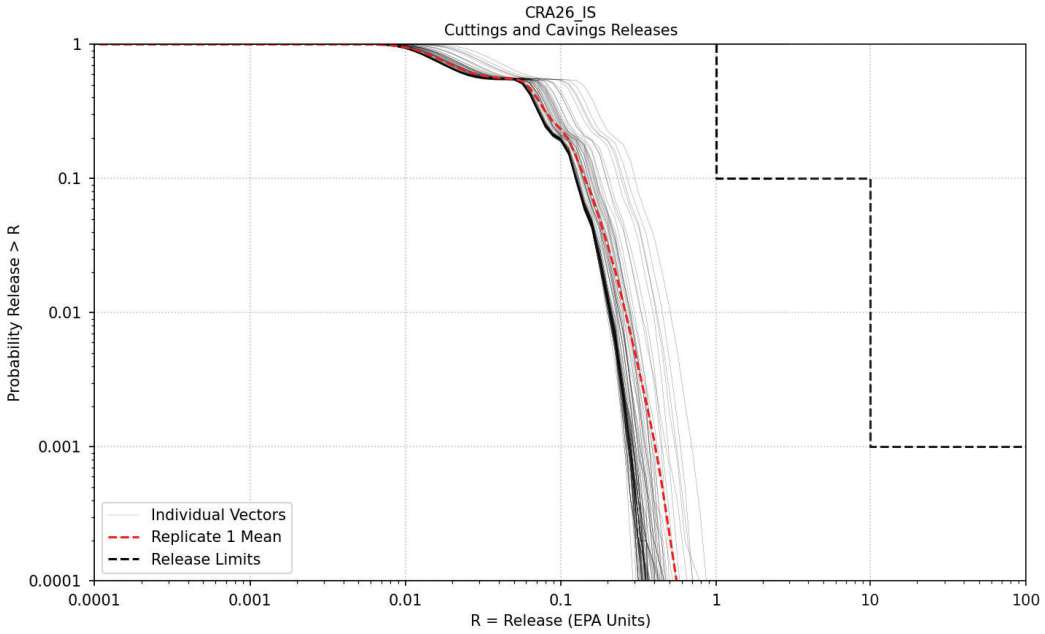


Figure 7 from King et al. (2025d).

Figure 29. Cuttings and Cavings Releases for Replicate 1 of the CRA26_IS

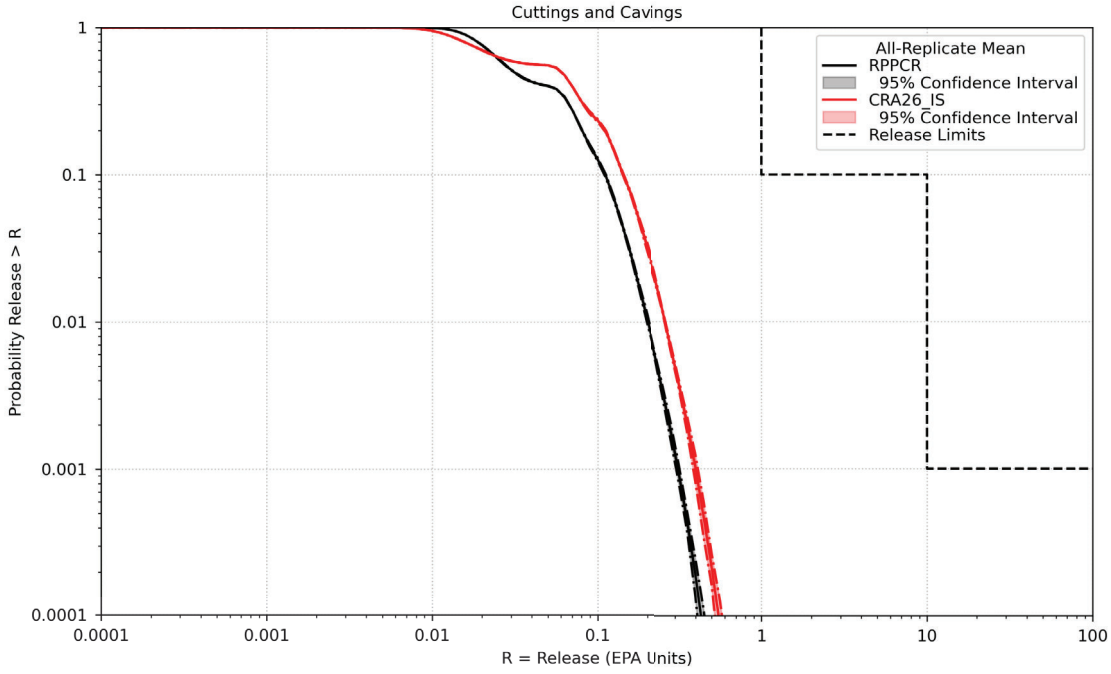


Figure 8 from King et al. (2025d).

Figure 30. Overall Mean Cuttings and Cavings Releases

Information Only

Table 18. Statistics on the Overall Mean Cuttings and Cavings Release

Analysis	P(R)>0.1 Lower CI (EPA Units)	P(R)>0.1 Mean (EPA Units)	P(R)>0.1 Upper CI (EPA Units)	P(R)>0.1 Release Limit (EPA Units)	P(R)>0.001 Lower CI (EPA Units)	P(R)>0.001 Mean (EPA Units)	P(R)>0.001 Upper CI (EPA Units)	P(R)>0.001 Release Limit (EPA Units)
RPPCR	0.1100	0.1111	0.1122	1	0.3074	0.3135	0.3204	10
CRA26_IS	0.1417	0.1429	0.1442	1	0.3898	0.4007	0.4164	10

4.8.3 Spallings Releases

Spallings releases are calculated based on spallings volumes and the average waste activity concentration in contact-handled waste. The combined effect of the smaller repository footprint and the increase in the drilling rate in the CRA26_IS results in fewer boreholes per future and smaller spallings volumes overall. However, when scaled by the FVW factor, spallings waste release volumes in the CRA26_IS are comparable to those observed in the RPPCR. Figure 31 shows the mean spallings volume scaled by the FVW factor for Replicate 1, illustrating the impact of repository configuration on waste release volumes.

CCDFs for spallings releases are presented in Figure 32 for Replicate 1 of the CRA26_IS. The overall mean spallings releases, along with the 95% confidence interval, are presented in Figure 33. Table 19 provides statistics on the overall mean spallings release at the compliance limit probabilities. The values in Table 19 indicate an increase in spallings releases for the CRA26_IS at both compliance limit probabilities. With the spalling waste release volumes being comparable to those in the RPPCR, the increase in releases is mainly attributed to the increase in waste activity concentration, as described in Section and Section 5.2.2 of Brunell and Kicker (2025).

Information Only

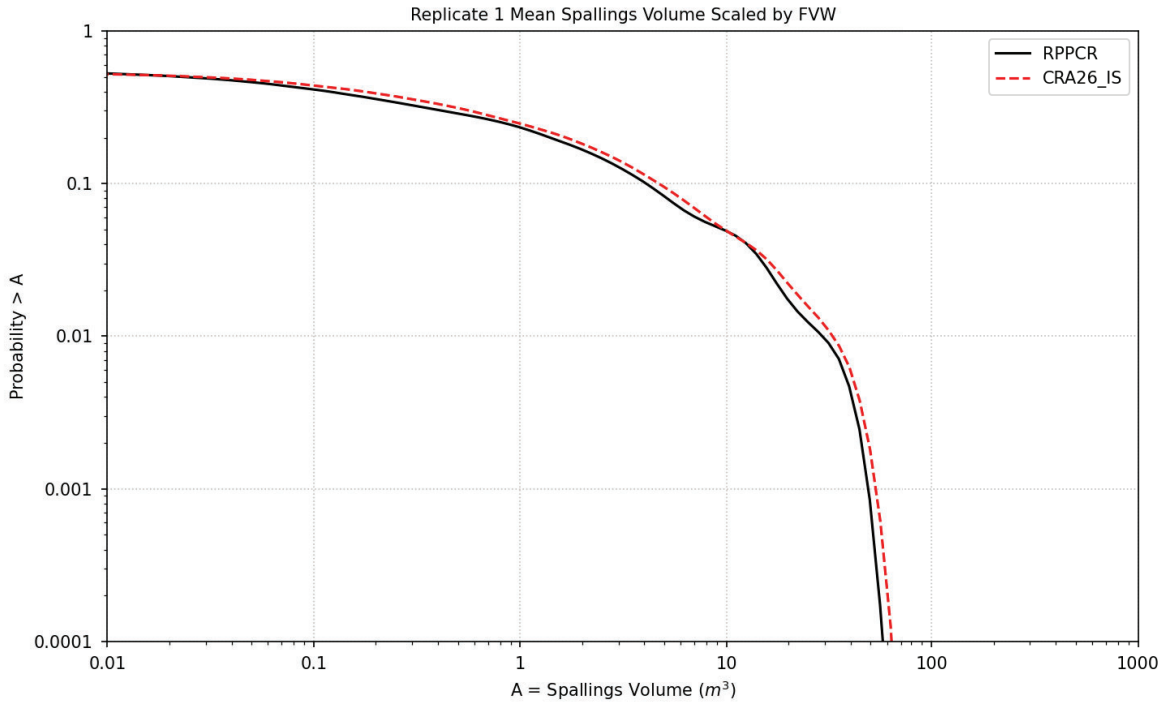


Figure 11 from King et al. (2025d).

Figure 31. Mean Spallings Volume Scaled by the FVW Factor for Replicate 1

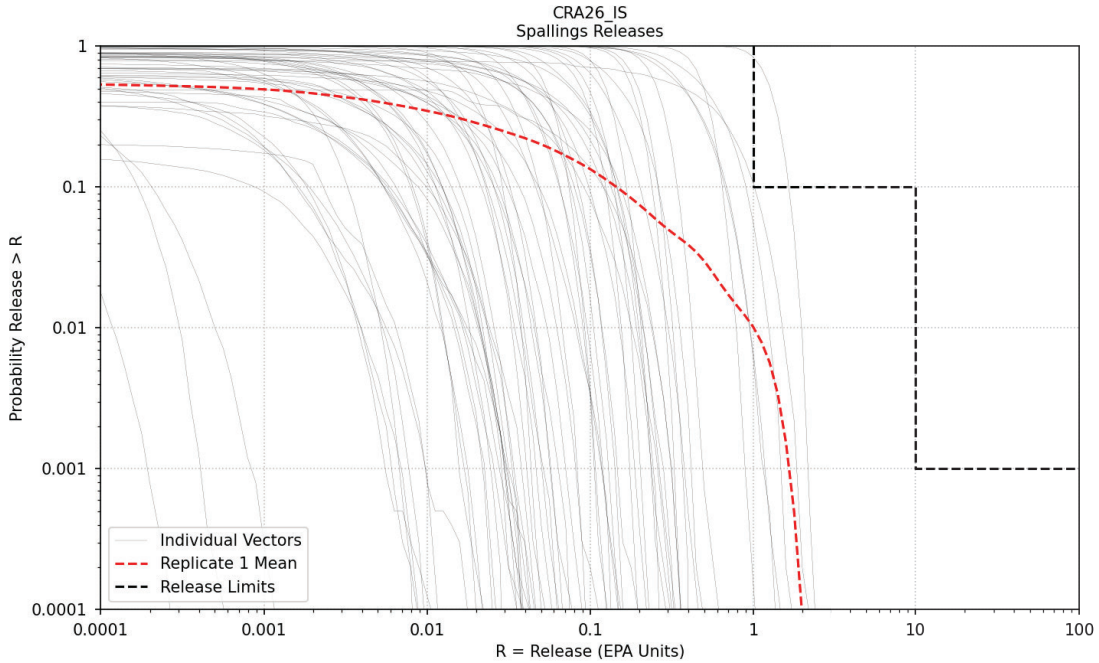


Figure 12 from King et al. (2025d).

Figure 32. Spallings Releases for Replicate 1 of the CRA26_IS

Information Only

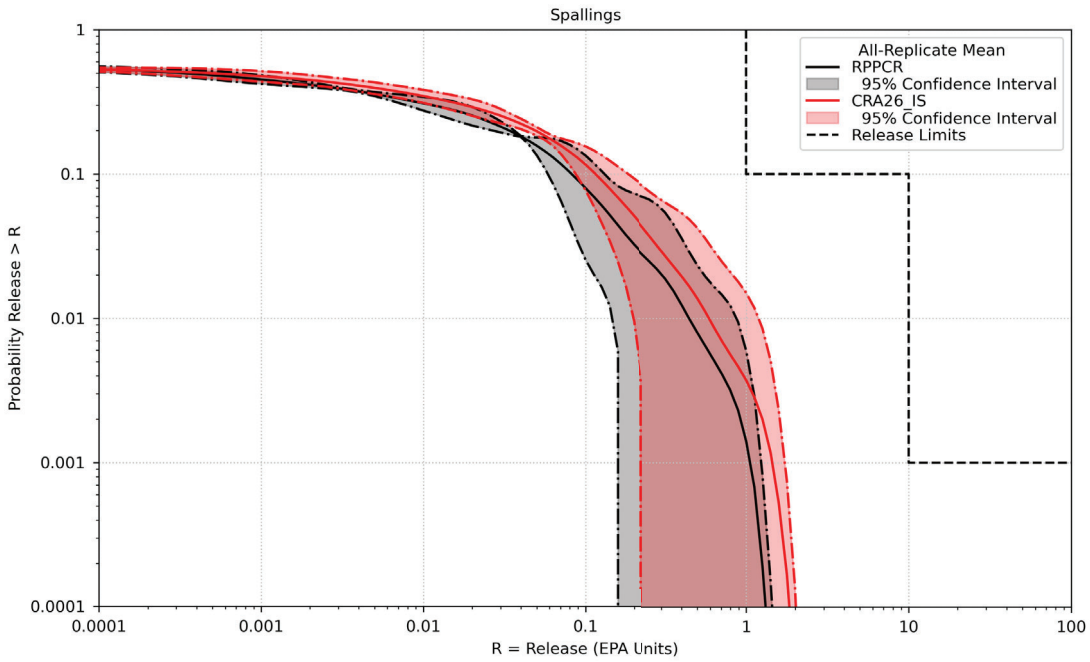


Figure 15 from King et al. (2025d).

Figure 33. Overall Mean Spallings Releases

Table 19. Statistics on the Overall Mean Spallings Release

Analysis	P(R)>0.1 Lower CI (EPA Units)	P(R)>0.1 Mean (EPA Units)	P(R)>0.1 Upper CI (EPA Units)	P(R)>0.1 Release Limit (EPA Units)	P(R)>0.001 Lower CI (EPA Units)	P(R)>0.001 Mean (EPA Units)	P(R)>0.001 Upper CI (EPA Units)	P(R)>0.001 Release Limit (EPA Units)
RPPCR	0.0587	0.0822	0.1312	1	0.1712	1.0674	1.2469	10
CRA26_IS	0.0871	0.1153	0.1833	1	0.2389	1.4579	1.7470	10

4.8.4 Direct Brine Releases

Direct brine releases (DBRs) occur when brine migrates up through an intruding borehole under conditions of sufficient brine pressure and saturation. Figure 34 shows the mean direct brine volume for Replicate 1 of the CRA26_IS, illustrating the combined impacts of repository configuration, drilling rate, and brine saturation/pressure on brine volumes. The mean direct brine volume CCDF is decreased due to: 1) the combined effects of the decreased repository footprint and increased drilling rate leading to a net decrease in the number of intrusions in CRA26_IS; and 2) the decreased brine volumes due to decreased brine saturations and brine pressures (Section 4.4). CCDFs for direct brine releases are presented in Figure 35 for Replicate 1 of the CRA26_IS.

Information Only

Increased mobilized radionuclide concentrations amplify releases. The combined impacts of decreased direct brine volumes and increased mobilized radionuclide concentrations result in a decrease in mean DBRs at higher probabilities and an increase in mean DBRs at lower probabilities, compared to the RPPCR. The result at lower probabilities is thus primarily attributed to increased mobile radionuclide concentrations, as the other changes, on the whole, tend toward DBR decreases. The overall mean direct brine releases, along with the 95% confidence interval, are presented in Figure 36. Table 20 provides statistics on the overall mean direct brine release at the compliance limit probabilities. The values in Table 20 indicate that while direct brine releases are lower at higher probabilities (P(R)>0.1) in the CRA26_IS, they are slightly higher at lower probabilities (P(R)>0.001).

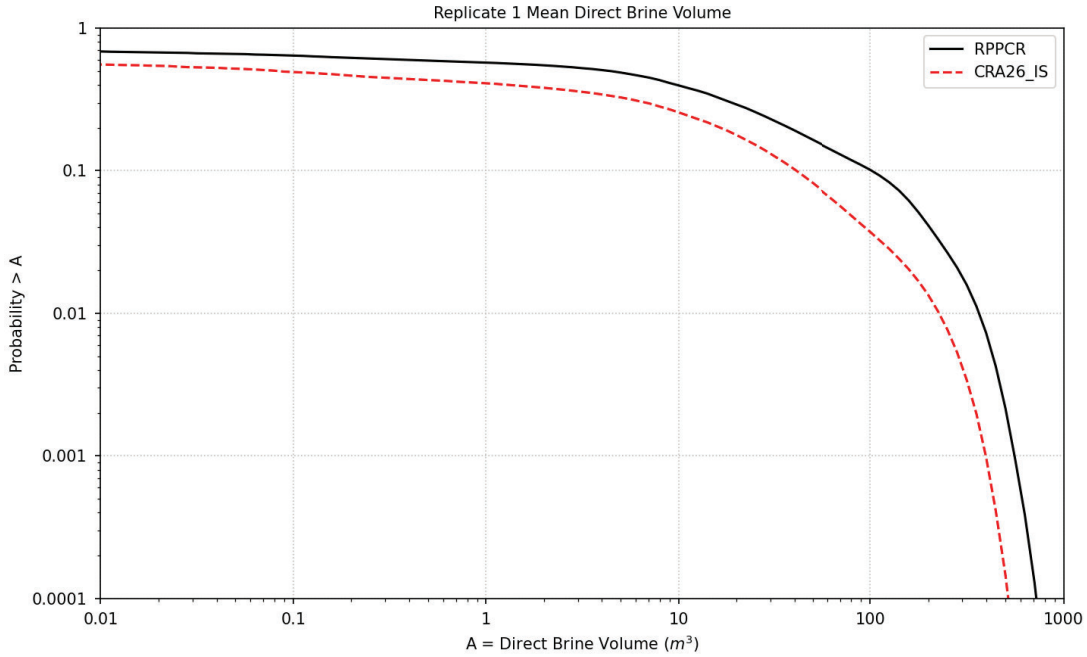


Figure 18 from King et al. (2025d).

Figure 34. Mean Direct Brine Volumes for Replicate 1

Information Only

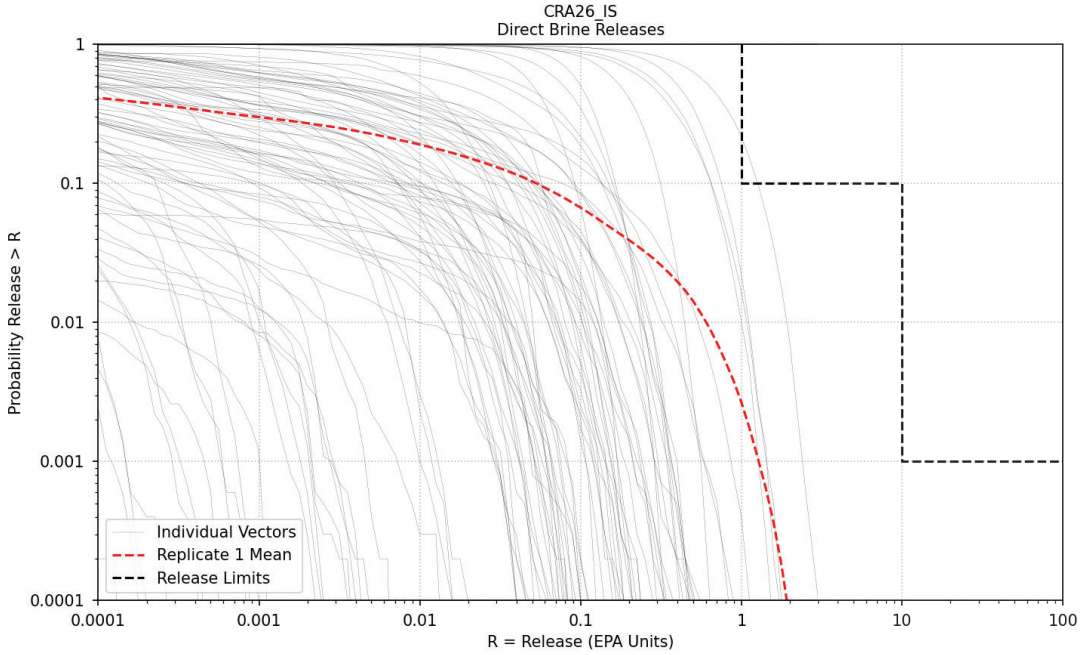


Figure 19 from King et al. (2025d).

Figure 35. Direct Brine Releases for Replicate 1 of the CRA26_IS

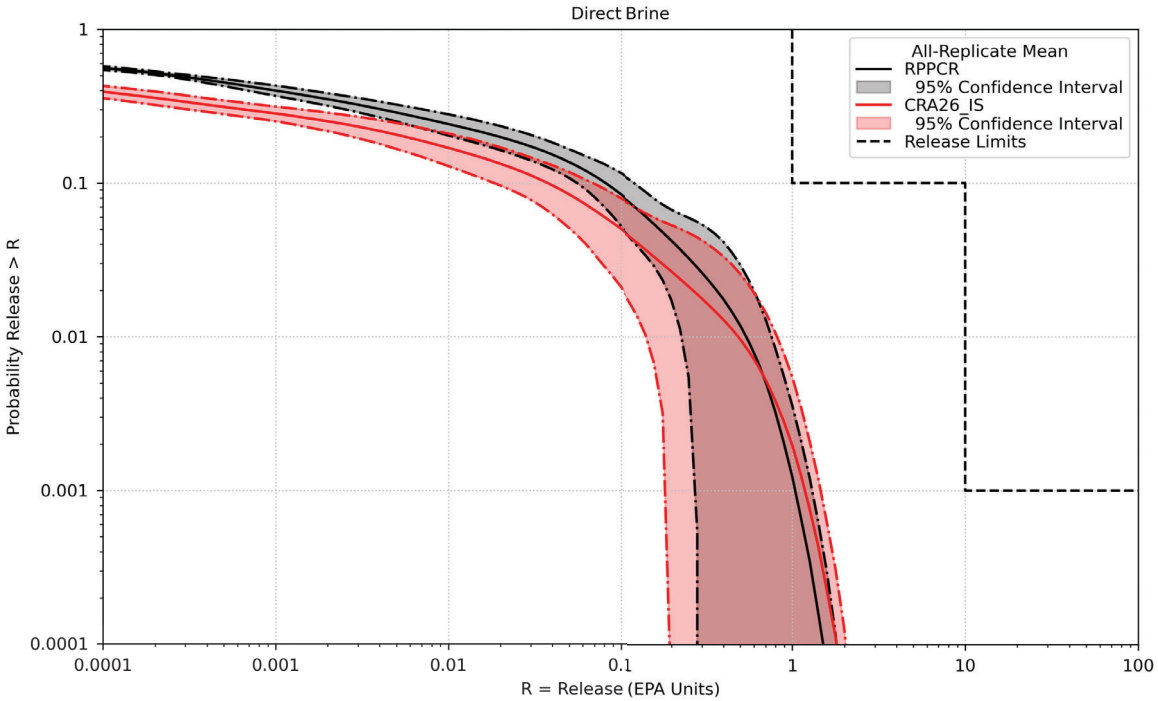


Figure 22 from King et al. (2025d).

Figure 36. Overall Mean Direct Brine Releases

Information Only

Table 20. Statistics on the Overall Mean Direct Brine Release

Analysis	P(R)>0.1 Lower CI (EPA Units)	P(R)>0.1 Mean (EPA Units)	P(R)>0.1 Upper CI (EPA Units)	P(R)>0.1 Release Limit (EPA Units)	P(R)>0.001 Lower CI (EPA Units)	P(R)>0.001 Mean (EPA Units)	P(R)>0.001 Upper CI (EPA Units)	P(R)>0.001 Release Limit (EPA Units)
RPPCR	0.0555	0.0813	0.1217	1	0.2790	1.0485	1.3139	10
CRA26_IS	0.0184	0.0376	0.0685	1	0.1929	1.1927	1.4710	10

4.8.5 Long-Term Radionuclide Transport

4.8.5.1 Activity Entering the Culebra

Activity entering the Culebra represents the radionuclide source term for transport through the Culebra Dolomite Member of the Rustler Formation. This activity is calculated based on brine flow through boreholes intersecting waste panels and is influenced by repository configuration, brine pressure, and radionuclide mobilization mechanisms.

Figure 37 shows the mean activity entering the Culebra by radionuclide for Replicate 1 of the CRA26_IS, illustrating the contributions of individual radionuclides. Activity entering the Culebra is dominated by ^{241}Am, followed by ^{239}Pu, with activity from ^{230}Th and ^{234}U being orders of magnitude smaller. Figure 38 presents the overall mean activity entering the Culebra, along with the 95% confidence interval, for the CRA26_IS. Table 21 provides statistics on the overall mean activity entering the Culebra at the compliance limit probabilities. The values in Table 21 indicate a slight reduction in activity entering the Culebra for the CRA26_IS compared to the RPPCR.

Information Only

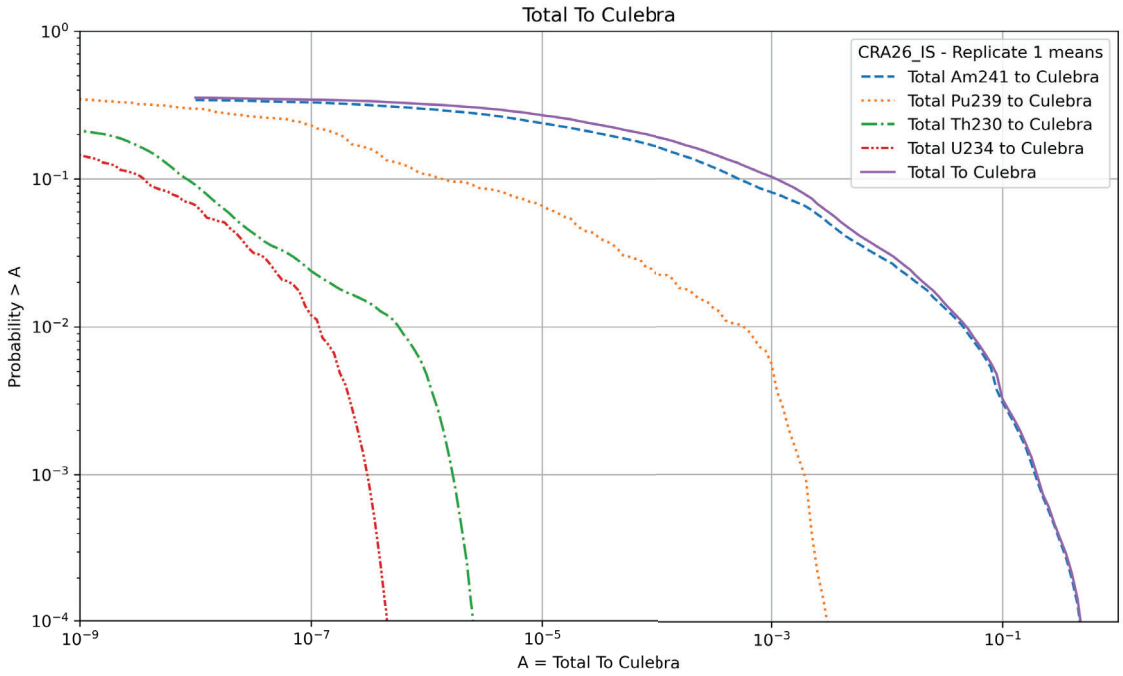


Figure 29 from King et al. (2025d).

Figure 37. Mean Activity Entering the Culebra by Radionuclide for Replicate 1 of the CRA26_IS

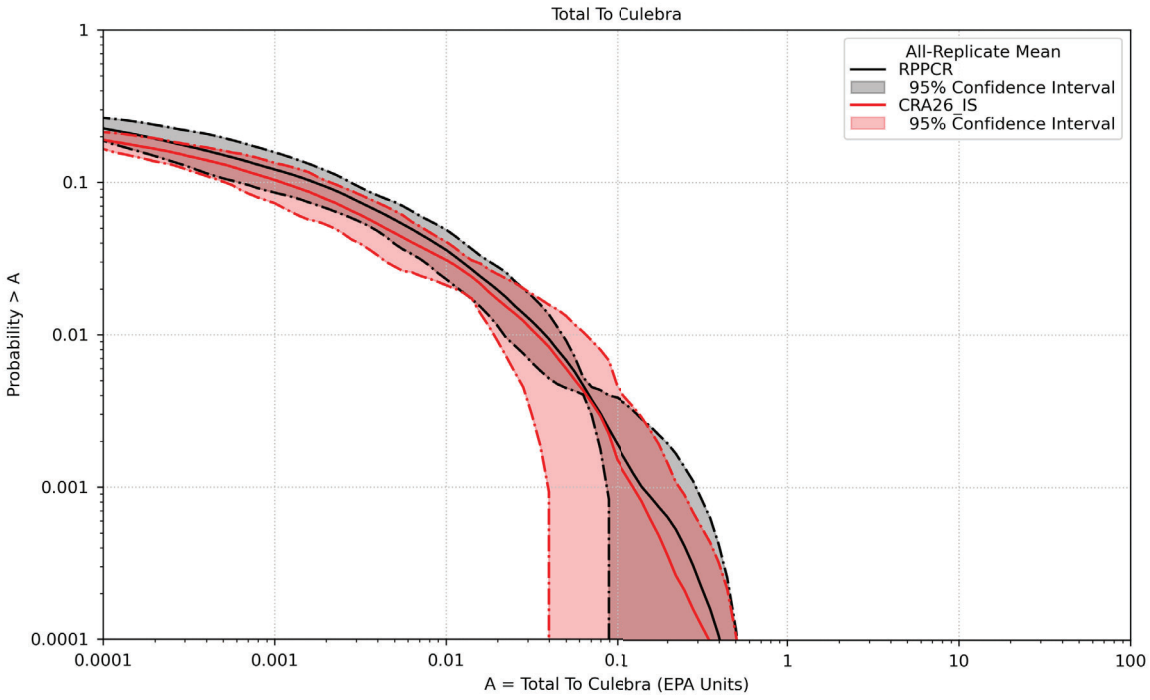


Figure 30 from King et al. (2025d).

Figure 38. Overall Mean Activity Entering the Culebra

Information Only

Table 21. Statistics on the Overall Mean Activity Entering the Culebra

Analysis	P(R)>0.1 Lower CI (EPA Units)	P(R)>0.1 Mean (EPA Units)	P(R)>0.1 Upper CI (EPA Units)	P(R)>0.001 Lower CI (EPA Units)	P(R)>0.001 Mean (EPA Units)	P(R)>0.001 Upper CI (EPA Units)
RPPCR	0.0006	0.0017	0.0028	0.0874	0.1429	0.2954
CRA26_IS	0.0005	0.0011	0.0021	0.0395	0.1263	0.2359

4.8.5.2 Releases Through the Culebra

Releases through the Culebra represent radionuclide activity transported from the Culebra Dolomite Member to the accessible environment. These releases are calculated based on radionuclide transport modeling and are influenced by the activity entering the Culebra, transmissivity fields, and radionuclide decay and sorption processes.

Figure 39 shows the mean releases through the Culebra by radionuclide and release point for Replicate 1 of the CRA26_IS. The x-axis in this figure has been extended to display releases below the normal cutoff of 0.0001 EPA units, highlighting the negligible radionuclide releases through the Culebra for the CRA26_IS. Despite ^{241}Am and ^{239}Pu dominating the activity entering the Culebra (Figure 37), ^{234}U is the principal component of releases through the Culebra. Figure 40 presents the overall mean releases through the Culebra, along with the 95% confidence interval, for the CRA26_IS. However, the mean CRA26_IS results and confidence interval are below the cutoff value of 0.0001 EPA units and do not appear in Figure 40. Table 22 provides statistics on the overall mean releases through the Culebra at the compliance limit probabilities. The values in Table 22 confirm that releases through the Culebra are effectively zero for the CRA26_IS, even at lower probabilities.

The CRA26_IS repository layout uses only the first and second Culebra release points (CRP 1 and CRP 2), as the interim state repository consists of 12 panels. In contrast, the RPPCR included four release points, with CRP 4 experiencing much higher releases due to westerly flow in the mining-impacted region. The exclusion of CRP 4 from the CRA26_IS significantly reduces the potential for radionuclide releases through the Culebra. The slight change of location for CRP 2 (Section 2.12) has little impact on radionuclide transport in the Culebra (Wilgus and Bethune 2025).

Information Only

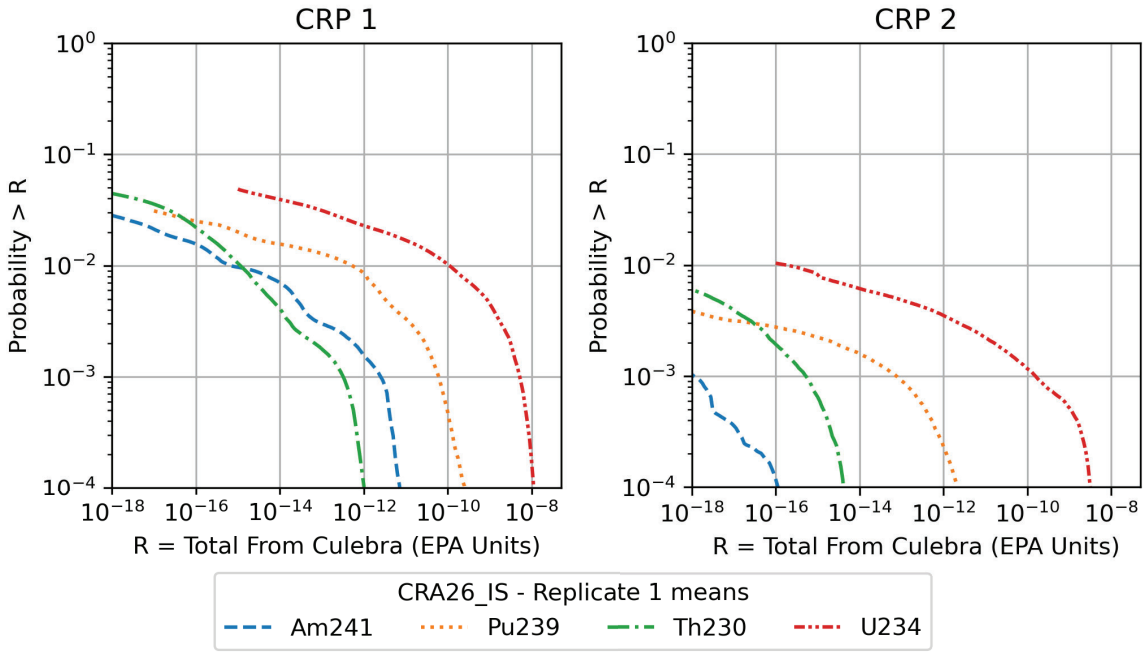


Figure 34 from King et al. (2025d).

Figure 39. Releases Through the Culebra by Radionuclide and Release Point for Replicate 1 of the CRA26_IS

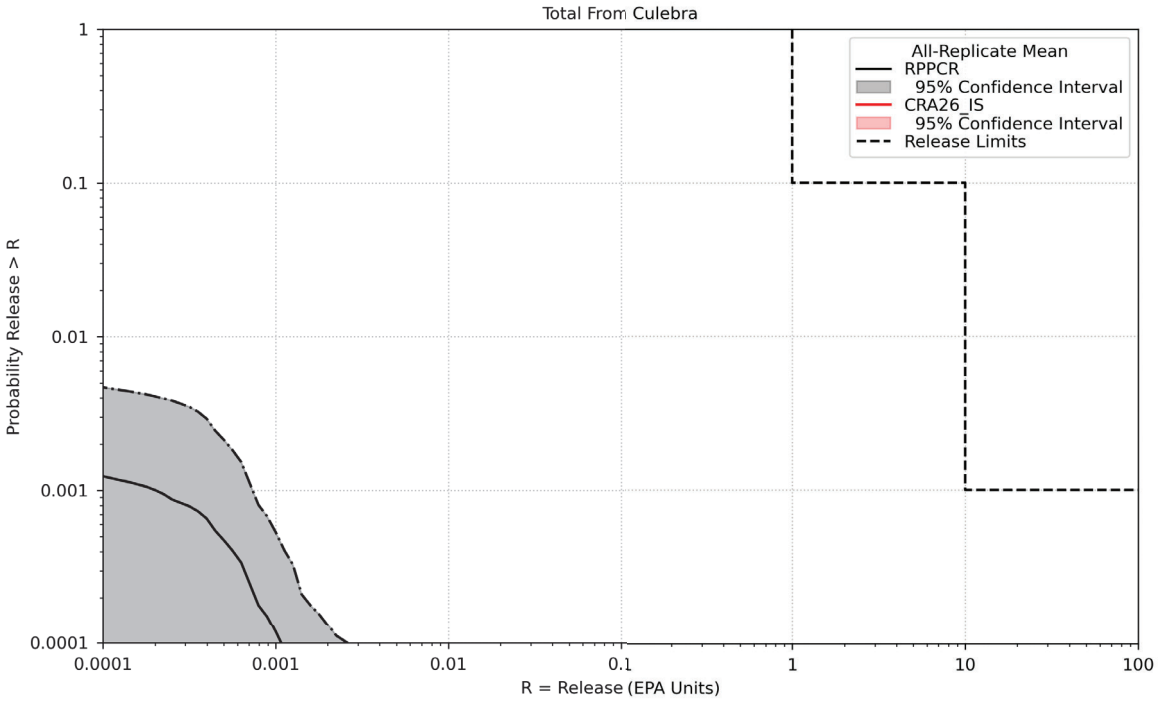


Figure 35 from King et al. (2025d).

Figure 40. Overall Mean Releases Through the Culebra

Information Only

Table 22. Statistics on the Overall Mean Releases Through the Culebra

Analysis	P(R)>0.1 Lower CI (EPA Units)	P(R)>0.1 Mean (EPA Units)	P(R)>0.1 Upper CI (EPA Units)	P(R)>0.1 Release Limit (EPA Units)	P(R)>0.001 Lower CI (EPA Units)	P(R)>0.001 Mean (EPA Units)	P(R)>0.001 Upper CI (EPA Units)	P(R)>0.001 Release Limit (EPA Units)
RPPCR	0.0000	0.0000	0.0000	1	0.0000	0.0002	0.0007	10
CRA26_IS	0.0000	0.0000	0.0000	1	0.0000	0.0000	0.0000	10

4.9 Total Releases

Total releases represent the combined radionuclide releases from all release pathways, including cuttings and cavings, spallings, direct brine releases, and releases through the Culebra. Figure 41 shows the overall mean release components for the CRA26_IS, illustrating the relative contributions of each release pathway to the mean total releases. The overall mean total releases, along with the 95% confidence interval, are presented in Figure 42. Table 23 provides statistics on the overall mean total releases at the compliance limit probabilities.

The values in Table 23 indicate slightly higher total releases for the CRA26_IS compared to the RPPCR at both compliance limit probabilities. This increase is primarily driven by higher spallings and direct brine releases. The CRA26_IS incorporates a waste inventory with higher activity concentrations and more radionuclides with long half-lives, which amplify the impact of spallings releases. Additionally, while the repository footprint is smaller in the CRA26_IS, the waste density (m^3 waste/m^3 repository) and the drilling rate have increased, contributing to the observed increase in total releases.

Despite the increase in total releases, the CRA26_IS results remain well below the regulatory limits of 1 EPA Unit for P(R)>0.1 and 10 EPA Units for P(R)>0.001. These findings demonstrate that the interim state repository continues to comply with containment requirements under 40 CFR Part 191.

Information Only

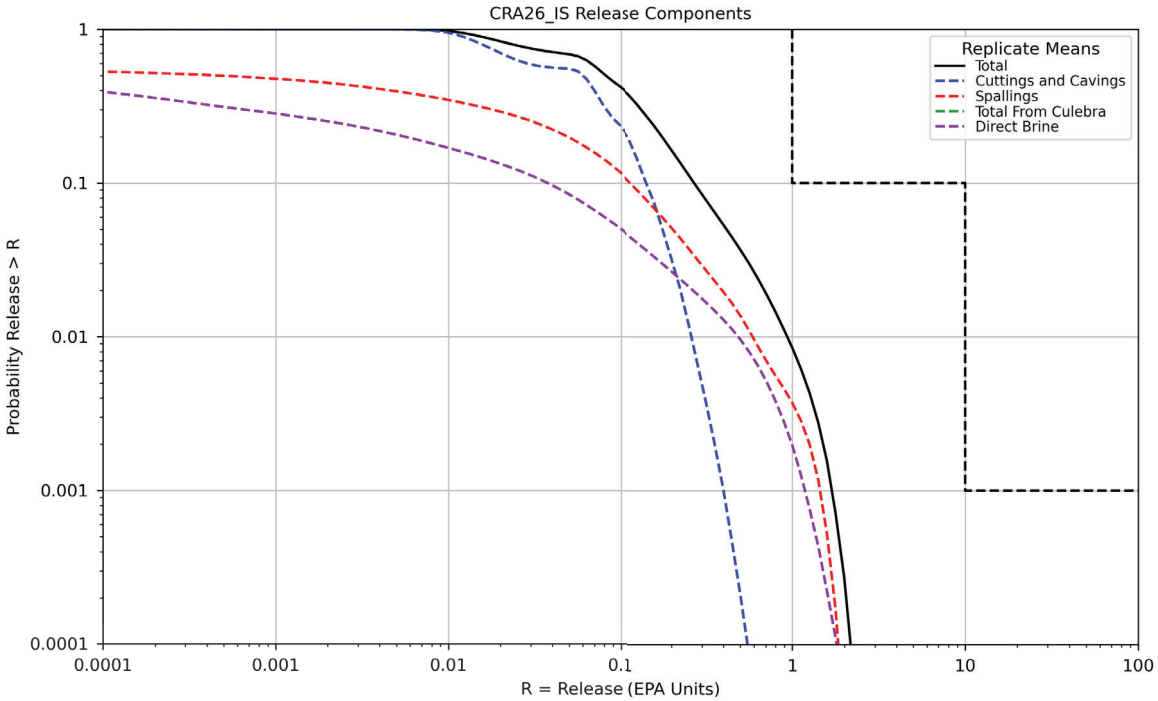


Figure 40 from King et al. (2025d).

Figure 41. Overall Mean Releases Components for the CRA26_IS

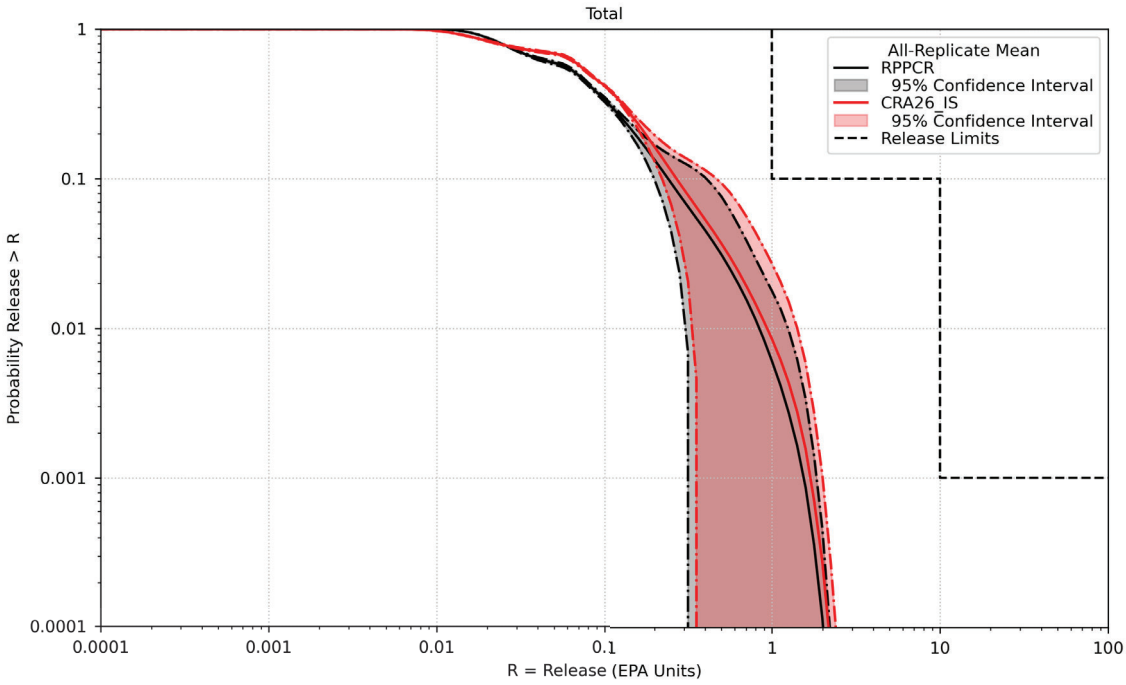


Figure 41 from King et al. (2025d).

Figure 42. Overall Mean Total Releases

Information Only

Table 23. Statistics on the Overall Mean for Total Release

Analysis	P(R)>0.1 Lower CI (EPA Units)	P(R)>0.1 Mean (EPA Units)	P(R)>0.1 Upper CI (EPA Units)	P(R)>0.1 Release Limit (EPA Units)	P(R)>0.001 Lower CI (EPA Units)	P(R)>0.001 Mean (EPA Units)	P(R)>0.001 Upper CI (EPA Units)	P(R)>0.001 Release Limit (EPA Units)
RPPCR	0.1990	0.2418	0.4073	1	0.3360	1.5541	1.8716	10
CRA26_IS	0.2219	0.2713	0.4679	1	0.3678	1.7121	2.0062	10

4.9.1 Sensitivity Analysis for Total Releases

In the sensitivity analysis results, the cumulative R^2 value represents the proportion of total uncertainty explained by the fitted rank regression using the listed variables, starting with the greatest contributor to the variance. The number of variables used in the regression model is determined by the stepwise regression procedure (King et al. 2025d). Regression analyses are conducted for each replicate separately, so results for the CRA26_IS and the RPPCR analyses are therefore compared on a per-replicate basis.

To aid in interpretation and discussion of the results, highlighting indicates parameters with a change in R^2 greater than 0.05 between the current step and the previous step. While this threshold of 0.05 is somewhat arbitrary, the highlighted parameters are clearly influential and tend to have a more consistent ranking. For a full discussion of STEPWISE, see Appendix A of King et al. (2025d).

Sensitivity analysis for mean total releases was conducted to identify the parameters contributing most to variability in total releases. Table 24, Table 25, and Table 26 summarize the stepwise ranked regression analysis results for each replicate of the CRA26_IS and RPPCR analyses. Across all replicates and both analyses, the porosity of intact Salado halite (S_HALITE:POROSITY) consistently emerged as the dominant parameter influencing variability in mean total releases.

In the CRA26_IS analysis, S_HALITE:POROSITY explains 18–27% of the variability in mean total releases, compared to 27–36% in the RPPCR analysis. This parameter's influence is attributed to its significant impact on repository pressure and brine saturation, which directly affect spallings and direct brine release volumes.

Other notable parameters include:

- BOREHOLE:TAUFAIL: This parameter, representing waste shear strength, was the second most influential across both analyses, explaining 6–13% of variability in total releases for the CRA26_IS. Its importance is tied to its role in cuttings and cavings releases.
- SPALLMOD:PARTDIAM: Particle diameter for spallings showed increased influence in the CRA26_IS, explaining up to 17% of variability, compared to 2–8% in the RPPCR. This reflects the increased contributions from spallings releases in the CRA26_IS due to changes in the waste inventory.

Information Only

The CRA26_IS analysis generally showed lower cumulative R^2 values across steps compared to the RPPCR, indicating slightly less variability explained by the regression models.

Overall, the sensitivity analysis results demonstrate that S_HALITE:POROSITY, BOREHOLE:TAUFAIL, and SPALLMOD:PARTDIAM are the primary drivers of variability in total releases for both the RPPCR and CRA26_IS. The CRA26_IS results show slightly higher variability for SPALLMOD:PARTDIAM, likely due to increased contributions from spallings releases driven by changes in the waste inventory.

Table 24. Stepwise Ranked Regression Analysis for Mean Total Releases for Replicate 1 of the RPPCR and CRA26_IS

	RPPCR Replicate 1			CRA26_IS Replicate 1		
Step [a]	Variable [b]	R^2 [c]	SRRC [d]	Variable	R^2	SRRC
1	S_HALITE:POROSITY	0.35	0.57	S_HALITE:POROSITY	0.27	0.49
2	BOREHOLE:TAUFAIL	0.41	-0.26	SPALLMOD:PARTDIAM	0.33	-0.25
3	CASTILER:PRESSURE	0.47	0.25	BOREHOLE:TAUFAIL	0.39	-0.23
4	SOLMOD3:SOLVAR	0.50	0.17	CASTILER:PRESSURE	0.43	0.22
5	STEEL:CORRMCO2	0.53	-0.19	STEEL:CORRMCO2	0.47	-0.22
6	WAS_AREA:PROBDEG	0.56	0.16	WAS_AREA:PROBDEG	0.49	0.17
7	DRZ_1:PRMX_LOG	0.58	0.16	SOLMOD3:SOLVAR	0.52	0.16
8	SPALLMOD:PARTDIAM	0.60	-0.14	SPALLMOD:REPIPERM	0.54	0.15
9	S_MB139:PRMX_LOG	0.62	0.14			

[a] Steps in stepwise regression analysis
[b] Variables listed in order of selection
[c] Cumulative R^2 value with entry of each variable into regression model
[d] Standardized Rank Regression Coefficient

Information Only

Table 25. Stepwise Ranked Regression Analysis for Mean Total Releases for Replicate 2 of the RPPCR and CRA26_IS

	RPPCR Replicate 2			CRA26_IS Replicate 2		
Step [a]	Variable [b]	R^2 [c]	SRRC [d]	Variable	R^2	SRRC
1	S_HALITE:POROSITY	0.36	0.61	S_HALITE:POROSITY	0.24	0.51
2	BOREHOLE:TAUFAIL	0.43	-0.28	BOREHOLE:TAUFAIL	0.31	-0.28
3	CASTILER:PRESSURE	0.51	0.28	GLOBAL:PBRINE	0.37	0.26
4	GLOBAL:PBRINE	0.56	0.22	CASTILER:PRESSURE	0.42	0.23
5	DRZ_1:PRMX_LOG	0.58	0.17	SPALLMOD:PARTDIAM	0.47	-0.23
6	WAS_AREA:BIOGENFC	0.60	0.14	WAS_AREA:BIOGENFC	0.50	0.19
7	SOLMOD3:SOLVAR	0.62	0.14	BH_SAND:PRMX_LOG	0.53	-0.15
8	SPALLMOD:PARTDIAM	0.64	-0.14	SOLMOD3:SOLVAR	0.55	0.16
9	BH_SAND:PRMX_LOG	0.66	-0.12	WAS_AREA:GRATMICI	0.58	0.16
10				STEEL:CORRMCO2	0.60	-0.14

[a] Steps in stepwise regression analysis
[b] Variables listed in order of selection
[c] Cumulative R^2 value with entry of each variable into regression model
[d] Standardized Rank Regression Coefficient

Table 26. Stepwise Ranked Regression Analysis for Mean Total Releases for Replicate 3 of the RPPCR and CRA26_IS

	RPPCR Replicate 3			CRA26_IS Replicate 3		
Step [a]	Variable [b]	R^2 [c]	SRRC [d]	Variable	R^2	SRRC
1	S_HALITE:POROSITY	0.27	0.49	S_HALITE:POROSITY	0.18	0.39
2	BOREHOLE:TAUFAIL	0.43	-0.39	SPALLMOD:PARTDIAM	0.35	-0.38
3	SPALLMOD:PARTDIAM	0.51	-0.28	BOREHOLE:TAUFAIL	0.48	-0.35
4	CASTILER:PRESSURE	0.55	0.20	(Composite):MKD_U	0.51	-0.15
5	SOLMOD3:SOLVAR	0.58	0.17	CASTILER:PRESSURE	0.54	0.18
6	(Composite):MKD_U	0.61	-0.18	WAS_AREA:SAT_WICK	0.57	0.14
7	WAS_AREA:SAT_WICK	0.64	0.17	WAS_AREA:GRATMICH	0.59	0.15
8	DRZ_PCS:PRMX_LOG	0.66	-0.14	WAS_AREA:BIOGENFC	0.61	0.15
9				SPALLMOD:REPIPOR	0.63	-0.14
10				S_HALITE:PRESSURE	0.64	-0.13
11				GLOBAL:PBRINE	0.66	0.13

[a] Steps in stepwise regression analysis
[b] Variables listed in order of selection
[c] Cumulative R^2 value with entry of each variable into regression model
[d] Standardized Rank Regression Coefficient

Information Only

4.9.2 Comparison to CRA-2019

In this section, overall mean total releases from the CRA26_IS are compared to releases from the 2019 Compliance Recertification Application (CRA19) releases. Releases are illustrated in Figure 43, with corresponding statistics provided in Table 27. Mean total releases for the CRA26_IS have increased compared to the CRA19. Additionally, the 95% confidence interval for the mean total release has expanded at lower probabilities since the CRA19.

The drivers for increased releases identified by Brunell et al. (2023) between the RPPCR and the CRA19 continue to apply to the increases observed between the CRA19 and the CRA26_IS. These changes include increased drilling frequency, factors contributing to heightened repository pressures, and increased radionuclide activity, which collectively contribute to the overall increase in releases.

Since there are no calculated releases from the repository in the undisturbed scenario, all releases are contingent upon drilling intrusions, making release levels highly sensitive to the frequency of drilling events. For the CRA26_IS calculation, the frequency of drilling events (parameter GLOBAL:LAMBDAD) was set at 1.534×10^{-2} boreholes/km^2/yr, representing a 55% increase from the 0.99×10^{-2} boreholes/km^2/yr value used in CRA19.

Brine pressure in the repository drives both spallings and direct brine releases, which have increased from CRA19 to CRA26_IS. The updated salt creep closure model predicts faster closure of the salt with smaller waste area porosity values, leading to higher pressures in the repository. Additionally, the increased inventory—comprising radionuclide activity, iron mass, and CPR mass—contributes to greater gas generation, further elevating repository pressures.

Finally, because releases are quantified in EPA units (a measure of activity normalized to the activity at closure), an increase in radionuclide activity does not necessarily lead to increased releases. However, the rise in radionuclide activity since CRA19 is driven by increases in long half-life radionuclides. This results in an increase in normalized activity over time, which in turn contributes to increased releases.

Information Only

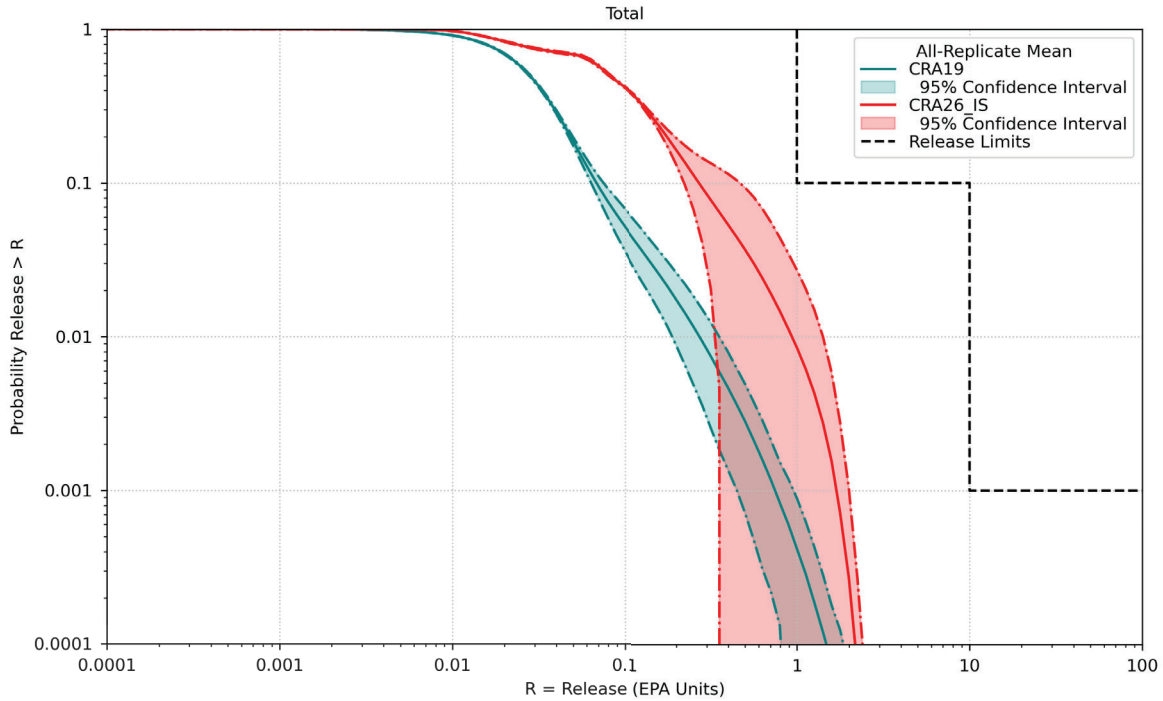


Figure 43. Overall Mean Total Releases

Table 27. Statistics on the Overall Mean for Total Release

Analysis	P(R)>0.1 Lower CI (EPA Units)	P(R)>0.1 Mean (EPA Units)	P(R)>0.1 Upper CI (EPA Units)	P(R)>0.1 Release Limit (EPA Units)	P(R)>0.001 Lower CI (EPA Units)	P(R)>0.001 Mean (EPA Units)	P(R)>0.001 Upper CI (EPA Units)	P(R)>0.001 Release Limit (EPA Units)
CRA19	0.0636	0.0685	0.0753	1	0.4487	0.7505	0.9595	10
CRA26_IS	0.2219	0.2713	0.4679	1	0.3678	1.7121	2.0062	10

Information Only

5.0 CONCLUSIONS

The CRA-2026 Interim State Repository Performance Assessment (CRA26_IS PA) supports the DOE's 2026 recertification application as described in Certification Criteria of Title 40 CFR Part 194. All previous WIPP certifications have been based on a repository consisting of the 10 original panels. In July 2025, the DOE received EPA approval for waste emplacement in two new panels, referred to as replacement panels, located to the west of the existing operations area (Bollinger 2024).

The addition of the two replacement panels is not expected to provide sufficient space for the disposal of the allowable waste volume designated for the WIPP under the Land Withdrawal Act (LWA). The 12-panel configuration considered in the CRA26_IS PA is thus regarded as an interim state of the repository. The DOE may seek approval for waste disposal in up to seven additional panels to accommodate the full allowable volume of waste. The 19-panel configuration is considered the anticipated final state of the repository. The RPPCR considered a 19-panel repository configuration.

Several changes beyond the number of panels have been incorporated into the CRA26_IS since the RPPCR, including updates to the following items: drilling rate, borehole plugging pattern probabilities, inventory, oxidation state model, baseline solubilities, solubility uncertainty distributions, MgO hydration parameters, the minimum brine volume needed for a DBR to occur, the location of Culebra release point 2, and colloid enhancement parameters.

There is a slight increase in mean total releases for the CRA26_IS compared to the RPPCR. This is mainly due to higher contributions of spallings and direct brine releases. The CRA26_IS incorporates a waste inventory with higher activity concentrations and more radionuclides with long half-lives, which amplify spalling releases. Additionally, while the volume of waste is reduced in the CRA26_IS compared to the RPPCR, the waste density (m^3 waste/m^3 repository) has increased. The inventory changes, along with the combined effect of the increased drilling rate, reduced repository footprint, and increased waste density in the CRA26_IS, contribute to the observed increase in total releases compared to the RPPCR.

Mean total releases in the CRA26_IS continue to be defined by direct releases: by cuttings and cavings at high probabilities, and by spallings and DBRs at lower probabilities. Releases from the Culebra provide a miniscule contribution to total releases.

Mean total releases from the CRA26_IS are below the regulatory limits. As a result, the 2026 Compliance Recertification Application PA for the interim state repository demonstrates that the WIPP repository with two replacement panels remains in compliance with the containment requirement of 40 CFR Part 191.

Information Only

REFERENCES

Bethune, J. 2023. Culebra Flow and Transport Analysis Report for the Replacement Panels Planned Change Request (RPPCR). ERMS 579725. Carlsbad, NM: Sandia National Laboratories.

Beauheim, R.L., and Holt, R.M. 1990. Hydrogeology of the WIPP site, in Powers, D.W., Holt, R.M., Beauheim, R.L., and Rempe, N., eds., Geological and Hydrological Studies of Evaporites in the Northern Delaware Basin for the Waste Isolation Pilot Plant (WIPP): Guidebook 14. Geological Society of America (Dallas Geological Society), p. 45-78.

Bollinger, M. 2024. Letter to Ms. L. Veal. Subject: Planned Change Request for the use of Replacement Panels 11 and 12. March 12, 2024. CBFO:ERCD:MG:SV:24-0168. Carlsbad, NM: U.S. DOE, Carlsbad Field Office.

Bowman, D., R. Kushnereit, M. Pedrazas, P. Johnson, N. Deeds, and J. Pinkard. 2023. Analysis Report Documenting the Data, Generation, and Calibration of T-fields for CRA-2024. ERMS 579507. Carlsbad, NM: Sandia National Laboratories.

Brunell, S. 2025. Update to CRA-2026 PA Input Parameters Due to Revised WIPP Repository Dimensions. EIMS-0004799007. Carlsbad, NM: Sandia National Laboratories.

Brunell, S. and D. Kicker. 2025. Analysis Report for Cuttings, Cavings, and Spallings in the 2026 Compliance Recertification Application Performance Assessment: Interim State Repository. EIMS-0005077055. Carlsbad, NM: Sandia National Laboratories.

Brunell, S., J. Bethune, P. Docherty, D. Kicker, S. Kim, S. King, J. Long, and T. Zeitler. 2023. Summary Report for the 2023 Replacement Panels Planned Change Request Performance Assessment. ERMS 579729. Carlsbad, NM: Sandia National Laboratories.

Burgess, A., T. Doe, T. Lowenstein, and J.A. Thies. 2008. Waste Isolation Pilot Plant Culebra Hydrogeologic Conceptual Model Peer Review Final Report. ERMS 551513. Carlsbad, NM: U.S. Department of Energy.

Cranston, C.C. 2009. Minable Potash Ore. ERMS 551120. Carlsbad, NM: Bureau of Land Management

Day, B. 2025a. BRAGFLO Grid Development for CRA-2026. EIMS-0004447000. Carlsbad, NM: Sandia National Laboratories.

Day, B. 2025b. Recommendation and Justification for Implementing a Lower Bound on Capillary Pressure in Marker Bed Materials S_MB139, S_ANH_AB, and S_MB138 using the CAP_MOD and PO_MIN Parameters for CRA-2026. EIMS-0004430534. Carlsbad, NM: Sandia National Laboratories.

Day, B. and S. King. 2025. Analysis Report for Salado Flow in the 2026 Compliance Recertification Application Performance Assessment: Interim State Repository. EIMS-0004944216. Carlsbad, NM: Sandia National Laboratories.

Docherty, P. and S. Kim. 2025. Analysis Report for Actinide Mobilization and Salado Transport in the 2026 Compliance Recertification Application Performance Assessment: Interim State Repository. EIMS-0005110990. Carlsbad, NM: Sandia National Laboratories.

Information Only

Domski, P. 2025a. Parameter Memorandum: Uncertainty Analysis of Actinide Solubilities for the 2026 Compliance Recertification Application (CRA-2026). EIMS-0004447122. Carlsbad, NM: Sandia National Laboratories.

Domski, P. 2025b. Th(IV), Np(V), and Am(III) Baseline Solubilities for the 2026 WIPP Compliance Recertification Application Performance Assessment Interim-State Analysis (CRA-2026 IS). EIMS-0004833660. Carlsbad, NM: Sandia National Laboratories.

Domski, P. 2025c. Prediction of Baseline Actinide Solubilities for the 2026 WIPP Compliance Recertification Application Performance Assessment Interim-State Analysis (CRA-2026 IS). EIMS-0004838025. Carlsbad, NM: Sandia National Laboratories.

Feng, L. and D. Kicker. 2025. Input Parameter Report for the 2026 Compliance Recertification Application Performance Assessment: Interim State Repository (CRA-2026 IS). EIMS-0005052992. Carlsbad, NM: Sandia National Laboratories.

Hansen, C., S. King, J. Bethune, and S. Brunell. 2023. Analysis Plan for the Performance Assessment for the Replacement Panels Planned Change Request. AP-204. ERMS 579449. Carlsbad, NM: Sandia National Laboratories.

Hansen, C., S. Brunell, B. Day, S. King, and J. Wilgus. 2025. Analysis Plan for the 2026 WIPP Compliance Recertification Application Performance Assessment. AP-214. Carlsbad, NM: Sandia National Laboratories.

Hart, D.B., R.M. Holt, and S.A. McKenna. 2008. Analysis Report for Task 5 of AP-114: Generation of Revised Base Transmissivity Fields. ERMS 552391. Carlsbad, NM: Sandia National Laboratories.

Holt, R.M. 1997. Conceptual Model for Transport Processes in the Culebra Dolomite Member of the Rustler Formation. SAND 97-0194. Carlsbad, NM: Sandia National Laboratories.

Kaplan, U., Swanson, J., and Kutahyali-Aslani, C. 2025. LANL ACRSP Parameter Recommendations for CRA-2026 Performance Assessment. Revision 1. LCO-ACP-41. Carlsbad, NM: Los Alamos National Laboratory.

Kicker, D. 2025. Analysis Report for Radionuclide Inventory Screening in the 2026 Compliance Recertification Application Performance Assessment: Interim State Repository. Revision 0. EIMS-0004832100. Carlsbad, NM: Sandia National Laboratories.

Kim, S., P. Docherty, D. Kicker, and S. King, 2024. Investigation of Radionuclide Screening on Total Curies versus Potentially Mobilized Curies. ERMS 581503. Carlsbad, NM: Sandia National Laboratories.

Kim, S. and D. Kicker. 2025. Analysis Report for Inventory EPA Units in the 2026 Compliance Recertification Application Performance Assessment: Interim State Repository. Revision 1. EIMS-0004940556. Carlsbad, NM: Sandia National Laboratories.

King, S. 2021. APPA 2D Salado Flow Grid Development. SAND2021-8603PE. Carlsbad, NM: Sandia National Laboratories.

King, S. 2025a. Constructed Cumulative Distributions for Approximation of Truncated Normal Distributions. EIMS-0004799476. Carlsbad, NM: Sandia National Laboratories.

Information Only

King, S. 2025b. Drilling Rate and Plugging Pattern Probabilities for the CRA-2026 PA Calculations. EIMS-0004437345. Carlsbad, NM: Sandia National Laboratories.

King, S. 2025c. Area for RH waste disposal for the interim state CRA-2026 PA calculation. EIMS-0004801801. Carlsbad, NM: Sandia National Laboratories.

King, S., S. Brunell, and T. Zeitler. 2025d. Analysis Report for Normalized Releases in the 2026 Compliance Recertification Application Performance Assessment: Interim State Repository. EIMS-0005040307. Carlsbad, NM: Sandia National Laboratories.

King, S. and T. Zeitler. 2025e. Analysis Report for Parameter Sampling in the 2026 Compliance Recertification Application Performance Assessment. EIMS-0004951492. Carlsbad, NM: Sandia National Laboratories.

Kirchner, T., A. Gilkey, and J. Long. 2014. Summary Report on the Migration of the WIPP PA Codes from VMS to Solaris. AP-162, Rev. 1. ERMS 561757. Carlsbad, NM: Sandia National Laboratories.

Kirchner, T., A. Gilkey, and J. Long. 2015. Addendum to the Summary Report on the Migration of the WIPP PA Codes from VMS to Solaris. AP-162. ERMS 564675. Carlsbad, NM: Sandia National Laboratories.

Kirkes, G.R. and J. McCormick. 2025. Features, Events, and Processes Assessment for the 2026 Compliance Recertification Application Performance Assessment. EIMS-0004940580. Carlsbad, NM: Sandia National Laboratories.

Knerr, R. 2020. Letter to Ms. Lee Ann B. Veal, U.S. Environmental Protection Agency, subject: “Planned Change Request for Alternative Panel Closure Locations for Panels 1 and 2,” Carlsbad, NM: U.S. DOE, Carlsbad Field Office.

Kuhlman, K. 2010. Analysis Report for the CRA-2009 PABC Culebra Flow and Transport Calculations. ERMS 552951. Carlsbad, NM: Sandia National Laboratories.

Leigh, C., and J. Trone. 2005. Calculation of Radionuclide Inventories for Use in NUTS in the Performance Assessment Baseline Calculation. ERMS 539644. Carlsbad, NM: Sandia National Laboratories.

Long, J. 2025. Computational Code Execution and File Management in the 2026 Compliance Recertification Application Performance Assessment: Interim State Repository (CRA-2026 IS). Revision 0. EIMS-0004900878. Carlsbad NM: Sandia National Laboratories.

Mariner, P. 2025. CRA-2026 IS updates to the WIPP humic colloids models for An(III) and An(IV). EIMS-0004838142. Carlsbad, NM: Sandia National Laboratories.

McCormick, J., Kirkes R., and Hansen C. 2024. Conceptual Models in WIPP Performance Assessment. EIMS-0004385596. Carlsbad, NM: Sandia National Laboratories.

Nemer, M. 2025. MgO Hydration Rates for the CRA-2026 Under AP-208. EIMS-0004445255. Albuquerque, NM: Sandia National Laboratories.

Information Only

Sanchez, L.C., J. Liscum-Powell, J.S. Rath, and H.R. Trellue. 1997. WIPP PA Analysis Report for EPAUNI: Estimating Probability Distribution of EPA Unit Loading in the WIPP Repository for Performance Assessment Calculations, Version 1.01. WBS 1.2.07.1.1. ERMS 243843. Albuquerque, NM: Sandia National Laboratories.

Shinta, A. A. 1997. User's Manual for NUTS, Version 2.05. ERMS 246002. Albuquerque, NM: Sandia National Laboratories.

U.S. Environmental Protection Agency (U.S. EPA). 1996. 40 CFR Part 194: Criteria for the Certification and Recertification of the Waste Isolation Pilot Plant's Compliance with the 40 CFR Part 191 Disposal Regulations: 61 Federal Register, 5223-5245 (February 9, 1996).

U.S. Environmental Protection Agency (U.S. EPA). 1998. 40 CFR Part 194: Criteria for the Certification and Recertification of the Waste Isolation Pilot Plant's Compliance with the Disposal Regulations: Certification Decision. Federal Register, vol. 63 (May 18, 1998): 27354 – 27406.

U.S. Environmental Protection Agency (U.S. EPA). 2025. Letter from Abigale Tardif to Mark Bollinger, Subject: EPA's Review and Approval of DOE's RPPCR for Waste Panels 11 and 12 at WIPP. July 31, 2025. Washington, DC: U.S. EPA.

U.S. Department of Energy (U.S. DOE). 2025. Waste Isolation Pilot Plant Delaware Basin Monitoring Annual Report. DOE/WIPP-24-2308. Carlsbad, NM: U.S. DOE, Carlsbad Field Office.

Van Soest, G. 2025. Interim State Performance Assessment Inventory Report – 2024. Revision 0. INV-IPA-24. Carlsbad, NM: Los Alamos National Laboratory.

Wallace, M. 1996. Summary Memo of Record for NS-11: Subsidence Associated with Mining Inside or Outside the Controlled Area. Records Package for Screening Effort NS-11: Subsidence Associated with Mining Inside or Outside the Controlled Area (November 21) (pp. 1–28). ERMS 412918. Albuquerque, NM: Sandia National Laboratories.

Ward, A. 2025. Performance Assessment Inventory for Analysis of a 12-Panel Repository Configuration. Letter to Bill McInroy. March 18, 2025. CBFO:ERCD:AW:RS:25-0197. Carlsbad, NM: U.S. DOE, Carlsbad Field Office.

Wilgus, J. and J. Bethune. 2025. Analysis Report for Culebra Flow and Transport in the 2026 Compliance Recertification Application Performance Assessment. EIMS-0005101531. Carlsbad, NM: Sandia National Laboratories.

Wilgus, J. and S. Brunell. 2025. Re-Calculation of the Location of Culebra Release Point 2 for Use in WIPP PA Rev. 1. EIMS-0004818700. Carlsbad, NM: Sandia National Laboratories.

WIPP PA. 2025. Design Document and User's Manual for BRAGFLO Version 8.00. EIMS-0004430695. Carlsbad, NM: Sandia National Laboratories.

Zeitler, T. 2025. Analysis Report for Direct Brine Releases in the 2026 Compliance Recertification Application Performance Assessment: Interim State Repository. EIMS-0004961699. Carlsbad, NM: Sandia National Laboratories.

Information Only

Sandia National Laboratories is a multimission laboratory managed and operated by National Technology & Engineering Solutions of Sandia, LLC, a wholly owned subsidiary of Honeywell International Inc., for the U.S. Department of Energy's National Nuclear Security Administration under contract DE-NA0003525. This research is funded by WIPP programs administered by the Office of Environmental Management (EM) of the U.S. Department of Energy.







Information Only